The Role of A1-MGBv Corticothalamic Feedback Explored with Mistuning of Harmonic Complex Tones using Ferrets

Natsumi Homma, B.Sc.
Merton College, University of Oxford

A thesis submitted for the degree of
Doctor of Philosophy
Hilary 2016

To my parents

Acknowledgements

Firstly, I would like to thank my supervisors, Professors Victoria Bajo and Andrew King. Without their continuous support and invaluable input throughout my DPhil this thesis would not have been possible.

I am very grateful for Andy's thoughtful advice and input on the project and also for the opportunity to learn from him and gain so much experience in his laboratory.

In particular, I would like to thank Vicky. Without her advice and intimate knowledge of the field this project would not have reached completion. I really appreciate that she gave up so much time for hands-on teaching and I am also indebted for her patience and guidance throughout this project.

Furthermore, I would like to thank Dr. Fernando Nodal. Equally, without his support this project could not have been completed. I am very grateful for all of his advice, input and hands-on teaching.

I also would like to thank Dr. Max Happel from the Leibniz Institute for Neurobiology, Magdeburg. I am grateful for his advice and input.

I am particularly obliged to my funding body, the Japan Student Services Organization. Without this scholarship, I could not have studied at Oxford University. I also appreciate the support grants from Merton College, Oxford.

Finally, I would like to thank all the lab members for their insightful advice on my project and for making my time in Oxford so memorable. Particular thanks goes to Amy, my good lab mate and friend, for cheering me up whilst sitting next to me in the office, and to all my little ferrets, with whom I spent so much time during this project.

Contributions

Chapter 3
Experimental design: N Homma (NH), V Bajo (VB), F Nodal (FN), M Happel (MH), A King (AK); Data collection and analysis: NH; MATLAB script for the go/no-go behaviour: NH, FN, MH.
A part of work was submitted as a manuscript: Natsumi Y. Homma, Victoria M. Bajo, Max F.K. Happel, Fernando R. Nodal and Andrew J. King. (In press - JASA-EL-00102) Mistuning detection performance of ferrets in a go/no-go task.

Chapter 4
Experimental design: NH, VB, FN, AK; Stimulus design: NH, FN; Recording data collection: NH, VB, FN; Histology: NH; Data analysis: NH.
The anatomical investigation of tonotopic organization in ferret MGBv was adapted from the poster (Nodal et al. 2006) with agreement.

Chapter 5
Experimental design NH, VB, FN, AK; Stimulus design: NH, FN; Recording data collection: NH, VB, FN; Data analysis: NH.

Chapter 6
Experimental design NH, VB, FN, MH, AK; Behavioural data collection: NH, MH; Surgical procedures: NH, VB, FN; Histology and stereology: NH, VB; Data analysis: NH; MATLAB script for the go/no-go behaviour: NH, FN, MH.
Dr. Nodal kindly provided the brain sections with BDA tracer injection in the MGBv for a control case. The figure 6.8 was prepared by Prof. Bajo.

We are grateful to Dr. Kerry Walker for providing initial MATLAB code for the go/no-go behaviour.

Abstract

The Role of A1-MGBv Corticothalamic Feedback Explored with Mistuning of Harmonic Complex Tones using Ferrets

Natsumi Homma, B.Sc.
Merton College, University of Oxford
A thesis submitted for the degree of *Doctor of Philosophy*
Hilary 2016

The A1-MGBv corticothalamic projection is one of the major descending pathways in the auditory system, projecting from the primary auditory cortex (A1) to the ventral division of medial geniculate body (MGBv). Recent evidence suggests that corticothalamic feedback can sharpen the spectral receptive fields of thalamic neurons and modulate the temporal precision of the responses. The aim of the work presented here was to investigate the role of A1-MGBv corticothalamic feedback using harmonic and mistuned complex tones (HCTs and MCTs) in adult ferrets. The MCTs used comprised a mistuned harmonic shifted to a higher frequency in the otherwise HCTs. The harmonic structure of sounds is an important grouping cue in auditory scene analysis.

We first measured the ability of ferrets to detect mistuned harmonics using a go/no-go behavioural task paradigm. Psychometric functions plotting sensitivity as a function of degree of mistuning were used to evaluate the behavioural performance using signal detection theory. The threshold for mistuning detection was 0.8 ± 0.1 Hz (mean ± sem), with sensitivity indices and reaction times

depending on the degree of mistuning. The threshold range for mistuning in ferrets is similar to that previously described in other species.

The responses to MCTs in MGBv neurons were explored using extracellular recordings in anaesthetised animals. The functional organization of the ferret auditory thalamus has not previously been investigated. The ferret MGBv was identified by the short response latency and the sharply tuned frequency response areas of the recorded units and by its tonotopic organization, which was found to be comparable to that of other species. Compared to their responses to HCTs, the firing rates of MGBv neurons were modulated depending on the degree of mistuning and the fundamental frequency of the MCTs. Distinctive temporal response patterns were also observed, phase locked to the periodicities of altered phases of the MCTs.

To investigate whether corticofugal modulation contributes to mistuning detection, A1-MGBv corticothalamic neurons were selectively eliminated bilaterally by chromophore-targeted laser photolysis. Using the behavioural paradigm established above, mistuning detection was tested before and after these lesions were made. Animals with corticothalamic lesions were impaired in their ability to detect a mistuned harmonic, as indicated by decreased *d'* values, increased thresholds, and a shift of the psychometric curves towards higher mistuning values.

Together, these results suggest a possible role for corticothalamic feedback in modulating the firing patterns of MGBv neurons in ways that contribute to accurate recognition of complex auditory stimuli. In other words, this top-down corticothalamic feedback may be important for auditory scene analysis.

List of Abbreviations

A1	Primary auditory cortex
AAF	Anterior auditory field
AC	Auditory cortex
ADF	Anterior dorsal field
AEG	Anterior ectosylvian gyrus
ANF	Auditory nerve fibre
AP	Antero-posterior
AVCN	Anteroventral nuclei of cochlear nucleus
AVF	Anterior ventral field
BBN	Broadband noise
BDA	Biotinylated dextran amine
BF	Best frequency
CF	Characteristic frequency
CN	Cochlear nucleus
CNIC	Central nucleus of inferior colliculus
DCN	Dorsal nuclei of cochlear nucleus
EG	Ectosylvian gyrus
EMG	Exponentially modified Gaussian distribution
EPSP	Excitatory postsynaptic potential
F0	Fundamental frequency
FA rate	False alarm rate
FRA	Frequency response area
HCT	Harmonic complex tone
IC	Inferior colliculus
ILD	Interaural level difference
ITD	Interaural time difference
LGN	Lateral geniculate nucleus
LSO	Lateral superior olive
LV	Pars lateralis
MCT	Mistuned complex tone
MEG	Middle ectosylvian gyrus
MGB	Medial geniculate body
MGBd	Dorsal division of medial geniculate body
MGBm	Medial division of medial geniculate body
MGBv	Ventral division of medial geniculate body
ML	Medio-lateral
MNTB	Medial nucleus of the trapezoid body

MSO	Medial superior olive
OV	Pars ovoidea
PB	Phosphate buffer
PBS	Phosphate buffer saline
PEG	Posterior ectosylvian gyrus
PPF	Posterior pseudosylvian field
PSF	Posterior suprasylvian field
PSTH	Post stimulus time histogram
PVCN	Posteroventral nuclei of cochlear nucleus
TRN	Thalamic reticular nucleus

Contents

List of Figures and Tables

Chapter 1

General introduction

1.1. **Preface**

In everyday life, we listen to many different kinds of sound at the same time. However, it is not difficult for us to understand what the next person is saying while other people are chatting or to pick up a sudden phone call while listening to music. We can segregate different sounds that occur simultaneously into perceptually meaningful categories and perceive the whole environment; this is called auditory scene analysis. In other words, we group and segregate mixtures of sounds in order to better perceive the acoustic environment. This processing is enabled by a complex and well-organized auditory system.

One of the fundamental questions in auditory neuroscience is to understand the mechanisms of segregation and grouping. Scene analysis has been addressed by psychoacoustic, anatomical, electrophysiological, computational studies, and by combinations of these approaches. In this thesis, I investigated the role of corticothalamic feedback, one of the major projections from the primary auditory cortex to the thalamus, in complex sound processing.

1.2. **Sounds in nature**

Pure tones are sounds generated as a sinusoidal wave and therefore consist of a single frequency. Because of their simplicity, they are routinely used in auditory laboratories to investigate basic properties of auditory responses. On the other hand, most sounds in nature have a more complex structure. They typically comprise a fundamental frequency (F_0) plus several harmonics and are therefore periodic. This includes human speech, animal vocalizations and the sounds produced by many musical instruments (Fig. 1.1). Furthermore, in a broad sense, natural sounds, such as the sound of waves in the sea and wind in the leaves, are also complex sounds, and are produced by natural sources.

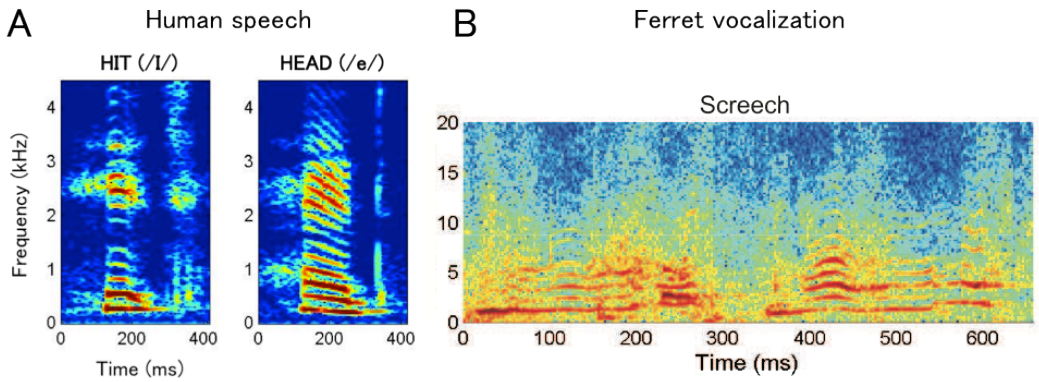

Figure 1.1 Example of harmonic structure in human speech and ferret vocalizations
(A) Spectrograms of the words, "hit" and "head" spoken by a native British English speaker. They represent the spectral profiles of the vowel /I/ and /e/ in the words, respectively (adapted and modified from Schnupp et al. 2011, figure 1.16). (B) The ferret 'screech' vocalization, recorded by Dr. Kerry Walker (adapted and modified from Walker 2008, figure 1.2).

In human speech, speakers generate a series of rapid clicks (glottal pulses) with their vocal folds, and the glottal pulse train travels through the resonant cavities of the vocal tract, which amplify and suppress some of the harmonics without introducing any new frequencies. The vocal tract includes the throat, mouth and nasal sinuses, and the generation of formant frequencies is controlled by moving articulators, such as the lips, jaws and tongue, to change the size and shape of the resonant cavities. In the example (Fig. 1.1A), both of word, “hit” and “head” have a clear harmonic structure with characteristic spectral profiles. The difference between the vowels /I/ and /e/ in each word is represented by their formant frequencies.

Animals use their vocal cords and tracts in a similar manner to humans and also generate vocalizations based on pulse-train and resonance mechanisms. For example, ferrets (*Mustela putorius furo*) produce a set of vocalizations, which are complex sounds spanning a range of 2 to 8 kHz (e.g. Fig. 1.1B). They make a loud chirp (‘bark’) when they are excited. When they are annoyed or mad, they produce a ‘hiss’. It is like that of cats, although it is not as scratchy. The ‘dock’ is produced when they are happy or playing, which sounds like a chicken clucking. The ‘screech’ is periodic, with high pitch and high amplitude, indicating that they in pain or fear and is observed during fighting (Walker 2008). The Siberian ferret (*Mustela eversmanni*) and other mustelid species produce similar vocalizations (Farley et al. 1987). Their ‘screech’ and ‘hiss-squeal’, which is similar to a ‘screech’ but starting with a loud hiss followed by complex tones comprising several frequency components, are periodic sounds and therefore have a harmonic structure (Fig. 1.1B). It is important for both humans and ferrets to discriminate and

recognize these vocalizations for their communication and interactions with their environment.

1.3. **Auditory scene analysis**

The analysis of the auditory scene is achieved based on the acoustic properties of 'auditory objects', with the complex integration of memory and learning. The process of scene analysis relies on spatial information, amplitude modulation, onset asynchrony and harmonicity of the constituent sounds (Bregman 1990). In addition, attention plays a key role in auditory scene analysis. A good example is the 'cocktail party effect,' where you can hear out what a person in front of you is saying by paying attention even in a noisy situation. Recent studies have attempted to investigate the neural basis for scene analysis (reviewed by Shamma et al. 2011; Christison-Lagay et al. 2014). In addition to the role of attention, learning allows us to generalize across different categories of sounds. For example, we are able to learn to distinguish tone qualities ('timbre') of different musical instruments through exposure to the sounds. Furthermore, we integrate information from other sensory modalities to better understand the auditory scene. The 'McGurk effect' is one of the well-known examples of audiovisual integration, in which the perception of an articulated syllable can be altered by seeing incongruent lip movements (McGurk and MacDonald 1976).

In addition to segregating sounds from different sources that are present simultaneously, it is important to be able to group or segregate sequences of sounds that occur at different times. For example, a tone sequence is perceived to be grouped or segregated according to the difference of frequencies and intervals

between the tones (e.g. Bregman and Campbell 1971). If high and low tones are presented alternately, with tones played in high-low-high/low-high-low order (ABA rhythm paradigm), the tone sequence is perceived as one stream of trills, or galloping, when the frequency separation is small (< ~3 semitones), whereas two streams are heard if the presentation rate is fast and the frequency separation large (Miller and Heise 1950; van Noorden 1975). This is an example of non-simultaneous grouping and segregation.

In the following, I summarize the principal grouping cues.

Spatial information

Spatial information plays a role in grouping and segregating sounds (Cherry 1953; O'Connor and Sutter 2000; Boehnke and Phillips 2005; Eramudugolla et al. 2008). As binaural sound localization cues for the horizontal plane ('azimuth'), interaural time differences (ITDs) and interaural level differences (ILDs) are mainly used, which originate from the differences of time of arrival and intensity between two ears, respectively. Psychophysical experiments in humans suggest that ITDs (and presumably other spatial cues) contribute less to the grouping of simultaneous sounds than other cues (Buell and Hafter 1991; Hill and Darwin 1996; Darwin and Hukin 1999). However, binaural cues do help to segregate sequences of tones, as adding ITD and ILD retrieves masked information from complex sound environment (e.g. Middlebrooks and Onsan 2012; Tolnai et al. 2015), suggesting that they play an important role in segregating a stream of speech (Culling et al. 2004).

Amplitude modulation

Amplitude modulation helps to distinguish signal or target tones over background noise. In comodulation masking release, thresholds for detecting a pure tone decrease as the bandwidth of an amplitude-modulated masker is increased beyond the so-called critical bandwidth, whereas this is not the case for an unmodulated noise masker (Hall et al. 1984). Auditory neurons that follow fluctuations in the envelope of the noise masker are found at various levels of the auditory pathway, but only at higher levels do neurons respond to low-level tones-in-noise in ways that suggest that responses to background noise are suppressed (Nelken et al. 1999; Las et al. 2005). This is likely to be helpful for segregating targets from noise, and suggests a role for thalamocortical processing, which will be considered further in the following sections.

Onset asynchrony

Sounds starting or finishing at the same time are usually grouped together. If several frequency components are presented with a common onset, they are more likely to be perceived as a single auditory object. On the other hand, if one frequency component (partial) starts or ends at a different time, complex tones composed of a few partials are more likely to result in streaming (Dannenbring and Bregman 1978). A similar trend was observed when one of the harmonics started or stopped at a different time from the rest of the vowel, causing a change in vowel perception (e.g. from /I/ to /e/) (Darwin 1984; Darwin and Sutherland 1984). Although Darwin and colleagues suggested that the perceptual grouping process

happens at higher levels of the auditory system, further studies suggested it was a broadband masking effect at the level of the cochlear nucleus (Roberts and Holmes 2006; Roberts and Holmes 2007; Bleeck et al. 2008). However, it seems unlikely that the effect of changing the synchrony of partials on vowel perception can be explained only by the low-level mechanisms, and the basis for this is not yet fully understood.

Harmonicity

Harmonicity or spectral regularity is a powerful cue for grouping. Harmonic complex tones (HCTs), which comprise an F_0 and multiple integer harmonics, are usually heard as one tone, not as separated several pure tones (Roberts and Bregman 1991; Roberts and Bailey 1993; Roberts and Bailey 1996b; Roberts and Bailey 1996a). F_0 differences between concurrent vowels or HCTs help to segregate them, with better performance observed as F_0 separation increases (Scheffers 1983; Zwicker 1984). This perceptual segregation is thought to reflect a combination of grouping harmonics with a common F_0 and fluctuations in the spectral envelope of the combined stimuli that result from beating (Culling and Darwin 1994). Beats elicit a sensation of 'roughness' and are thought to derive from interactions between neighbouring harmonics that fall within the same auditory filter. Mistuned complex tones (MCTs) contain a partial or frequency component that is not harmonically related to the HCT, and can also give rise to beating. The harmonically unrelated partial (or mistuned harmonic) is heard to 'pop out' as a separate tone from a complex tone when its frequency is relatively low or

produces a sensation of roughness in the tone quality when it is relatively high frequency (Moore et al. 1985; Moore et al. 1986; Hartmann et al. 1990).

Another important source of information for scene analysis is provided by the temporal fine structure of sounds (e.g. Moore 2008) due to the way acoustic signals, such as speech, change rapidly over time. Inserted mistuned harmonics in HCTs alter both the envelope and temporal fine structure of the HCT, which provides 'temporal cues' as well as 'spectral cues' that could assist in their detection. The relative contributions of these cues in the perception of complex tones have been investigated by psychophysical and modelling studies. In the concept of 'harmonic sieves' (Goldstein 1973), templates are calculated as multiple harmonic series of HCTs based on a F_0, and MCTs are perceived as inharmonic when the spectral components deviate from the templates. On the other hand, mistuning detection may be based on the temporal excitation pattern produced in the auditory periphery by the envelope of complex tones (Licklider 1951; Meddis and Hewitt 1991a; Meddis and Hewitt 1991b). It has been proposed that place and temporal models contribute to the perception of low and high frequency harmonics, respectively, according to whether they can be resolved by cochlear filtering (Houtsma and Smurzynski 1990). Furthermore, broadband harmonic templates have been proposed as a way of detecting mistuned harmonics (Lin and Hartmann 1998). Neural correlates have been studied electrophysiologically in animals, showing enhanced firing rates for specific spectral components and temporal patterns locked to the envelope and fine structure of MCTs (Sinex et al. 2005; Sinex and Li 2007; Sinex 2008; Fishman and Steinschneider 2010).

1.4. Processing of complex sounds in the auditory system

The auditory system comprises a well-organized neural network that carries information from the periphery to the cortex, and sounds are processed at each stage throughout the network. Auditory pathways are complex with multiple projections of afferent and efferent neurons in the subcortical and cortical areas, communicating with each other through feedforward and feedback loops and interconnecting ipsilaterally and contralaterally.

Peripheral system

Sounds are generated by vibrating objects. They are pressure waves and their properties are characterised by the physical properties of the objects. Hearing starts when the pressure waves are collected in the external ear (‘pinna,’ ‘concha’ and ‘auditory meatus’) and reach the eardrum, which transforms sound induced vibrations to mechanical displacements on the tympanic membrane. The human external ear has evolved for selectively amplifying a major speech frequency range 2 to 5 kHz, and as a result of its size and shape generates spectral cues that aid in the localization of sound (Middlebrooks and Green 1991). In the middle ear, the vibrations of the tympanic membrane are transmitted by three small bones (or ‘ossicles’) to the oval window of the fluid-filled cochlea, a process that serves to offset the loss in pressure that would otherwise occur due to the higher impedance of the cochlear fluids. Transmission across the ossicles chain is controlled by the reflex contraction of the tensor tympani and stapedius muscles, protecting the inner ear from continuous loud sounds. In the inner ear, the amplified vibrations propagate in the fluid, inducing travelling waves along the basilar membrane. On

the basilar membrane, one row of inner hair cell and three rows of outer hair cells are arranged so that deflection of their hair bundles modulates the opening of transduction channels through which potassium ions enter to depolarize the cells. While inner hair cells works as sensory receptors to transmit signals to the brain, outer hair cells amplify the basilar membrane vibrations as a result of their rapid electromotility involving the motor protein 'prestin' (Ashmore 2008). Since the tuning of the basilar membrane varies logarithmically from the base to the apex, the hair cells that sit upon it are tuned to specific frequencies. Thus, the operation of the basilar membrane approximates a Fourier transform, giving rise to a cochleotopic or tonotopic map along its length. Because of changes in bandwidth – the range of frequencies to which each hair cell responds – the harmonics of complex sounds are 'resolved' at the lower frequency region, where they respond exclusively to a single harmonic and 'unresolved' at the higher frequency region, where they respond to several harmonics (Moore and Gockel 2011).

Auditory nerve

Connections to auditory nerve fibres (ANFs) are different for inner and outer hair cells. Outer hair cells connect to type II fibres, which represent a small (~5%) proportion, and are thin and unmyelinated. On the other hand, the excitation of inner hair cells is delivered through type I fibres that rapidly conducts signals through thick myelinated axons (Liberman and Simmons 1985). ANFs preserve the tonotopic map as the type I fibres innervate a single inner hair cell. Therefore, ANFs are equally selective to specific frequencies and have a characteristic frequency (CF, the frequency of sound at which the fibre responds with the lowest

intensity) that varies topographically to form a 'place code'. The firing rates of the ANFs encode the intensity of sounds (a 'rate code'); as the intensity of sounds increases, the number of action potentials per unit of time monotonically increases until this saturates at a certain sound level. Most ANFs have high spontaneous firing rate and are sensitive to low intensity sounds, while a minority have low spontaneous firing rates, less steep rate-intensity function and do not saturate up to > 80 dB SPL (Heil and Peterson 2015). The firing pattern can be phase-locked to sound frequencies up to a few kilohertz, which provides the basis for a 'temporal code.' In the phase locked response, spikes occur at a particular phase of the sound envelope with a high probability. ANFs phase lock to the stimuli is degrades above 1-2 kHz (Rose et al. 1967; Palmer and Russell 1986) and to interactions between different components of complex sounds (Horst et al. 1986; Sinex et al. 2003). Their responses across frequencies carry essential information for complex sounds processing (Horst et al. 1986; Cariani and Delgutte 1996a; Cariani and Delgutte 1996b; Sinex et al. 2003).

Cochlear nucleus

ANFs innervate the cochlear nucleus (CN) in the brainstem, which comprises three divisions: dorsal, anteroventral and posteroventral nuclei (DCN, AVCN and PVCN). Each of them is tonotopically organized and contains different populations of neurons with distinct anatomical locations, morphology and firing properties (Pfeiffer 1966; Brawer et al. 1974; Young and Brownell 1976). Cues for the segregation and grouping of complex sounds are processed at this stage. For example, wideband inhibition, which reduces excitation of other neurons as the

bandwidth of stimuli is increased, may allow a partial to be heard out by the rebound in the excitatory response through release from inhibition (Roberts and Holmes 2006; Roberts and Holmes 2007; Bleeck et al. 2008). Neural correlates of comodulation masking release have been observed showing more salient responses to tones when wideband fluctuating noise were added and reduced neural responses to the masker modulation (Pressnitzer et al. 2001; Neuert 2004). However, this is less pronounced than that observed in the cortex, and the addition of a low level tone does not suppress phase locked responses to modulated maskers, suggesting that higher levels of processing play a key role in differentiating targets from noise (Nelken et al. 1999; Las et al. 2005). Chopper neurons are a distinct cell type in the AVCN where several ANFs and other type of inputs converge. Segregation of two concurrent vowels may be achieved by 'channel selection', in which the relative synchronization of chopper neurons to the two F_0s determines which vowel they will respond best to (Keilson et al. 1997). Furthermore, 'harmonic cancelation' contrasts two concurrent vowels by suppressing responses as a harmonic masker. It assumes a cancellation filter that comprises a delayed input and an inhibitory synapse, which enables the periodic spikes of one vowel to be cancelled out and contrasted with the periodicity of the responses to the other vowel (de Cheveigné 1995; de Cheveigné 1997; de Cheveigné et al. 1997a; de Cheveigné et al. 1997b). Indeed, it is difficult to explain how to discriminate inharmonic vowels only by channel selection (de Cheveigné 1995; de Cheveigné et al. 1997b) and the effects on vowel discrimination of introducing an intensity difference between two vowels are easier to explain in terms of harmonic cancellation (de Cheveigné et al. 1997a). Nevertheless, electrophysiological evidence for harmonic cancellation has not been

found yet. For MCTs, primary-like neurons in the CN synchronize their responses to the individual stimulus components, much like the ANFs from which they receive their inputs, while chopper neurons show phase locking to the periodicity of the envelopes derived from the interaction of adjacent stimulus components (Sinex 2008).

Superior olivary complex

Binaural information first converges in the superior olivary complex, and spatial cues, such as ITDs and ILDs, are extracted at this stage. Neurons in the lateral superior olive (LSO) receive excitatory inputs from ipsilateral CN neurons and inhibitory inputs from contralateral CN neurons via the medial nucleus of the trapezoid body (MNTB), and ILDs are computed by integrating these inputs as a sum of firing rates (Sanes 1990; Tollin and Yin 2002a; Tollin and Yin 2002b). Since ILDs are localization cues that work better for high frequency sounds, the tonotopic organization of the LSO is biased toward higher frequencies (Tsuchitani and Boudreau 1966; Guinan et al. 1972). On the other hand, the medial superior olive (MSO) is biased more toward lower frequencies, and is thought to processes ITDs by acting as a coincidence detector (Jeffress 1948). It receives excitatory inputs from both ipsilateral and contralateral CN neurons, and, according to the Jeffress model, neurons are tuned to different ITDs as a result of delay lines from each CN (Carr and Konishi 1988; Yin and Chan 1990). However, in mammals, ITD tuning varies (McAlpine et al. 2001), which is not compatible with place coding, the mechanism of ITD detection also appears to involve glycinergic inhibitory inputs (Brand et al. 2002).

Inferior colliculus

Ascending pathways arising from the SOC and CN, as well as the nucleus of the lateral lemniscus, converge in the inferior colliculus (IC) of the midbrain, and these various inputs are essential for further processing of signals in the IC. ITD and ILD cues extracted in the SOC remain segregated in different parts of the IC laminae (Oliver et al. 1997; Loftus et al. 2004), although more recent electrophysiological data has shown that some IC neurons are sensitive to all localization cues (Chase and Young 2008). The central nucleus (CNIC) has a tonotopic organization with a low-to-high frequency gradient from dorso-lateral to ventro-medial (Aitkin et al. 1975). IC has abundant inhibitory inputs and is involved in processing complex temporal patterns (Oliver et al. 1994). Many neurons are sensitive to amplitude-modulated sounds (Langner and Schreiner 1988), and phase locking to pure tones is observed up to ~1000 Hz (Kuwada et al. 1984; Liu et al. 2006). Binaural integration for the harmonicity cues present in HCTs has been described in the IC (Nakamoto et al. 2015), while monaural responses can again represent the interaction between adjacent components of double HCTs as well as MCTs (Sinex et al. 2002; Sinex et al. 2005; Sinex and Li 2007). The temporal discharge pattern is locked to beats with increasing firing rate compared to HCTs, and this is observed across neurons with different CFs (Sinex et al. 2002; Sinex et al. 2005; Sinex and Li 2007)

Auditory thalamus

Except for the olfactory system, all sensory information is relayed to the cortex via the thalamus. Although the thalamus was thought to be a simple relay station, growing evidence suggests that converging inputs are further processed here. The auditory thalamus, the medial geniculate body (MGB), comprises three distinct divisions. The ventral division (MGBv) has a clear tonotopic organization, receiving major inputs from the ipsilateral CNIC and projecting to the primary auditory cortex (Calford and Aitkin 1983; Rouiller and de Ribaupierre 1985), with collaterals that terminate in the thalamic reticular nucleus (TRN) (Jones 1985). MGB contains a substantial number of GABAergic neurons, although the proportion varies among species (Winer and Larue 1996; Huang et al. 1999), and receives inhibitory feedforward inputs from IC (Winer et al. 1996) and TRN (Jones 1975). MGBv contains large principal neurons with bushy and tufted dendrites, which mainly transmit information to the other brain regions, and smaller Golgi type II interneurons with short axons (Winer et al. 1988). MGBv is divided into two anterior and posterior regions, which project to the primary auditory cortex and adjacent core cortical fields, respectively (De La Mothe et al. 2006; Storace et al. 2010; Read et al. 2011). Rostral MGBv shows narrower frequency tuning and better synchronization to temporal modulation with shorter latency responses compared to posterior MGBv (Calford 1983; Rodrigues-Dagaeff et al. 1989; Rouiller and de Ribaupierre 1989).

In general, MGBv neurons have short response latencies and sharp tuning curves (Calford 1983; Morel et al. 1987; Rodrigues-Dagaeff et al. 1989; Redies and Brandner 1991; Bordi and LeDoux 1994; Edeline et al. 1999) and are

sensitive to temporal modulation (Rouiller et al. 1981; Bartlett and Wang 2011), and the majority show phase-locking to pure tones limited to ~520 Hz (Wallace et al. 2007). On the other hand, the medial and dorsal divisions (MGBm and MGBd) are non-tonotopic and integrate auditory and non-auditory information, showing complex polymodal receptive fields (Rouiller et al. 1989; Anderson et al. 2007). MGBd contains large stellate and bushy cells as principal neurons (Winer and Morest 1983b). Neurons in MGBd do not phase lock to tonal stimuli, but do respond with high temporal precision to amplitude modulation (Bartlett and Wang 2011). MGBm consists of morphologically heterogeneous neuron types (Winer and Morest 1983a), showing heterogeneous response properties (Rouiller et al. 1989; Anderson and Linden 2011). A small population of MGBm neurons can phase lock up to ~1000 Hz, and synchronized responses to rapid modulation can be comparable to those observed in MGBv (Rouiller et al. 1981; Wallace et al. 2007). Although major projections go to the auditory cortex, MGBm also innervates the amygdala, which is thought to produce emotional reactions to sounds (LeDoux et al. 1991). Their functions have not been elucidated enough, however, and may be more concerned with the integration of auditory and other sensory inputs.

MGBv is specialized to extract spectral and temporal information from the auditory signals it receives. There is a clear distinction in response properties from IC – MGBv – A1, suggesting that the thalamus may be a transformation or gating stage (Miller et al. 2002; Las et al. 2005; Bartlett and Wang 2007). Although sensitivity to spectral modulation is similar in the thalamus and cortex, recordings made simultaneously in both structures indicate that the thalamus exhibits faster temporal modulation rates and sharper tuning than the cortex does (Fig. 1.2)

(Miller et al. 2002). In addition, while the majority of IC neurons show temporally synchronised responses and cortical neurons can exhibit either synchronised or non-synchronised responses, thalamic neurons transit between synchronised responses to long inter-click intervals and non-synchronised responses to short inter-click intervals (Bartlett and Wang 2007). Furthermore, MGB and A1 neurons can be very sensitive to low level tones-in-noise, with thresholds lower than the tone threshold in silence, as a result of suppression of responses to modulated noise, whereas IC neurons represent acoustic properties of noise and tones equally well (Las et al. 2005). Thus, the thalamus and cortex appear to be well adapted for extracting sounds that are characterized by their spectrotemporal modulations, which may reflect the strong connections between MGBv and A1 that are mediated by the thalamocortical and corticothalamic loops described in a later section.

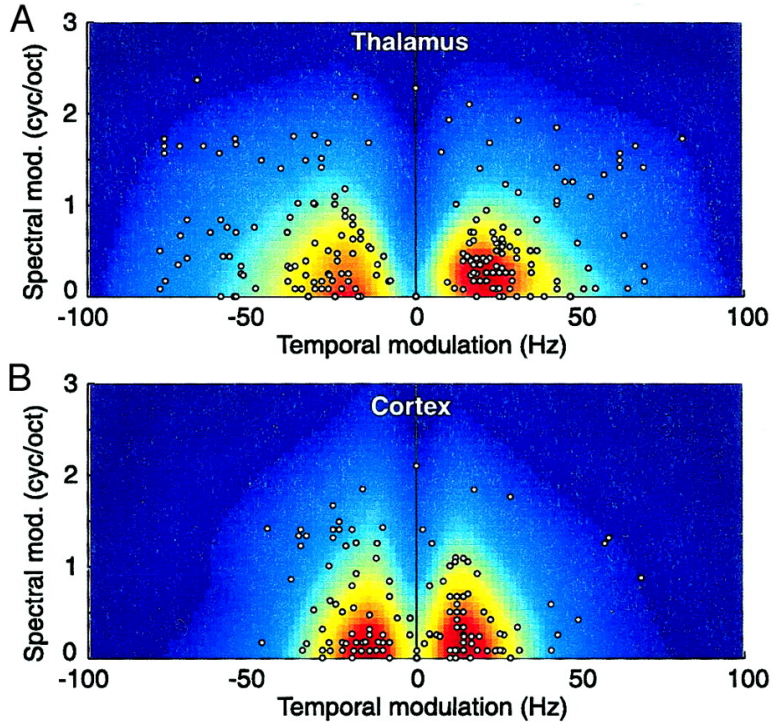

Figure 1.2 Population modulation transfer functions of the thalamus and cortex
Modulation transfer functions were obtained by presenting dynamic ripple sounds while recording in thalamus (A) and primary auditory cortex (B) of cats. These sounds are synthetic random chords that vary constantly and randomly in frequency and amplitude. The dots indicate best temporal and spectral modulation values for individual neurons. The colour represents the averaged modulation transfer functions (adopted and modified from Miller et al. 2002, figure 8).

Auditory cortex

Auditory cortex (AC) contains several fields, defined on the basis of their physiological and anatomical features. Although there are species differences, all mammalian auditory cortex can be distinguished into primary and second-order areas (Hackett et al. 2001; Bizley et al. 2005; Winer and Lee 2007). For example, the auditory cortex of ferret, the species used in this study, comprises the middle, posterior and anterior ectosylvian gyri (MEG, PEG, AEG), which have been characterized physiologically (Nelken et al. 2004; Bizley et al. 2005) and anatomically (Bajo et al. 2007) (Fig. 1.3). MEG is a core region, comprising two cortical fields, the primary auditory cortex (A1) and the anterior auditory field (AAF). PEG and AEG contain what are likely to be secondary or higher order areas. Neurons in the posterior pseudosylvian and suprasylvian fields (PPF and PSF) within PEG show longer latency and more sustained responses. The anterior dorsal and ventral fields (ADF and AVF) in AEG are more multisensory in nature, with many neurons showing sensitivity to both auditory and visual stimuli (Bizley et al. 2007; Bizley and King 2008).

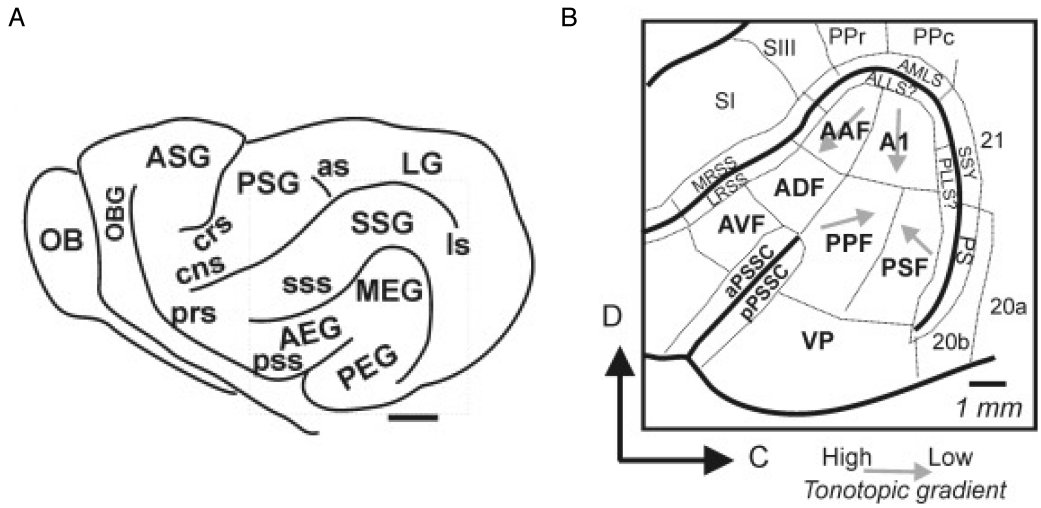

Figure 1.3 Schematic of the ferret auditory cortex
(A) Schematic of a whole ferret brain showing the main sulci and gyri. The auditory cortex is located on the ectosylvian gyrus. OB, olfactory bulb; OBG, orbital gyrus; ASG, anterior sygmoid gyrus; PSG, posterior sygmoid gyrus; SSG, syprasylvian gyrus; LG, lateral gyrus; prs, presylvian sulcus; crs, cruciate sulcus; cns, coronal sulcus; as, anseate sulcus; sss, suprasylvian sulcus; pss, pseudosylvian sulcus; ls, lateral sulcus. (B) Schematic showing the identified sensory areas within and around the ectosylvian gyrus. The auditory areas characterized to date comprise the primary auditory cortex (A1), the anterior auditory field (AAF), the posterior pseudosylvian field (PPF), the posterior suprasylvian field (PSF), the ventral posterior field (VP), and the anterior dorsal field (ADF). Multisensory (anterior ventral field [AVF]; anterior and posterior pseudosylvian sulcal cortex [PSSC]), parietal (rostral and caudal posterior parietal fields [PPr, PPc]), visual (areas 20 and 21, the suprasylvian sulcal fields [SSY], PS, and anteromedial lateral suprasylvian [AMLS]), and somatosensory areas (SI, SIII, and the medial bank of the rostral suprasylvian sulcus [MRSS]) are also shown. D, dorsal; C, caudal. The direction of high–low frequency gradients within tonotopically organised fields is shown with grey arrows. Scale bar = 5 mm in A, B. (adapted and modified from Bizley et al. 2015, figure 1)

The primary auditory cortex receives inputs preferentially from the ipsilateral MGBv (Morel and Imig 1987; De La Mothe et al. 2006; Lee and Winer 2008c). The tonotopic organization is preserved from CN, SOC, CNIC, MGBv, to A1, and all of these are referred as 'lemniscal' or 'core' regions. The second-order areas are weakly tonotopic or non-tonotopic, in other words, 'non-lemniscal,' and receive inputs from MGBd as well as MGBv and other cortical areas (Lee and Winer 2008a; Lee and Winer 2008c; Bizley et al. 2015). The cortico-cortical connection between the primary and second-order areas is thought to be important for higher level processing. The commissural connections are strong within the same cortical fields but also innervate the functionally similar areas (e.g. tonotopic to tonotopic, nontonotopic to nontonotopic, multisensory to multisensory) (Lee and Winer 2008b), while ipsilateral projections are strong between fields in the same region of the ectosylvian gyrus (Lee and Winer 2008a; Bizley et al. 2015). Furthermore, the fields in the core region innervate the adjacent secondary order areas (e.g. A1 to PPF and PSF, AAF to ADF, in ferrets), whereas the terminals of secondary areas are widely distributed across different fields (Bizley et al. 2015). MGBm innervates all areas of AC and seems to provide synchronized activity across cortical areas (Huang and Winer 2000; Jones 2001).

A1 neurons represent acoustic properties of HCTs and MCTs in ways that may be important in segregation and grouping complex tones. Low-frequency resolved harmonics are better represented as a rate-place code than higher harmonics, while lower F_0s are encoded temporally by phase locking to the periodic waveform of the HCTs (Steinschneider et al. 1998; Fishman et al. 2013). As in IC, synchronized responses to the low frequency beats produced by the

interaction between adjacent harmonics in MCTs and double HCTs are also observed (Fishman and Steinschneider 2010; Fishman et al. 2014). This temporal envelope representation is limited to 250 Hz (Kalluri et al. 2008), consistent with the lower upper limit of phase locking in the cortex (Wallace et al. 2002; Miller et al. 2002). Furthermore, a subpopulation of cortical neurons have multi-peaked frequency response areas, enabling them to respond to several harmonics even in the absence of a response to F_0, indicating that they might help fuse HCTs (Sutter and Schreiner 1991; Kadia and Wang 2003). A1 neurons are sensitive to amplitude-modulated sounds, but whether their best modulation frequencies form a periodicity map is controversial (Schulze et al. 2002; Nelken et al. 2008; Langner et al. 2009). In addition, event-related brain potentials in humans have been used to reveal that the perception of mistuned harmonics in complex sounds is associated with early responses, while later responses are elicited when subjects attend to the stimuli (Alain et al. 2001; Alain et al. 2002). Together, these studies highlight the importance of cortical processing in encoding acoustic signals based on their harmonic structure and temporal modulation in ways that may contribute to perceptual grouping and segregation.

Semantic processing is clearly important for understanding human speech. When speech is time reversed, it still sounds speech-like but becomes incomprehensible, although it is still comprehensive when it is flipped every ~50 ms (Saberi and Perrott 1999). The A1 neurons of marmosets show higher spike rates in response to their own normal vocalizations than to time-reversed ones (Wang et al. 1995), whereas the responses of A1 neurons in cats do not distinguish between normal and time-reversed marmoset calls (Wang and Kadia 2001).

However, after training ferrets to discriminate normal marmoset vocalizations, it was found that the temporal discharge patterns of their A1 neurons become more informative about the vocalizations without showing any selectivity in their firing rates for normal calls (Schnupp et al. 2006). Ferret A1 neurons encode temporal patterns of the vocalizations at a time resolution of <40 ms, suggesting that cortical processing has a wider temporal integration window as a readout frame. Furthermore, responses to normal and time-reversed conspecific vocalizations are distinctive in their discharge patterns and consistent between MGB and A1 of guinea pigs, particularly in awake animals (Huetz et al. 2009). These findings suggest that the temporal precision of action potential firing is important for complex sound processing, and that both the thalamus and cortex are involved.

1.5. **Corticothalamic pathways**

In addition to the ascending pathway, there are descending projections from the central to the peripheral system, and this feedback system modulates ascending inputs at almost every stage.

Descending pathways are also characterised by their tonotopic organization (Fig. 1.4). Lemniscal regions target mainly subcortical lemniscal nuclei (MGBv), while non-lemniscal regions project to non-lemniscal nuclei (MGBd) (Winer 2006). A1 also projects to MGBd (Winer et al. 2001). The cerebral cortex has a laminar structure that comprises different cell types functionally organized across its six layers, and corticothalamic and corticocollicular projections have different layers of origin. Corticothalamic projection neurons are found in layer VI (Ojima 1994), whereas corticocollicular

projection neurons occupy layer V (Games and Winer 1988; Winer and Prieto 2001; Bajo and Moore 2005; Bajo et al. 2007). Furthermore, a descending feedforward projection from A1 to MGBd originates in layer V, which is routed via non-primary AC (Rouiller and Welker 1991; Ojima 1994; Bajo et al. 1995; Winer et al. 1999; Bartlett et al. 2000; Llano and Sherman 2008). This connection is referred to as a cortico-thalamo-cortical pathway, and is essential for corticocortical communication and higher level processing of converged inputs. In the lemniscal pathway, descending axons preserve the tonotopic organization (Budinger et al. 2013). Compared to thalamocortical and corticocollicular projections, corticothalamic projections are particularly strong, as is also the case in the visual system (Van Horn et al. 2000; Winer et al. 2001).

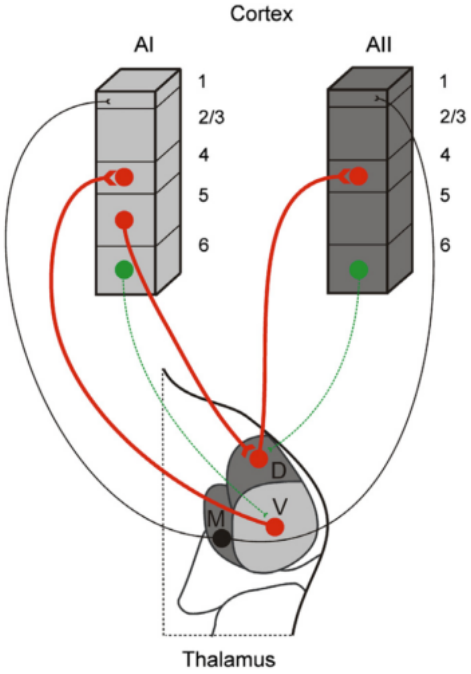

Figure 1.4 Corticothalamic projection neurons.
Red shows thalamocortical feedforward projections, while green is the corticothalamic feedback projection. Black indicates modulatory projection from MGBm. AI, primary auditory cortex; AII, second-order areas; D, M, V, the dorsal, medial and ventral division of MGB. The numbers indicate the cortical layers. (adapted from Lee 2013, figure 1)

In addition to MGBv, corticothalamic feedback projection neurons innervate layer IV and the thalamic reticular nucleus (TRN) (Jones 1975; Stratford et al. 1996). Cortical layer IV is the major thalamic recipient layer, projecting to upper cortical layer II/III (Huang and Winer 2000; Linden and Schreiner 2003). Layer II/III connects to other cortical areas and to layers V and VI, which in turn project to sub-cortical nuclei (Wallace and He 2011). TRN is formed from a sheet of GABAergic cells that surround dorsal and lateral thalamic nuclei (Jones 1975). Together with local and external GABAergic inputs (Winer et al. 1996; Winer and Larue 1996; Huang et al. 1999), this provides inhibition to MGB (Zhang et al. 2008). If the collaterals spread to the adjacent thalamic cells, the corticoreticular pathway could sharpen thalamic receptive fields by lateral inhibition. If the projection is strictly reciprocal, the combination of corticothalamic and corticoreticular pathways could modulate thalamic cells by controlling the gain of these responses. In the somatosensory system, both types of connections are observed (Lam and Sherman 2010). Recent studies suggest that corticothalamic projection neurons in layer VI modulate response gain across cortical layers by recruiting local inhibitory circuits in the visual system (Olsen et al. 2012; Bortone et al. 2014).

Glutamatergic projection neurons in the thalamus are classified into Class 1 and Class 2 based on structural and functional properties, and they are often referred to as driver and modulators, respectively, according to their roles (Sherman and Guillery 2011; Sherman and Guillery 2013). Drivers simply relay the input information to the cortex, while modulators regulate drivers and control how the input is relayed. Corticothalamic feedback projection neurons are

classified as Class 2 modulators, while corticothalamic feedforward neurons are classified as Class 1 drivers (Sherman and Guillery 1998).

Tracer injection results support the morphological characteristics of Class 2 corticothalamic neurons, which have major small distal terminals with thin axons and convergent endings (Rouiller and Welker 1991; Ojima 1994; Bajo et al. 1995; Winer et al. 1999; Bartlett et al. 2000; Llano and Sherman 2008). Large buttons are found in MGBd, which derives from cortical layer V and is distinguished as descending corticothalamic feedforward projections (Rouiller and Welker 1991; Bajo et al. 1995).

Physiological properties also support the notion that corticothalamic feedback neurons are Class 2 modulators. Class 2 afferents activate metabotropic receptors showing paired-pulse facilitation with small excitatory postsynaptic potentials (EPSPs), whereas Class 1 afferents only activate ionotropic receptors showing paired pulse depression with large EPSPs. Corticothalamic inputs from layer VI activate type I metabotropic glutamate receptors (Godwin et al. 1996; Vidnyanszky et al. 1996) and EPSP amplitude increases by repetitive stimulation in thalamic neurons and layer IV (Granseth 2004; Lee and Sherman 2008; Lee and Sherman 2009). Corticothalamic neurons modulate thalamic neurons by affecting their overall excitability, the voltage gated conductance and the synaptic potentials.

1.6. The role of corticothalamic feedback

The possible roles of corticothalamic feedback have been considered in the auditory system as well as other sensory systems (e.g. He 2003; Briggs and Usrey 2008). Generally, two major roles have been proposed. First, the tuning properties of thalamic neurons are re-organized by corticofugal modulation. Second, corticothalamic feedback modulates the firing pattern in a gain control manner. However, compared to growing physiological evidence, the significance of corticothalamic feedback has not been studied yet at the behavioural or perceptual level.

Changes in tuning properties

Stimulation of cortical neurons can alter the response properties of neurons that receive inputs from the ones stimulated (reviewed in Suga 2012). There are three major types of changes. First, when the best frequency (BF, the frequency of sound at which the neuron responds with the highest firing rate) of the thalamic neurons matches that of neurons at the site of cortical stimulation, their frequency tuning is sharpened by augmentation of the response at BF and by inhibition at lower and/or higher frequencies. Then, when a neuron has a different BF from that of the neurons at the site of cortical stimulation, the frequency tuning shifts due to facilitation of the response outside the BF and inhibition at its BF. This is called ‘BF shift’ and classified into two types: ‘centripetal’ and ‘centrifugal’ depending on the direction of the BF shift. Examples are shown in figure 1.5. These three types of changes have been observed in A1 of the Mongolian gerbil (Sakai and Suga 2002), rat (Talwar and Gerstein 2001) and big brown bat (Chowdhury and

Suga 2000; Ma and Suga 2001), in MGBv of mouse (Luo et al. 2011), in CNIC of mouse (Yan and Ehret 2002; Wu and Yan 2007) and big brown bat (Ma and Suga 2001; Zhang and Suga 2005), in CN of mouse (Luo et al. 2008) following cortical focal electric stimulation. Similar changes are also induced by conditioning in MGBv of mouse (Zhang and Yan 2008) and in IC of moustached bat (Gao and Suga 1998), and abolished when AC is inactivated (Zhang and Suga 1997; Zhang and Yan 2008). The direction of the BF shifts (i.e. centripetal or centrifugal) can be reversed by applying agonist and antagonist of inhibitory synaptic transmitter receptors (Ma and Suga 2004) and changes in AC are extended following application of acetylcholine (Ma and Suga 2005). The auditory system of the moustached bat is well developed for echolocation, and sensitivity to a range of acoustic properties, such as duration, frequency modulation and intensity, have been shown to change in a similar manner (e.g. Ma and Suga 2007). Overall, these results suggest that corticofugal projections can modulate thalamic tuning properties and that these effects are controlled by the balance of excitation and inhibition and neuromodulators as a basis for learning induced plasticity.

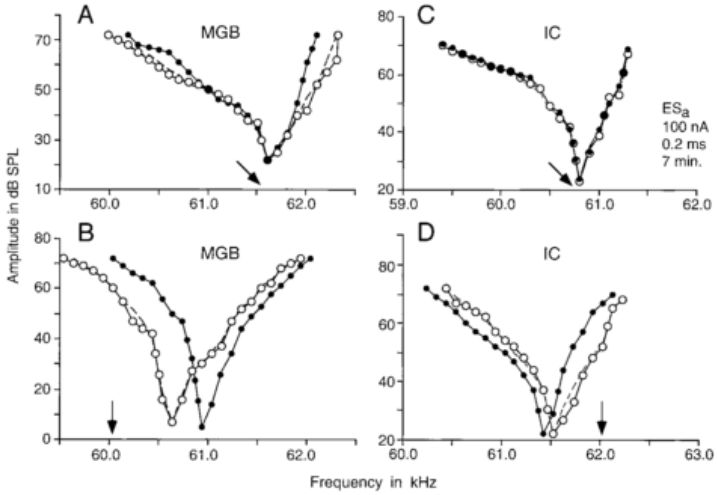

Figure 1.5 Corticofugal modulation
Tuning curve was sharpened when cortical neuron that had the same BF as recorded neuron in MGB (A) and IC (C), whereas it was shifted away from the frequency stimulated when cortical neuron had different BF from recorded neuron in MGB (B) and IC (D). (adapted from Zhang and Suga 2000, figure 5)

Gain control

Thalamocortical neurons have two distinct modes of firing for receiving inputs from IC (reviewed in Sherman 2001; Sherman and Guillery 2013) (Fig. 1.6). One is referred to as 'burst mode', in which the cells are hyperpolarized and de-inactivate voltage-gated T-type Ca^{2+} channels. In this mode, spontaneous firing is low. On the other hand, in 'tonic mode', the cells are depolarized and the firing pattern changes linearly depending on input strength.

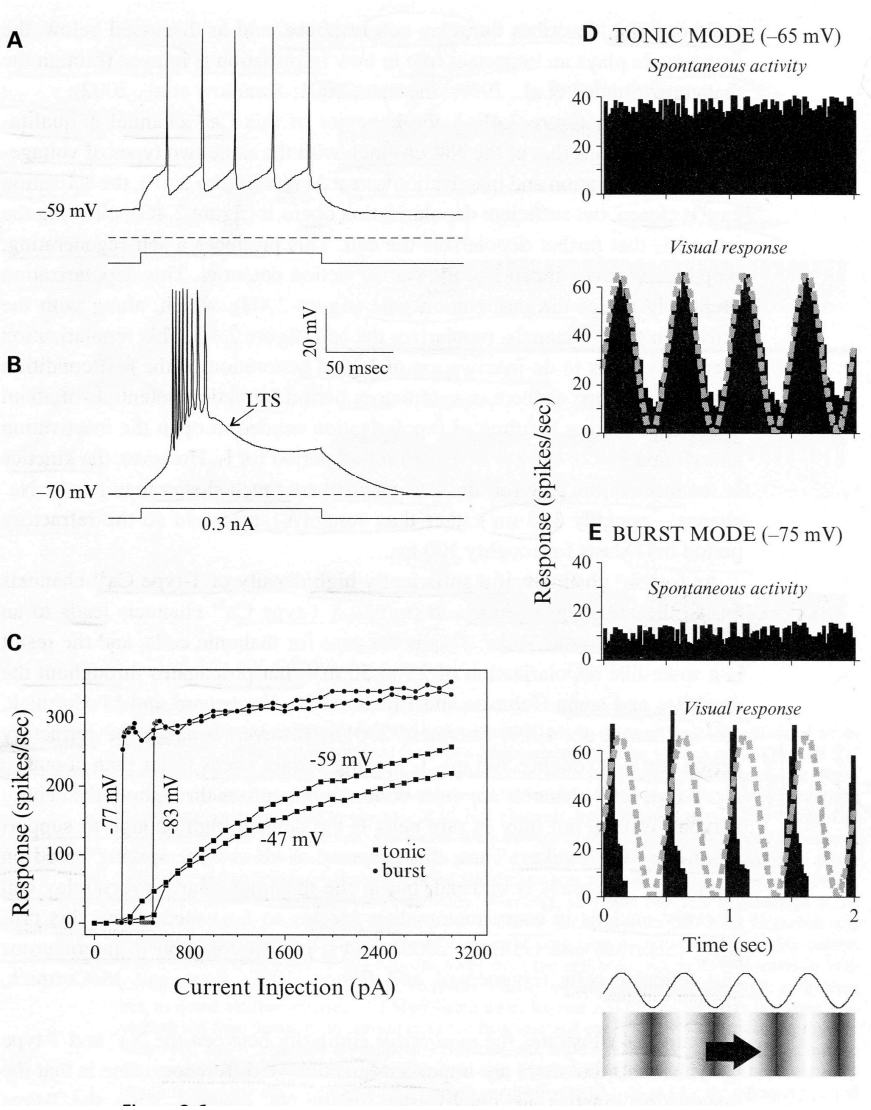

Figure 1.6 Tonic and burst mode
Spikes recorded intracellularly in principal neurons in the cat lateral geniculate nucleus, in an *in vitro* slice preparation (A-C) and in an anesthetized *in vivo* preparation (D, E). Voltage dependent firing is demonstrated by applying current in a relatively depolarized condition (tonic mode, A) or relatively hyperpolarized condition (burst mode, B). (C) Input-output relationship. (D, E) Responses to a drifting sinusoidal grating with the current injection to adjust the membrane potential to -65 mV (tonic mode, D) or -75 mV (burst mode, E). (adapted from Sherman and Guillery 2013, figure 2.6).

A strong facilitatory effect on excitability has been observed in MGBv of cats (Ryugo and Weinberger 1976; Orman and Humphrey 1981; Villa et al. 1991; He 1997) and guinea pigs (He et al. 2002; Yu et al. 2004), suggesting that corticothalamic projection neurons modulate the firing pattern of MGBv neurons. The spontaneous firing rate in MGBv neurons decreases when AC is deactivated (Ryugo and Weinberger 1976; Orman and Humphrey 1981; Villa et al. 1991), while responses are amplified when AC is activated (He 1997; He et al. 2002). MGBv neurons have also been shown to depolarize in response to cortical stimulation (Yu et al. 2004). However, inhibition and hyperpolarization to cortical activation are also observed, suggesting that inhibitory inputs, such as from TRN, also play a key role. A recent study has shown that the facilitatory effect of corticothalamic stimulation is switched to long suppression via TRN inhibition depending on stimulus rate (Crandall et al. 2015), which may explain both excitation and inhibition observed by cortical stimulation.

It has been proposed that the thalamus detects novel stimuli in burst mode (‘wake up call’) and responds more accurately to the stimuli in the tonic mode, when it is receiving corticothalamic feedback (Sherman 2001). This is similar to the theory that TRN works as a searchlight (Crick 1984). Thus, another role of corticothalamic feedback is thought to be a gating function.

Hypothesized roles of A1-MGBv corticothalamic feedback in mistuning detection

I would like to propose two possible roles of A1-MGBv corticothalamic feedback in the discrimination of HCTs and MCTs. First, it will sharpen the receptive fields

of MGBv neurons, facilitating the use of spectral cues to detect mistuned harmonics. In other words, sharper receptive fields may enable the listener to hear out mistuned harmonic more easily. Second, corticothalamic feedback will modulate temporal precision in thalamocortical neurons, enhancing the ability to use temporal cues to detect mistuning. After tones are detected by a 'wake up' call or searchlight (i.e. in burst mode), thalamocortical neurons will be switched into tonic mode by corticothalamic feedback. In this mode, these neurons may represent the envelope of complex tones more accurately by phase locking. This would be not only helpful in detecting MCTs but also important to discriminate speech and vocaliation in complex sound processing, and the importance of corticothalamic feedback was tested in this thesis, motivated by the two possible roles proposed above.

Finally, the ferret, the species used in this study, is a good model for investigating the neural networks in complex sound processing. Numerous behavioural studies have been conducted to investigate both spatial (Kavanagh and Kelly 1987; Nodal et al. 2008; Nodal et al. 2010; Leach et al. 2013; Keating et al. 2013; Keating et al. 2014; Tolnai et al. 2014) and non-spatial (Kalluri et al. 2008; Walker et al. 2009; Yin et al. 2010; Bizley et al. 2013a; Mill et al. 2014; Gold et al. 2015; Town et al. 2015) aspects of hearing. In particular, they are sensitive to low-frequency sounds (Kelly et al. 1986), which makes this species suitable for studying various aspects of pitch perception (Kalluri et al. 2008; Walker et al. 2009; Yin et al. 2010; Bizley et al. 2013b). Moreover, anatomical studies have revealed their auditory pathways and the connectivity (Bajo et al. 2007; Bizley et al. 2007; Bizley et al. 2015), and

physiological studies have investigated neural responses to simple and complex sounds (Kowalski et al. 1995; Nelken et al. 2004; Bizley et al. 2005; Nelken et al. 2008). The growing availability of methods for recording (Fritz et al. 2005; Bizley et al. 2013b) and manipulating (Bajo et al. 2010; Nodal et al. 2012) neural activity during behavioural testing has also led to the ferret becoming a popular model for hearing research.

1.7. **Thesis overview**

In this chapter, a general introduction and literature review were provided. I have described aspects of auditory scene analysis, the processing of complex sounds in the auditory system, the corticothalamic pathway, and the possible roles of corticothalamic feedback to support the purpose of this study.

Chapter 2 is a general methods chapter to describe common procedures used in this thesis, including methods for surgery, electrophysiology, histology and stereology.

Chapter 3 presents the results of a behavioural study using a mistuning detection task. Mistuning detection is thought to be important in auditory scene analysis in humans. Six ferrets were tested for their ability to detect mistuned harmonics using a go/no-go paradigm. The main aim of this study was to validate mistuning detection performance in ferrets. The threshold of detecting mistuned harmonic was found to be 0.8 ± 0.1 Hz, which is comparable to the values reported in other non-human species. Reaction times were dependent on the degree of mistuning, adding to the evidence that they discriminated complex tones using mistuning as a cue.

In Chapter 4, I present the data for recordings in the auditory thalamus. The purpose of this chapter is to examine general response properties of neurons in the auditory thalamus. I show that the functional organization of ferret auditory thalamus is comparable to that of other mammalian species. MGBv neurons were sharply tuned and organized with a tonotopic gradient similar to that previously described in other animal models.

In Chapter 5, I explore how MGBv neurons respond to MCTs. The main focus is to describe spike rate change and distinctive temporal response patterns to different MCTs. Firing rate was greatly changed when the frequency of mistuned harmonic was close to the tuned frequency of the recorded neurons, and phase locked responses to the temporal modulation of MCTs were observed. These represent spectral and temporal cues that could be used in mistuning detection and in line with the previous studies in the IC and A1, support the gradual emergence of complex sound processing at higher levels of the auditory pathway.

Chapter 6 is a behavioural study combined with chromophore-targeted laser photolysis, which enables us to selectively eliminate corticothalamic neurons. It has been suggested that the corticothalamic feedback system sharpens spectral receptive fields of neurons in the thalamus and modulates their temporal precision. The goal of this study was to investigate the effect of corticothalamic lesion on mistuning detection and to explore the role of the A1-MGBv corticothalamic feedback system. The behaviour performance was compared before and after the lesion, and the corticothalamic cell loss was evaluated by histology and stereology.

Chapter 7 is general discussion, which summarizes the results presented in Chapters 3 to 6, and places them in the context of the possible role of

corticothalamic feedback in complex sounds processing. I also highlight future directions for work in this field.

Chapter 2

Methods

This chapter describes common procedures of behavioural testing, surgery, electrophysiology, histology and stereology as well as specific procedures of data analysis for mistuning detection behaviour, thalamic recordings and selective elimination of A1-MGBv corticothalamic pathway.

2.1. **Subjects**

Nineteen female ferrets (*Mustela putorius furo*) sourced from Marshall BioResources (North Rose, NY) were used in this thesis. All experimental procedures were approved by the local ethical review committee and were carried out under license from the UK Home Office.

Animal	Behavioural training	Thalamic recording	Experimental group	Histology
F1204	✔	✔	-	-
F1206	✔	✔	-	-
F1207	✔	✔	-	-
F1224	✔	✔	-	-
F1302	✔	✔	-	Fluorescent
F1303	✔	✔	-	Fluorescent
F1405	✔	✔	-	-
F1418	-	With mistuning	-	Nissl
F1442	-	With mistuning	-	Nissl
F1443	-	With mistuning	-	Nissl
F1205	✔	✔	Corticothalamic lesion	Fluorescent
F1209	✔	✔	Corticothalamic lesion	Fluorescent
F1223	✔	✔	Control	Fluorescent
F1225	✔	✔	Control	Fluorescent
F1325	✔	✔	Control	Fluorescent
F1429	With correction	-	-	-
F1430	With correction	-	Corticothalamic lesion	Fluorescent
F1433	With correction	-	Control	Fluorescent
F1444	With correction	-	Control	Fluorescent

Table 2.1 Procedures performed on each ferret in this thesis.
The table shows procedures applied on nineteen ferrets. Check marks indicate the procedure was performed. 'With correction' indicates that animals were trained for mistuning detection with correction trials (see below for details). Thalamic recordings were performed for different purposes. One was to identify the location of MGBv for injections of microbeads and the other was to investigate responses to complex tones in the auditory thalamus. The latter case is indicated by 'with mistuning' in the table. When the role of corticothalamic feedback was investigated in Chapter 6, the experimental groups are indicated by either 'corticothalamic lesion' or 'control' case in the column. Histology was performed after all the procedures to visualize electrode tracks ('Nissl') or microbeads injection sites and retrogradely labelled cells ('fluorescent'). The grey colour indicates that histology is to be planned.

How each ferret was used is shown in table 2.1. Seven out of nineteen ferrets were used for refining go/no-go behavioural paradigm, recordings in the MGB and chromophore-targeted laser photolysis technique in ferret A1-MGBv pathway. Three other ferrets were used for investigating responses to pure and complex tones in the auditory thalamus in Chapters 4 and 5, and mistuning detection was measured in the remaining nine ferrets. Six of them were used to describe general behavioural trends in mistuning detection in Chapter 3, and eight of them, including five from the six, were used for studying the role of corticothalamic feedback in Chapter 6.

2.2. **Mistuning detection behaviour**

2.2.1. Apparatus

Animals were trained in a custom-built test chamber, 40 cm wide, 45 cm long, and 50 cm high (Fig. 3.1A). On the front side of the chamber were two poke holes each equipped with an infrared sensor and a spout for water delivery. All acoustic stimuli were presented via one loudspeaker (Visaton FRS8, Crewe, UK) mounted above the poke holes at a height of 20 cm from the floor. The behavioural task, data acquisition, and stimulus generation were controlled by personal computers communicating with a system 3 TDT RP2 real-time signal processor (Tucker-Davis Technologies, Alachua FL) using custom-written scripts in MATLAB software (MathWorks, Natick, MA).

2.2.2. Acoustic stimuli

The reference stimulus was a harmonic complex tone (HCT) of 350 ms duration composed of 16 harmonics that started in sine phase with a 400 Hz F_0, smoothed by a 25 ms Hanning window at the beginning and end of each tone to reduce side lobes in the frequency spectrum (Fig. 3.1B, F). The target stimulus was the same complex harmonic tone as the reference except that its 4th harmonic was mistuned (mistuned complex tone, MCT, Fig. 3.1B, G). We produced sets of target stimuli with their 4th harmonic shifted to a higher frequency by varying amounts that ranged from 0.1 to 192 Hz (23 fixed values were chosen based on a logarithmic separation within this range). In the initial training phase, a target stimulus with its 4th harmonic mistuned by 200 Hz was used. Reference and target stimuli were separated by 200 ms silence. All stimuli were generated by an RP2.1 real time processor (TDT) at a sampling rate of 25 kHz.

2.2.3. Behavioural paradigm

The animals were trained by positive reinforcement using water as reward in a go/no-go task. The training schedule comprised blocks of 14 or 5 days of training interspersed with 3 or 2 days off training, respectively. During training blocks animals had access to water only during the twice daily training sessions, and this was supplemented as mash comprising ground food pellets and water if the total daily amount consumed during the sessions was < 60 mL/kg, the average daily consumption measured when ferrets are provided with free access to water. Body weight was measured on a daily basis and compared to individual baseline weights

recorded before the start of each testing block. Water access regulation was suspended if animals lost >10 % of their baseline weight.

Before testing the animals' ability to detect MCTs, they underwent a series of procedural training steps. They were first trained to maintain a nose poke at the trigger spout for an increasing amount of time (0.2 to 2.0 s) before a water reward was delivered at the reward spout. Acoustic stimuli, comprising a pair of identical complex tones, were then introduced for which the animal had to wait before withdrawing from the trigger spout poke hole to get a reward. The animals were next trained to discriminate reference tones from subsequent target tones. They were required to initiate the stimulus presentation by poking their nose at the trigger spout and cease nose poking as soon as they heard a target tone or remain at the trigger spout until the end of the series of reference tones in order to receive a reward (Fig. 3.1A, C). To assist the animals with the initial discrimination, target tones with the 4th harmonic mistuned by 200 Hz (Fig. 3.1B) were presented at 70 dB SPL, whereas the reference tones were presented at 30 dB SPL. This intensity difference was gradually reduced as the animals' performance improved, until all tones were presented at 70 dB SPL. In the mistuning detection test, all stimuli were presented at this level.

The number of reference tones preceding the 2 target tones was randomized from 2 to 6 to reduce the predictability of the timing of the target tones and prevent stereotyped responses. The number of target tones was always two except that the first two animals were tested with 1 to 3 target tones. The probability of trials that comprised reference tones only (i.e. no-go trials; Fig. 1C) was 10 or 20%, in which the number of reference tones was randomized from 3 to

7. In the data analysis, go trials comprising 2 to 4 reference tones plus 2 target tones and no-go trials comprising 4 to 6 reference tones were used. To prevent uneven presentation of the different MCTs within a session, the original set of 23 MCTs was subdivided into 4 blocks, each containing 7 MCTs equally distributed within the set. In each behavioural session, only one of those 4 blocks was tested. For the first four animals, testing was performed for ~15 different degree of mistuning without presenting smaller mistuning (<0.5 Hz). To ensure the animals were attentive at the beginning of each trial, the stimulus presentation started 100 ms after the nose poke at the trigger spout. The duration and therefore number of trials in each session depended on the motivation of the animals, which, in turn, depended on how satiated they were; typically it corresponded to ~100 rewarded trials per session.

After misses (staying at the trigger spout even after the target tones were presented) and early releases (leaving the trigger spout while the reference tones were being presented), a burst of broadband noise was played to provide feedback and signal the lack of reward. Following a miss, a 1-s time-out was given before the animal was able to trigger the next trial. In contrast, a 12-s time-out was used after early releases to reinforce the performance of the animals on trials that required a long waiting time. To reduce the number of early releases, for the last four animals, we increased proportion of no-go trials from 10 to 20 % and introduced correction trials with the same stimulus composition that were presented after early releases. If 1 or 2 successive correction trials were presented, this time-out was shortened to 8-s or 5-s, respectively, and the stimulus composition was reset after 2 consecutive correction trials. One of the characteristics of our

experimental design was that every trial comprised a different number of reference tones from the previous trial, unless it was a correction trial.

2.2.4. Data analysis

For every session, behavioural performance was assessed by the overall correct response rate, defined as correct responses on go trials and correct rejections on no-go trials (i.e. where the animal stayed at the trigger spout). Hit rate (number of correct responses on go trials / total number of go trials) and false alarm (FA) rate (number of trials of incorrect responses on no-go trials / total number of no-go trials) were also calculated. Behavioural data were accumulated over sessions that had FA rates < 0.6 only, a criterion adopted as a measure that the animals were sufficiently motivated to perform the task. This FA rate was computed from all no-go trials. However, we only analysed trials comprising up to 6 tones to correct a general bias toward go responses on the longest trials. Accordingly, only no-go trials comprised of 4 to 6 reference tones that were of equivalent duration to the go-trials were included in the analysis. A minimum between 749 and 2073 trials in total were analysed from each animal, and the resulting FA rate was 0.4. Using signal detection theory (Wickens 2002), a sensitivity index (*d'*) was calculated for each degree of mistuning from the z-transformed hit rate and FA rate according to the formula:

d' = Z(hit rate)-Z(FA rate).

Psychometric functions were derived by fitting *d'* values using unconstrained nonlinear optimization to a cumulative Gaussian distribution:

$$D'(x \mid \alpha, \beta, \mu, \sigma) = \alpha\left(\frac{1}{\sigma\sqrt{2\pi}}\int_{-\infty}^{x} e^{\frac{-(t-\mu)^2}{2\sigma^2}}\,dt\right) + \beta$$

where x is the degree of mistuning (Hz) on a log scale, α and β are constants to rescale the function in the y direction, μ is the mean, and σ the standard deviation. Mistuning values corresponding to a criterion *d'* = 1 were taken as threshold values.

Since post-lesion animals showed fluctuating *d'* values, the sensitivity index (*d'*) was computed using the formula above and psychometric functions were obtained by smoothing the *d'* values based on model-free estimation (Zychaluk and Foster 2009). The weight function was assigned using a triangular kernel function with bandwidth 40:

$$W(i) = 1 - \frac{|x_i - x_{i+1}|}{40} \quad (i = 1, \ldots, m-1)$$

where x_i is mistuning (Hz) at *i*th of *m* stimuli, and d'_{smoothed} was computed by a locally weighted averaging of neighbouring values:

$$d'_{smoothed}(i)$$

$$= \begin{cases} \dfrac{d'_i \times W(i) + d'_{i+1} \times W(i+1)}{W(i) + W(i+1)} & (i = 1) \\ \dfrac{d'_{i-1} \times W(i-1) + d'_i \times W(i) + d'_{i+1} \times W(i+1)}{W(i-1) + W(i) + W(i+1)} & (i > 1, i < m) \\ \dfrac{d'_{i-1} \times W(i-1) + d'_i \times W(i)}{W(i-1) + W(i)} & (i = m) \end{cases}$$

where d'_i is d' value for ith stimulus calculated from the formula above. The thresholds were obtained as the first point to cross the criterion $d' = 1$. The estimated thresholds were not significantly different from those obtained by fitting to a cumulative Gaussian distribution.

In order to understand the effect of different degrees of mistuning, the values used were grouped into two categories, small (<3 Hz) and large (3 to 8 Hz), based on the shape of the psychometric functions, which indicated that the animals' maximal performance was achieved for mistuning values >3 Hz (Fig. 3.2A). To balance the number of trials in each group, hit rates for large mistuning values were calculated from trials in which the degree of mistuning lay between 3 and 8 Hz. For the first two animals, small (<8 Hz) and large (8 to 192 Hz) categories were used instead based on their psychometric functions.

Mistuning reaction times were fitted using maximum likelihood estimation of an exponentially modified Gaussian distribution (EMG):

$$\text{EMG}(x \mid \mu, \sigma, \tau) = \frac{1}{2\tau} e^{\left(\frac{\mu - x}{\tau} + \frac{\sigma^2}{2\tau^2}\right)} \left(1 + \frac{2}{\sqrt{\pi}} \int_0^{\frac{x-\mu}{\sigma} - \frac{\sigma}{\sqrt{2}\tau}} e^{-t^2} dt\right)$$

where μ is the estimated mean of the Gaussian component, σ is the estimated standard deviation of the Gaussian component, and τ is the estimated mean of the exponential component (Lacouture and Cousineau, 2008; https://github.com/bramzandbelt/exgauss). Because the histograms of reaction time were not normally distributed and showed two peaks corresponding to the two target tones presented, a double ex-Gaussian distribution (double-EMG) was defined as below, by combining two EMGs linearly using a probability α to represent the relative contribution of the two distributions corresponding to the two target tones in a go trial:

$$\text{double-EMG} = \alpha EMG(x|\mu1,\sigma1,\tau1)+(1-\alpha)EMG(x|\mu2,\sigma2,\tau2)$$

where μ1, σ1 and τ1 represent three constants for the first EMG, and μ2, σ2 and τ2 are three constants for the second EMG. The best fit model was then obtained based on the corrected Akaike's Information Criterion (AIC):

$$AIC = 2k-2\ln(L)+2k(k+1)/(n-k-1)$$

where k is the number of parameters in the model, ln(L) the log-likelihood function for the model, and n is the sample size. In order to examine the effect of degree of mistuning, fitting of reaction times was performed for small and large mistuning groups and seven parameters were obtained in each case, while parameters for overall performance were obtained using all go trials with correct responses.

In order to investigate responses bias, we calculated:

$$\lambda_{\text{center}} = -\frac{1}{2} \times [\text{Z(hit rate)} + \text{Z(FA rate)}].$$

In order to understand the effect of degree of mistuning and trial length on hit and FA rates, regression lines were fitted to the plots of hit and FA rates as a function of trial length by least squares fitting ($R^2 > 0.83$), and correlation coefficients were calculated between trial length and hit or FA rates. Furthermore, a two-way ANOVA was performed on *d'* values to examine the interaction of degree of mistuning and trial length, and Tukey-Kramer post hoc tests were performed for multiple comparisons. Parameter values obtained from reaction time fitting across different degrees of mistuning were compared using paired *t*-tests between small and large mistuning groups.

Paired *t*-tests were performed to compare thresholds between different psychometric function fittings, and pre- and post-laser period. *T*-tests were used to compare performance for pre- and post-injection of microbeads, as well as differences between *d'* values and thresholds between pre- and post-laser period. A two-way ANOVA was performed on reaction time as a function of procedure groups (corticothalamic lesion and controls) and two mistuning groups. Multiple comparisons were conducted using Tukey-Kramer tests for each procedure group if significant differences were first revealed by the one-way ANOVA.

2.3. Surgical procedures

2.3.1. Thalamic recording

Anaesthesia was induced with a single intramuscular injection of medetomidine hydrochloride (Domitor, 0.022 mg/kg body weight, Orion Pharma, Espoo, Finland) and ketamine hydrochloride (Narketan10, 5 mg/kg, Vetoquinol, Buckingham, UK) and maintained with an intravenous infusion (3-4 mL/h) of medetomidine hydrochloride (Domitor, 0.022 mg/kg/h) and ketamine hydrochloride (Narketan10, 5 mg/kg/h) in 0.9% saline solution supplemented with 5% glucose. Atropine sulphate (Atrocare, 0.06 mg/kg, s.c., Animalcare Ltd., York, UK) and dexamethasone (Dexadreson, 0.5 mg/kg, s.c., Intervet UK Ltd., Milton Keynes, UK) were administered to minimize pulmonary secretions and prevent cerebral oedema, respectively. Doxapram hydrochloride (Dopram-V Injection, 4 mg/kg, s.c., Pfizer, Surrey, UK) was administered to maintain respiratory rate. Perioperative analgesia was provided with buprenorphine hydrochloride (Vetergesic, 0.01 mg/kg, s.c., Sogeval UK Ltd., York, UK) and meloxicam (Metacam, 0.2 mg/kg, s.c., Boehringer Ingelheim, Germany). Depth of anaesthesia, respiratory rate, ECG and end-tidal CO_2 were monitored and maintained throughout the experiment. Temperature was monitored using a rectal probe, and maintained at 38 °C using a forced-air warming system (Bair Hugger, 3M Health Care, St. Paul, MN).

The ferret was mounted in a sterotaxic frame and its eyes were protected with a carmomer liquid eye gel (Viscotears, Alcon Laboratories (UK) Ltd., Surrey, UK). The skull was exposed and a stainless steel bar was attached above the mid-sagittal ridge using dental cement. After craniotomies were made, animals

were moved to an anechoic chamber. The dura was removed, and single or double shank Michigan electrodes (Neuronexus, Ann Arbor, MI) with 16 or 16×2 recording sites spaced at 100 μm intervals were inserted 1.8-2.5 mm anterior to the caudal end of the ectosylvian gyrus and 3.9-4.7 mm lateral from the midline. The electrode was slowly advanced perpendicularly until the responses to a set of light and broadband noise stimuli were observed and sites responding exclusively to auditory stimuli were found. In order to protect the surface and improve recording stability, 1.5 % agar solution or silicon oil (viscosity 50 cSt, 378356, Sigma-Aldrich, St Louis, MO) was applied.

2.3.2. Recovery surgery

Anaesthesia was induced with a single intramuscular injection of medetomidine hydrochloride (Domitor, 0.022 mg/kg) and ketamine hydrochloride (Narketan10, 5 mg/kg), and maintained with Isoflurane (ISoFlo, 2%, Abbott Laboratories Ltd., Maidenhead, UK, administered in 1 L of O_2 through a endotracheal cannula). An intravenous infusion (3-4 mL/h) of 0.9% saline solution supplemented with 5% glucose was used to maintain body fluids and the balance of electrolytes, and amoxicillin and clavulanic acid (Co-amoxiclav, 20 mg/kg, i.v., Wockhardt UK Ltd., Wrexham, UK) were administrated through the IV line every 2 hours to prevent infections. Once animals were stabilized, atipamezole hydrochloride (Antisedan, 0.5 mg/kg, s.c., Orion Pharma, Espoo, Finland) was administered. Other medications and monitoring procedures followed those described for thalamic recordings. For postoperative analgesia, buprenorphine hydrochloride (Vetergesic, 0.01 mg/kg, s.c.) was administrated twice a day for two days. Amoxicillin and

clavulanic acid (Synulox, 20 mg/kg, s.c., Pfizer, Surrey, UK) and meloxicam (Metacam, 0.1 mg/kg, oral, Boehringer Ingelheim, Germany) were administered for five days as antibiotic and nonsteroidal anti-inflammatory drug, respectively.

2.3.2.1. Injection of microbeads

Conjugated microbeads (see Appendix) were injected in the thalamus of anaesthetised ferrets. After exposing the skull, a 5 mm^2 craniotomy was performed centred at ~2.0 mm from the caudal end of the ectosylvian gyrus and 4.5-5.0 mm lateral from the midline for both hemispheres. Thalamic recordings were conducted to identify the position of MGBv on both sides in the first set of five animals and only on the left side in the second set of seven animals. The stereotaxic coordinates established from these experiments were used for the last set of four animals without conducting recordings. Pressure injections of conjugated microbeads were made with a microinjector (Nanoject II, Drummond Scientific, Broomall, PA) bilaterally in the left and right thalamus using a glass micropipette with a 15–30-µm tip diameter. Four to five individual injections of 18.4 nL were made in each of the penetrations at a depth of 6 to 9 mm below the cortical surface.

2.3.2.2. Laser illumination

After 3–4 weeks, during which pre-laser data in the mistuning detection test were collected, animals were again anaesthetised with Isoflurane using a recovery surgery procedure and the left and right middle MEG were exposed and illuminated with a 670 nm wavelength near-infrared light from a 300 mW laser diode (OPTC 5M-G25-60sMA) (Flatbeam-Laser 670, Schäfter + Kirchhoff,

Hamburg, Germany). The laser light was adjusted with beam-shaping optics to create a 1.35 mm spot focused at the level of layer VI, ~1 mm from the pial surface (working distance 20.71 mm). The centre of the spot was always placed in the centre of the MEG, where A1 is located. The laser intensity was increased to 280 mW and maintained for 10 minutes.

2.4. **Electrophysiology**

2.4.1. Stimulus presentation

Stimulus generation and data acquisition were controlled by computers using BrainWare program (Tucker-Davis Technologies) running customized MATLAB scripts (MathWorks), which communicated with system 3 TDT RP2 and RX5 real-time signal processors (Tucker-Davis Technologies). All auditory stimuli were delivered bilaterally using Panasonic headphone drivers (RPHV297, Panasonic, Bracknell, UK) with an inverse filter generated by closed field calibrations using an 1/8-inch condenser microphone (Type4138, Bruel and Kjær, Naerum, Denmark). Visual stimulus was delivered from an LED (2.7 V light amplitude, 20 mA, amber, 12.7 mm), located at 0° in front of the animal's head.

2.4.2. Identification of MGBv

A set of light and broadband noise (BBN) stimuli was used for searching for and identifying visual and auditory thalamus. BBN bursts at 80-90 dB SPL with or without light stimulus was presented for identifying acoustically and/or visually driven neural activity during recordings. When units appeared to be responsive, the

complete set of stimuli was pseudorandomly presented. In the stimulus set, light and BBN duration was 100 ms and sound attenuation was varied between 50 and 90 dB SPL in 10 dB steps. Each stimulus was presented 20 times, and the sweeplength was 1000 ms. Once acoustically-responsive units were identified on the basis of post stimulus time histograms (PSTHs) and raster plots, a set of 26 pure tones was presented for identifying the tonotopic organization of MGBv. The tones were composed of different frequencies and intensities, ranging from 0.1 to 32 kHz in one forth octave steps, 100 ms duration with 5 ms cosine ramps and intensity levels were varied between 0 and 80 dB SPL in 10 dB increments. Each frequency-level combination was presented pseudorandomly ≥5 times at a rate of once per second. The electrodes were moved deeper by 0.1-0.2 mm based on the observed responses during recordings.

2.4.3. Data processing

Manual spike sorting was performed offline in BrainWare on the basis of different spike features (e.g. amplitude, width and area), and all the units were analysed as multi-unit since the purpose of study is to investigate the overall responses in auditory thalamus. However, automated k-means clustering performed in some of the multi-units suggested that single units were recorded in most of the cases. The spike timing data were exported as binary data for further analysis in MATLAB.

2.4.4. Analysis of general responses properties

Only the data whose spike counts in a 150-ms window following stimulus presentation were significantly different from the spike counts in the same duration

window at the end of the sweep were analysed (paired *t*-test, $P < 0.01$). Some units showed inhibitory responses, and those were not included in the following analysis. Response windows were defined as follows: onset response, 1-50 ms after stimulus onset; sustained response, 51-100 ms after stimulus onset; offset response, 1-50 ms after stimulus offset. Spontaneous activity was measured from a 50 ms window at the end of the sweep. Paired *t*-tests were performed to analyse responses in each of the response windows, comparing with the activity in the spontaneous window ($P < 0.01$). Raster plots were obtained by showing the timing of each spike with a black dot for each stimulus presentation on the horizontal axis. Pooled PSTHs were obtained by summing spike counts per bin (1 ms) across stimulus repetitions. For the analysis of response to pure tones, PSTHs was obtained by pooling only responses to unit CF ± 0.25 octaves above 40 dB SPL.

The response patterns were classified into 5 types following previous studies in the auditory thalamus (Calford and Webster 1981; Calford 1983) and auditory cortex (Bizley et al. 2005; Walker et al. 2011). Peak response latencies were computed as the time in ms until the highest spike rate was driven in the pooled response, and minimum response latencies were computed as the time until the spike rate first exceeded a criterion defined as 20 % of the difference between peak and mean spontaneous firing rates (Bizley et al. 2005).

Frequency response areas (FRAs) were determined by summing activity in respective response windows for all combinations of level and frequency. Tuning curves were constructed using mean spontaneous rate plus 20% of the peak spike rate as a response criterion (Sutter and Schreiner 1991; Bizley et al. 2005). Thresholds (lowest amplitude in dB SPL that evoked a significant response) and

characteristic frequency (CF), defined as the frequency that showed a response at this threshold, were calculated. Q10 (CF divided by the bandwidth at 10 dB above threshold) was further extracted from FRAs of each unit.

Since response latencies were not normally distributed, Kruskal-Wallis test was performed for comparing the values among three divisions in MGB and response patterns. Tukey-Kramer post hoc tests were performed for multiple comparisons. For the comparison between responses in BBN and pure tones, Wilcoxon rank sum test was used.

2.4.5. Analysis of responses to complex tones

Stimulus

A set of complex tones was used for investigating responses to MCTs in the auditory thalamus. HCTs comprised 16 harmonics. The F_0s used were 200, 400 and 800 Hz. For MCTs, the 2^{nd}, 4^{th} or 8^{th} harmonic was shifted to a higher frequency by 0.05, 0.2, 0.8, 3 or 12% (e.g. Fig. 5.1). The sound attenuation was varied between 40 and 90 dB SPL in 10 dB steps, and each tone was presented pseudorandomly 5 to 10 times with a tone duration of 350 ms. The complex tones were smoothed by a 25 ms Hanning window at the beginning and end to reduce side lobes in the frequency spectrum.

Data analysis

The responses properties to complex tones were analysed for the units in the MGBv that presented sharp tuning curves to pure tones. Only units whose spike

counts in a 400 ms window following stimulus presentation were significantly different from the spike counts in the same duration window at the end of sweep were considered to be responsive to complex tones (paired *t*-test, $P < 0.01$). Response patterns were classified using the same 5 types for BBN and pure tones, although response windows were adjusted for complex tone duration (Onset, 1-50 ms; sustained 51-350 ms; offset 351-400 ms).

Firing rate

Firing rates were computed for each stimulus condition during the tone presentation, pooling all responses for a complex tone defined by F_0 (200, 400 or 800 Hz), mistuned harmonic position (2^{nd}, 4^{th}, 8^{th}, or no shift if it is a HCT) and the degree of mistuning (0, 0.05, 0.2, 0.8, 3 or 12%). A one-way ANOVA was used to compare the firing rates of HCTs with 200, 400 or 800 Hz F_0. To exclude individual variability, the difference of firing rate between MCTs and HCTs were further calculated.

When the spectral distance between the frequency of mistuned harmonics and unit CF was < 0.7 octaves (Fig. 5.3A), a repeated measures ANOVA was performed to investigate the effect of degree of mistuning and the interaction with F_0 and mistuned harmonic position on the difference of firing rate between MCTs and HCTs. The Tukey-Kramer test was used as a post hoc test.

To investigate the effect of spectral distance between the frequency of mistuned harmonics and unit CFs on firing rate, responses were categorised into three groups (Fig. 5.6A). When the spectral distance between the frequency of mistuned harmonics and unit CF is less than 0.7 octaves, it was grouped as ‘Shift at

CF' (Group 1). If the frequency of mistuned harmonic is > 0.7 octaves *below* CF, they were grouped as 'Shift at > 0.7 Oct *below* CF' (Group 2). If it is > 0.7 octaves *above* CF, responses were grouped as 'Shift at > 0.7 Oct *above* CF' (Group 3). A repeated measures ANOVA was performed to examine the effect of degree of mistuning with the interaction of spectral distance and F_0 on the difference of firing rate between MCTs and HCTs. The Tukey-Kramer test was used as a post hoc test.

Temporal response pattern

PSTHs were obtained for the units with sustained responses (51 to 350 ms from tone onset) to look for temporal patterns in the response. After excluding the first 50 ms onset response, vector strength (Goldberg and Brown 1969) was computed as a Fourier analysis.

$$R_T = \frac{1}{n}\sqrt{x^2 + y^2},\ x = \sum_{i=1}^{n} \cos\theta_i\ , y = \sum_{i=1}^{n} \sin\theta_i\ ,\ \theta_i = 2\pi\frac{t_i}{T}$$

In the formulae, n is the total number of spikes, t_i is the time of spike occurrence, and T is a period (6.6 to 488.3 Hz in 3.3 Hz step). This is known as synchronization index (Young and Sachs 1979), which is the values of discrete Fourier transform divided by the mean firing rate. Frequencies lower than 3.3 Hz were excluded from this analysis since the 300 ms window did not allow analysis of components lower than that. Statistical significance was evaluated using Rayleigh statistics, $2nR^2$, (Lu and Wang 2000).The criterion used was $2nR^2$ >13.8, which corresponds to $P < 0.001$ for Rayleigh test (Mardia and Jupp 2000). Estimated phase locked periodicities, *F_0*, *Beating, Mistuning* and *Interaction*, were

computed for each MCT (see Appendix Table A.1). F_0 was defined as the frequency of the F_0 of the stimuli, and the degree of mistuning was changed into hertz as *Mistuning*:

$$Mistuning\ (\text{Hz}) = \frac{\text{degree of mistuning (\%)}}{100} \times F0 \times \text{mistuned harmonic position}$$

Beating was computed from the frequencies of mistuned harmonic and next higher harmonic based on the F_0 and mistuned harmonic position according to the formula:

$$Beating\ (\text{Hz}) = F0\times(\text{mistuned harmonic position} + 1) - (F0\times\text{mistuned harmonic position} + Mistuning)$$

Thus, *Mistuning* can be calculated as the difference of F_0 and *Beating*:

Mistuning (Hz) = F_0 (Hz) – *Beating* (Hz)

Interaction was calculated as the frequency difference of *Beating* and *Mistuning* according to the formula:

Interaction (Hz) = *Beating* (Hz) – *Mistuning* (Hz)

2.5. Histology and stereology

2.5.1. Tissue processing

Animals were perfused transcardially with 0.5 L 0.9 % saline solution (wt/vol) and 1L 4% paraformaldehyde (wt/vol) in 0.1 M phosphate buffer (PB), pH 7.4, after sedation with medetomidine hydrochloride (Domitor, 0.022 mg/kg, im) followed by overdosing with pentobarbital sodium (Euthatal, 2 ml of 200 mg/ml, ip, Merial Animal Health, Harlow, UK). The brain was dissected from the skull and post-fixed with the same fixative. After 2-3 days, the fixative was replaced by 30 % sucrose in 0.1 M PB. Coronal sections were obtained using a cryotome (Leica SM2000 R sliding microtome, Leica Biosystems, Milton Keynes, UK) with a thickness 45-50 μm (see below) and mounted on double subbed slides for Nissl staining and florescent investigation. The slides had been coated twice by 1.4 % gelatine solution (wt/vol) supplemented with 0.05 % chrome alum (chromium(III) potassium sulphate 12 hydrate, 2775845, BDH Laboratory Supplies, Poole, UK).

2.5.2. Data analysis

2.5.2.1. Electrode tracks

Brain sections were prepared with the thickness 50 μm, and all the sections that included the thalamus were stained for Nissl substance (see Appendix). The positions of the recording electrodes were investigated under the microscope, and photographs were taken using a Leica DMR microscope (Leica Microsystems,

Milton Keynes, UK) with a digital camera (Microfire, Optronics UK, Milton Keynes, UK).

2.5.2.2. Evaluation of corticothalamic cell loss

Fluorescent investigation and NeuN immunostaining were performed after all the behavioural testing was completed. The aim was to identify the microbeads injection sites and to quantify the number of retrogradely labelled cells in the auditory system. Stereological analysis was conducted using brain sections with NeuN immunostaining to estimate the cell density in layer VI of auditory cortex (AC).

Brain sections were prepared with the thickness 45 μm, and five sets were made by distributing every fifth section into one set. Two of the sets were used for fluorescent inspection of microbeads injection sites, and a set was used for evaluating the cell density in AC. The rest was kept for Nissl staining and backup.

Slides with brain sections, which had fluorescent signal, were dehydrated in 100 % Ethanol for 3 min and 100 % Xylane for 2 min three times. They were then cover-slipped using toluene based mounting medium (HARLECO Krystalon, EMD Chemicals Inc., Gibbstown NJ). A fluorescent microscope (Leica DMRD, Leica Microsystems) was used to identify the microbeads injection sites in the brain, and the number and distribution of retrogradely labelled flourescent cells in the auditory cortex were examined. Photographs were obtained using a Leica DMR microscope, fitted with filters for fluorescence (448 nm or 530 nm light emission for green and red, respectively), and a digital camera (Microfire) and edited in

Photoshop (Version CS, Adobe Systems, San Jose CA) for laying on top of the pictures taken under visible light without the filters.

Unbiased stereological estimation of number of neurons and volumes of cortical layer VI were performed using the optical fractionator probe with StereoInvestigator (Version11, MBF Bioscience, Williston VT). A set of brain sections was stained using NeuN (see Appendix). The population size was estimated by setting the parameters to obtain a coefficient of error of <0.05. To investigate the effect of lesion procedure and hemispheric differences on the three auditory regions of the MEG, a repeated measures ANOVA was performed with Scheffé post hoc tests. For the multiple comparisons of relative layer VI cell density in auditory cortex, the Tukey-Kramer test was used.

Chapter 3

Mistuning detection performance in ferrets

3.1. Abstract

The harmonic structure of sounds is an important grouping cue in auditory scene analysis. In this chapter, we measured the ability of ferrets, a species increasingly used in auditory research, to detect mistuned harmonics using a go/no-go task paradigm. Complex tones composed of 16 harmonics with a 400 Hz fundamental frequency (F_0) were presented as a reference tone versus a target sound that consisted of the same reference complex tone but with a mistuned 4th harmonic (shifted to a higher frequency, so that it was no longer an integer multiple of the F_0). Psychometric functions plotting sensitivity as a function of degree of mistuning (spectral distance of the mistuned 4th harmonic) were used to evaluate behavioural performance using signal detection theory. The mean (± sem) threshold for mistuning detection across animals was 0.8 ± 0.1 Hz, which is comparable to the values reported in other animal species. Reaction times were not normally distributed and were fitted using a double ex-Gaussian distribution. We found that sensitivity indices and reaction times were dependent on the degree of mistuning. Together, these data indicate that ferrets can discriminate complex tones using

harmonic mistuning as a cue, providing a basis for investigation of the neural basis for the perception of complex sounds in this species.

3.2. Introduction

Complex tones are abundant in naturalistic environments. For example, they are part of animal vocalizations, human speech and music. Consequently, the ability to discriminate and segregate them plays a fundamental part in auditory scene analysis (Bregman, 1990). Harmonicity is one of the most important cues in segregation and grouping of simultaneous sounds. Harmonic complex tones (HCTs), which are composed of harmonics that are integer multiples of the fundamental frequency (F_0) are usually heard as a whole entity rather than as individual sounds with different frequencies. In contrast to HCTs, inharmonic or mistuned complex tones (MCTs) comprise different frequency components or partials that are not all harmonically related. In human listeners, unrelated partials can be heard to 'pop out' when their frequencies are close to resolved low harmonics, and as rough 'beats' when they are close to unresolved higher harmonics (Moore et al. 1985; Hartmann et al. 1990).

Because of the way acoustic signals, such as speech, change rapidly over time, another important source of information for scene analysis is provided by the temporal fine structure of sounds (e.g. Moore 2008). Insertion of a mistuned harmonic in a HCT alters both the envelope and temporal fine structure of the HCT, providing temporal cues in addition to spectral cues that could help in its detection. Psychophysical and modelling studies have attempted to identify the relative contributions of these cues in the perception of complex tones (Goldstein 1973;

Terhardt 1974; Houtsma and Smurzynski 1990). Furthermore, neural responses to harmonic and mistuned complex tones have been investigated in various animal species, showing enhanced responses and phase locking to MCTs and supporting psychoacoustic results at physiological levels (Sinex et al. 2002; Sinex et al. 2005; Sinex 2008; Fishman and Steinschneider 2010; Fishman et al. 2013; Fishman et al. 2014).

Mistuning detection in harmonically complex stimuli has been measured behaviourally in several animal species, including gerbils (Klinge and Klump 2009; Klinge and Klump 2010), zebra finches and budgerigars (Lohr and Dooling 1998). Interestingly, these species showed substantially better thresholds than humans, raising questions about whether the same neural mechanisms are involved. In this chapter, we have developed a go/no-go task design in ferrets, for the first time in this species, to investigate the detection of mistuning in complex tones. Using psychometric analyses to quantify their ability to detect a mistuned harmonic in an otherwise harmonic complex, we found that detection thresholds were comparable to those reported in other animal species.

3.3. **Results**

Mistuning detection sensitivity

Six ferrets were tested for their ability to detect a mistuned harmonic from HCTs using a go/no-go task (Fig. 3.1). Animals were trained to report when the target MCTs were presented. We found that ferrets are able to discriminate MCTs from HCTs and that the relationship between the sensitivity index, *d'*, and the degree of mistuning followed a cumulative Gaussian distribution (Fig. 3.2A). The maximal performance (indicated by the asymptote in the *d'* values) was obtained for mistuning values > 3 Hz, with a mean (± sem) threshold of 0.8 ± 0.1 Hz obtained from a criterion of *d'* = 1. The psychometric functions of individual animals showed similar trends, and their thresholds varied between 0.4 and 1.2 Hz.

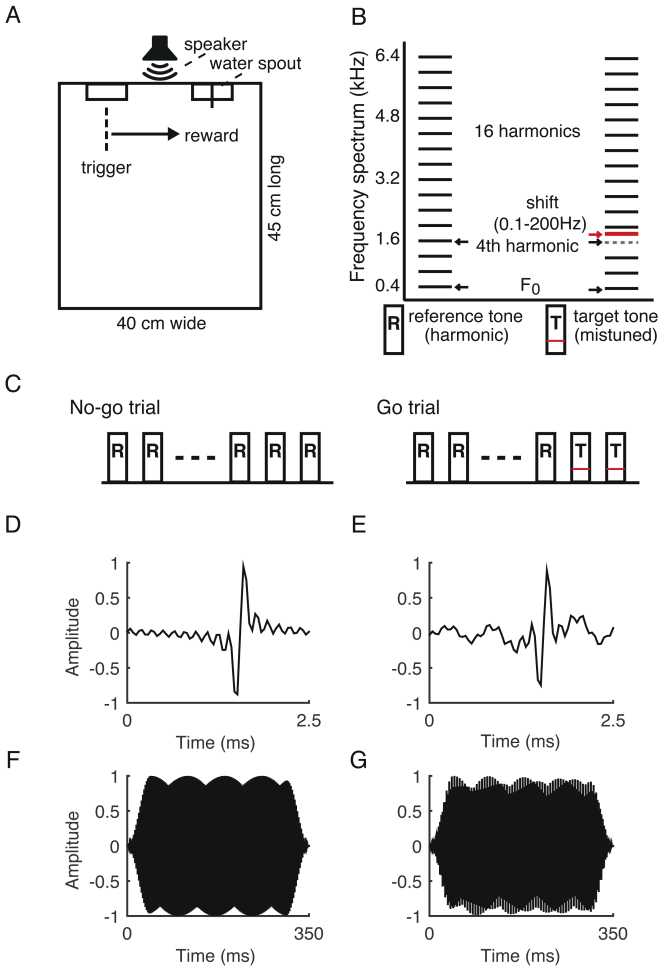

Figure 3.1 Experimental design.
(A) Behavioural test chamber (40 cm wide, 45 cm long and 50 cm high). A loudspeaker was mounted at the centre of the front side at a height of 20 cm between two water spouts, referred as trigger (left) and reward (right) spouts. (B) The reference tone was a harmonic complex tone composed of 16 harmonics with a 400 Hz F0. The target tone included a mistuned 4th harmonic component shifted to a higher frequency by 0.1 to 200 Hz. (C) No-go trials comprised 3-7 reference tones, whereas go trials comprised 2-6 reference tones followed by 2 target tones. Only data from trials comprising 4 to 6 tones (4-6 reference tones in no-go trials and 2-4 reference tones plus 2 target tones in go trials) were used to measure mistuning detection (see text). (D, E) Envelopes of the reference tone (D) and a target tone with a 192 Hz shift in the 4th harmonic (E) for one cycle of F0 (2.5 ms). (F, G) Envelopes of the reference tone (F) and the same target tone (G) for the whole tone duration of 350 ms with a 25 ms Hanning ramp at the onset and offset of tone.

Response bias was examined by calculating and plotting λ_{center} as a function of mistuning (Fig. 3.2B). As λ_{center} estimates a shift of decision criterion from a non-biased point, the value of zero represents the point without any bias. It was expected that the values of λ_{center} would be around zero above the mistuning threshold, and be positive below the threshold as the hit rates should be lower than the false alarm (FA) rates (see Chapter 2 for detail). In fact, we found that λ_{center} for each mistuning value above the threshold of ~0.8 Hz was negative, indicating that the animals were biased to make go responses. This tendency to move toward the reward spout is perhaps not surprising, given that no-go trials comprised only 10-20% of all trials and that it is relatively difficult to train inquisitive animals like ferrets to wait at the same location.

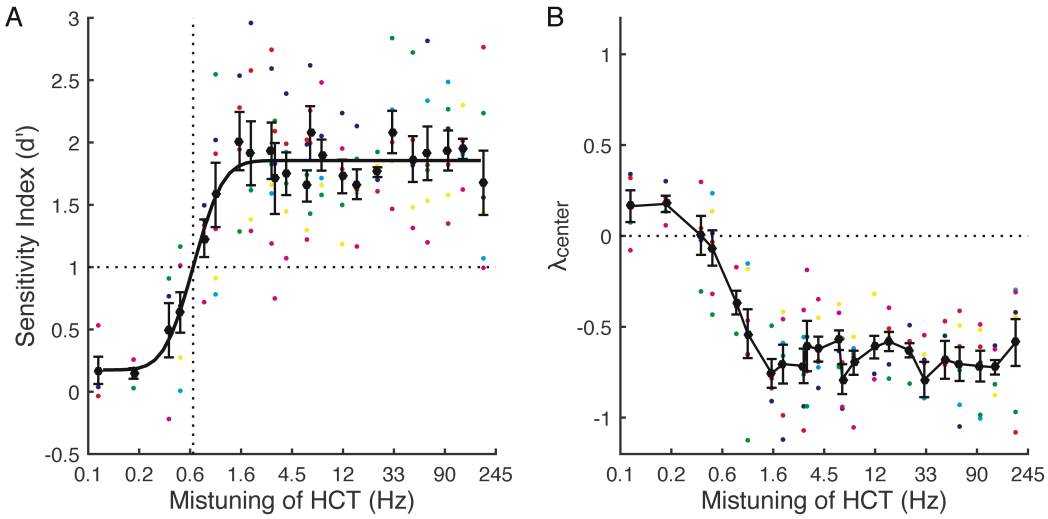

Figure 3.2 Psychometric function for mistuning detection and response bias.
Large black circles represent the mean (± sem) across all animals (n=6), while different colours represent the values for individual animals. (A) *d'* values are plotted as a function of mistuning (on a log scale) of the 4th harmonic of a harmonic complex tone (HCT). A cumulative Gaussian distribution was used to fit the psychometric function. The vertical dotted line indicates the mean threshold for the ferrets used in this study using a criterion of *d'* = 1. (B) The response bias measure λ_{center} as a function of mistuning. The horizontal dotted line indicates the value for no bias.

Sensitivity depends on the degree of mistuning and is independent of waiting time

To investigate the effect on the animals' performance of the degree of mistuning and waiting time at the trigger spout, as determined by the number of reference tones on each trial, hit rate, FA rate and *d'* values were calculated for each trial duration. The bias towards go responses observed above may reflect a tendency of the animals to respond quickly after the onset of the first target tones, resulting in a higher FA rate for trials that require longer waiting times. The 23 different MCTs were divided into two groups according to the shape of the psychometric functions while balancing the number of trials in each case (small: < 3 Hz; large: 3 to 8 Hz). To examine the effect of waiting time in go and no-go trials in parallel, trial length was divided into short, medium and long groups for go trials composed of 2 to 4 reference tones and no-go trials with 4 to 6 reference tones (waiting time ~2.3s, ~2.85s, ~3.4s).

Hit and FA rates increased as trial length increased and were significantly correlated with trial length within these groups (for each group; $R > 0.63$, $P < 0.01$). *d'* values varied with the degree of mistuning (two-way ANOVA; $F_{(1, 30)} = 19.7$, $P = 0.0001$), but not with trial length, and no interaction between these parameters was detected (trial length; $F_{(2, 30)} = 1.29$, $P = 0.29$, degree of mistuning × trial length; $F_{(2, 30)} = 0.5$, $P = 0.6$).

Reaction time was dependent on the degree of mistuning

Reaction time was calculated from go trials on which correct responses were made as the time from the first target tone onset until the animal ceased contact with the

trigger spout. The histograms of reaction time were not normally distributed and showed two peaks corresponding to the two target tones presented (Fig. 3.3). In previous studies, a non-normal distribution of reaction times has been fitted using an ex-Gaussian function (Lacouture and Cousineau 2008). In this study, two ex-Gaussian distributions (double-EMG) were combined linearly with the probability of responding representing the contribution of each.

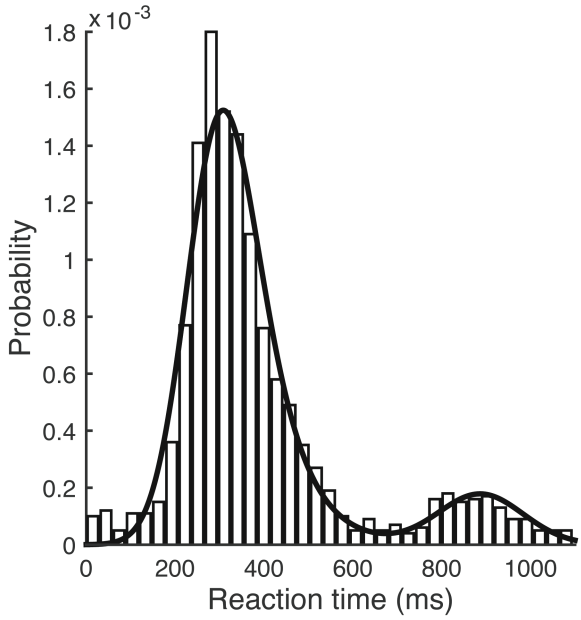

Figure 3.3 Fitting of reaction time.
Fitting of reaction time to the whole dataset using a double ex-Gaussian distribution to account for the non-normal distribution of these data. We combined two ex-Gaussian distributions, with the probability of the first peak defined by the value α. Another six parameters were obtained for describing the shape of the fit (see text) (α = 0.89, μ1 = 259, σ1 = 699, τ1 = 73, μ2 = 867, σ2 = 94, τ2 = 21).

We examined how reaction time varied with the degree of mistuning. Fitted curves showed that animals were generally more likely to respond to the first target tone than to the second (compare the height of the two peaks in Figure 3.3). In the small mistuning group (< 3 Hz), however, the response was delayed and showed a broader distribution at the second target tone compared to the large mistuning group (3 to 8 Hz) (Fig. 3.4A). A delayed response to the first target tone was observed in all animals, whereas increased reaction times to the second target tone were observed in 3 out of 6 animals. Significant differences in the parameters μ1 and σ1 from the double-EMG fitting were obtained between trials with different degrees of mistuning (paired *t*-test; μ1: $t_{(5)} = 4.39$, $P = 0.007$; σ1: $t_{(5)} = 5.30$, $P = 0.003$) (Fig. 3.4B, C). This analysis provides further confirmation that the performance of the ferrets on this task was determined by the degree of mistuning.

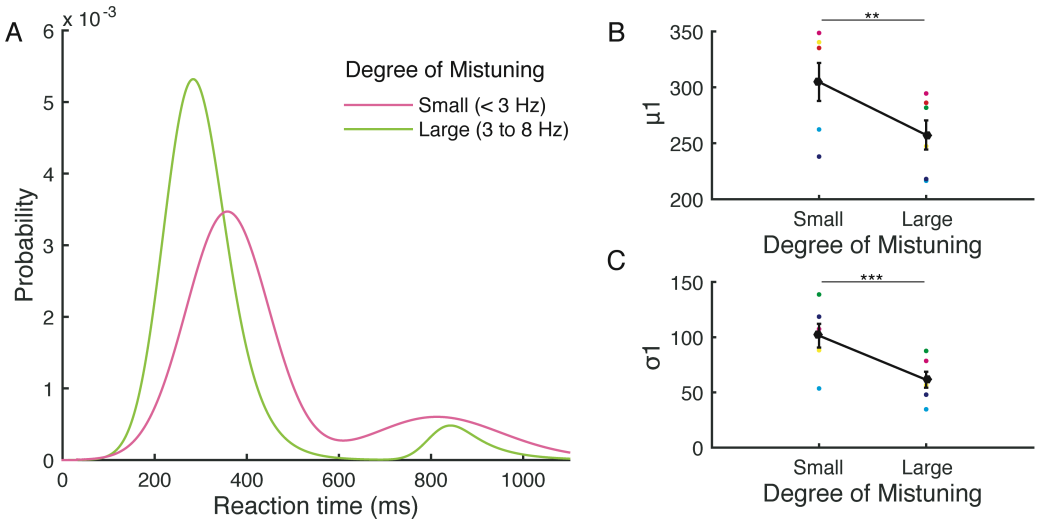

Figure 3.4 Effect of mistuning on reaction time.
(A) Fitted reaction time for different degrees of mistuning (pink: small, < 3 Hz; green: large, 3-8 Hz). (B, C) Parameter values obtained from the ex-Gaussian distribution (B: μ1; C: σ1) are plotted for the two mistuning groups. Black indicates mean ± sem. Coloured dots represent data from individual animals. Paired *t*-tests revealed significant differences in the value of these parameters between the small and large mistuning groups (μ1: $t_{(5)} = 4.39$, $P = 0.007$; σ1: $t_{(5)} = 5.30$, $P = 0.003$). $^{**}P < 0.01$, $^{***}P < 0.005$.

3.4. Discussion

In this chapter we have shown that ferrets, a species increasingly used in auditory research, are readily able to discriminate MCTs from HCTs. A previous study has shown that ferrets have the capacity to spontaneously distinguish harmonic from inharmonic tones without being trained or rewarded for doing so, and that this is likely to be on the basis of differences in perceived fusion of the individual tone components due to their harmonic relationships (Kalluri et al. 2008). The discrimination thresholds for ferrets in this study are in line with those reported for other animal species (Lohr and Dooling 1998; Klinge and Klump 2009; Klinge and Klump 2010) and lower than those measured in humans (Moore et al. 1985; Hartmann et al. 1990). This behavioural sensitivity to harmonicity and the availability of established methods for the measurement (e.g. Fritz et al. 2005; Bizley et al. 2013b) or manipulation (Bajo et al. 2010; Nodal et al. 2012) of neuronal activity opens the possibility of using the ferret as a model for scene analysis studies.

Task design

In this study, the mistuning detection ability of ferrets was explored using a modified go/no-go paradigm. Similar paradigms have been employed for measuring mistuning detection in gerbils (Klinge and Klump 2009; Klinge and Klump 2010) and birds (Lohr and Dooling 1998; Klinge et al. 2010). The advantage of using a go/no-go paradigm is the simplicity of the task, although the performance in general can be affected by the animals' motivation and change of criteria across sessions (Carandini and Churchland 2013). We found that higher FA

rates were observed in trials that required longer waiting time at the trigger spout, resulting in increased bias towards go responses (Fig. 3.2B). It has been shown that decision criteria are adjusted based on the statistics of stimuli and difficulty of the task (Dorfman and Biderman 1971; Thomas 1975; Mill et al. 2014). Because the go/no-go paradigm increases the probability of correct responses on longer trials, it is not surprising that both hit rate and FA rate increased in trials with long waiting times. Therefore, we pooled data only from sessions on which the FA rate was relatively low, and trials with the longest waiting times were not included in our analysis. By defining specific criteria in this way, it is possible to achieve stable behavioural performance in ferrets using a go/no-go mistuning detection paradigm.

In contrast to typical go/no-go paradigms, we introduced correction trials to reinforce the animals to stay at the trigger spout and decrease their FA rate, yielding less response bias. Because response bias was not investigated in previous mistuning detection studies in other species, it is not clear how this might have affected the reported behaviour and thresholds or even if there are interspecies differences in bias. It is possible, for example, that, because they are carnivores, ferrets might be particularly prone to make go responses. In previous studies in birds and gerbils (Lohr and Dooling 1998; Klinge and Klump 2009; Klinge and Klump 2010), data were analysed for sessions in which the FA rate did not exceed 20%. Here we used different criteria as we considered the effect of trial length on hit and FA rates and *d'* values, and did not include trials with the longest waiting time in our analysis. Consequently, the FA rate was 0.4 on average in our experiments. Despite these considerations, the mistuning detection thresholds in ferrets are very similar to those measured in other animal species using similar

paradigms. Moreover, these experiments show that a go/no-go task can be used to measure auditory perceptual abilities in ferrets.

Reaction time

We also studied the relationship between reaction time and performance on the go/no-go task. Using an ex-Gaussian distribution to parameterise the distribution of reaction times (Lacouture and Cousineau 2008), we found that responses to the first target tone were delayed and became much less precise to the second target tone when the degree of mistuning was reduced (Fig. 3.4). These findings indicate that the animals require more time to correctly judge the target tones as mistuned when the harmonic shift is small. Furthermore, we found that not only τ but all parameter values from the ex-Gaussian distribution were affected, appearing to contradict the classical view that the exponentially distributed component represents the time for decision making (Hohle 1965). This finding supports the view that parameters from fitting should be used for purely descriptive purposes without interpreting them in terms of the underlying cognitive processes (McGill 1963; Luce 1986; Matzke and Wagenmakers 2009). Indeed, previous studies have highlighted the value of using parameters from ex-Gaussian fitting for analysing reaction time distributions (e.g. Heathcote et al., 1991; Yap et al., 2006; Leach et al., 2013).

Comparisons with other species

Our results show that the threshold for mistuning detecting in ferrets is 0.8 ± 0.1 Hz. This corresponds closely to the thresholds reported for gerbils (Klinge and Klump

2009; Klinge and Klump 2010), zebra finches and budgerigars (Lohr and Dooling 1998), which are often < 1 Hz, whereas those measured in humans can be as much as an order of magnitude higher (Moore et al., 1985; Hartmann et al., 1990; Lohr and Dolling 1998; Klinge and Klump 2009). Importantly, this does not reflect differences in task design. Although two-alternative forced choice and matching tasks are commonly used in humans (Moore et al., 1985; Hartmann et al., 1990), similarly high thresholds have been obtained using procedures modelled on the go/no-go tasks employed in the animal studies (Lohr and Dolling 1998; Klinge and Klump 2009).

It has been suggested that the ferret auditory system closely resembles that of cats (Moore et al. 1983; Kelly et al. 1986; Phillips et al. 1988), although the tuning properties of auditory nerve fibres in ferrets are broader and closer to those of smaller animals, such as guinea pigs and chinchillas (Sumner and Palmer 2012). Because thresholds for the detection of mistuning in gerbils and birds increase when sine phase complex tones were replaced with random phase complex tones, whereas human thresholds are not affected (Lohr and Dooling 1998; Klinge and Klump 2009), it has been suggested that animals may rely relatively more on temporal fine structure (Lohr and Dooling 1998; Dooling et al. 2002; Klinge and Klump 2009; Klinge et al. 2010). This is also likely to be the case in ferrets since their ability to discriminate HCTs appears to rely more on temporal periodicity cues in unresolved harmonics than on spectral cues in resolved harmonics (Walker et al. 2014). It should be noted that 1600 Hz, which is the harmonic frequency that was shifted in this study, lies at the edge of the ferret's auditory nerve phase locking range (Sumner and Palmer 2012). However, phase locking has been

demonstrated in other species not only to mistuned harmonics, but also to the lower frequency beats corresponding to the difference in frequency between the mistuned and adjacent harmonics (Sinex et al. 2002; Sinex et al. 2005; Sinex 2008; Fishman and Steinschneider 2010).

The behavioural thresholds measured in gerbils, ferrets and birds for detecting a mistuned harmonic in a HCT are substantially smaller than the frequency difference limens for pure tones in these species, whereas the converse is true in humans (Moore 1973; Fay 1988; Lohr and Dooling 1998; Klinge and Klump 2009; Walker et al. 2009; Klinge et al. 2010). It has been proposed that animal species with a short cochlea are less able to rely on the spatial distribution of excitation for discriminating different frequencies (Fay 1992; Klinge et al. 2010). This may therefore account for the difference in frequency difference limens for pure tones between humans and animals and the greater dependence of the latter on temporal cues for discrimination tasks of this sort.

Concluding remarks

In this chapter, we have shown that trained ferrets have excellent thresholds for discriminating sounds on the basis of their harmonicity. Together with previous evidence that at least some cortical neurons in this species can distinguish between harmonic and inharmonic complex tones (Kalluri et al. 2008) and encode pitch judgments (Bizley et al. 2013b), this study highlights the value of using this species for exploring the neural basis for pitch perception and auditory scene analysis.

Chapter 4

Functional organization of the ferret auditory thalamus

4.1. Abstract

In this chapter, we describe the functional organization of the ferret auditory thalamus. Acoustically-evoked response patterns and response latencies were examined in the ventral, medial and dorsal divisions of medial geniculate body (MGBv, MGBm and MGBd). Furthermore, frequency response areas (FRAs) were investigated to characterize the tuning properties in each division. Onset responses were dominant in all the divisions, and response latencies were consistent with the values previously reported for other species. While MGBd and MGBm showed broadly tuned or multipeaked FRAs, MGBv showed sharply tuned FRAs with a tonotopic gradient similar to that described in other animal models, with a high to low frequency gradient from the anterior-dorsal to posterior-ventral aspect of this division. These results show that the functional organization of the ferret auditory thalamus is comparable to that of other species.

4.2. Introduction

The mammalian auditory thalamus, the medial geniculate body (MGB), has been classified into three divisions. The ventral division of medial geniculate body (MGBv) is a lemniscal or core region, which is involved in processing auditory information, with neurons well-tuned to specific sound frequencies. In contrast, the MGB dorsal and medial divisions (MGBd and MGBm, respectively) are non-lemniscal regions, with neurons in MGBd less driven by sounds of specific frequencies, while those in MGBm respond to both auditory and non-auditory information and seem to be involved in higher cognitive processing (Bartlett 2013). MGBv receives ascending inputs from the ipsilateral central nucleus of the inferior colliculus (CNIC) and descending inputs from the primary auditory cortex (A1) (Calford and Aitkin 1983; Rouiller and de Ribaupierre 1985; LeDoux et al. 1985; González-Hernández et al. 1991). In addition to the excitatory inputs, MGBv receives inhibitory GABAergic input from the inferior colliculus (IC) and the thalamic reticular nucleus (TRN), which are thought to control firing patterns in the thalamus (Jones 1975; Winer et al. 1996; Peruzzi et al. 1997).

Neurons in MGBv mainly project to layer III-IV of the primary auditory cortical areas, while MGBd and MGBm target layer III-IV of the secondary auditory cortical areas with terminals from MGBm projection neurons also ending in layers I and VI throughout auditory cortex (Morel and Imig 1987; Huang and Winer 2000; De La Mothe et al. 2006; Lee and Winer 2008c). MGBv has a clear tonotopic organization, with a frequency gradient resembling that in the cochlea. The orientation of the tonotopic gradient in MGBv varies in different species, and neurons are also sensitive to the periodicity of sounds and their temporal

modulation (cat: Rouiller et al. 1979; Rouiller et al. 1981; Calford 1983; Morel et al. 1987; Rodrigues-Dagaeff et al. 1989; guinea pig: Redies and Brandner 1991; Edeline et al. 1999; Wallace et al. 2007; Anderson et al. 2007; rat: Bordi and LeDoux 1994; Kimura et al. 2009; Storace et al. 2010; mouse: Hackett et al. 2011; marmoset: Bartlett and Wang 2007; Bartlett and Wang 2011). The ferret is becoming one of the most frequently used animal models in auditory neuroscience research, however, the organization of the auditory thalamus in this species has not been investigated yet.

Thus, the aim of this study was to examine the responses of thalamic auditory neurons to conventional auditory stimuli, broadband noise (BBN) and pure tones, in order to characterize ferret MGB physiologically prior to the more specific investigation of its role in mistuning detection to be addressed in the next two chapters. Our results show that ferret MGB has a similar organization to other species, with MGBv neurons showing relatively short response latencies and sharply tuned FRAs that are organized tonotopically.

4.3. **Results**

We searched for the auditory thalamus by making dorso-ventral penetrations using single or double shank Neuronexus probes with a vertical linear configuration (16 or 16×2 recording sites, 100 μm apart, Fig. 4.1A, but see also Methods in Chapter 2). The probes were positioned at 1.8-2.5 mm anterior to the caudal end of the ectosylvian gyrus (EG) and 3.9-4.7 mm lateral from the midline. In a typical penetration, visual responses in the cortex were firstly observed until ~ 4 mm below the pial surface. This was followed by large spontaneous spikes that were

observed between ~ 4 to 5.5 mm deep, which we identified as the hippocampus. Strong responses to an LED were obtained from ~ 5.5 to 7.5 mm deep, corresponding to the visual thalamus, the lateral geniculate nucleus (LGN) (Fig. 4.1B and 1C). Finally, auditory responses were recorded from ~ 7.5 to 9.5 mm deep in the auditory thalamus.

In a total of 3 ferrets in which the recording probes were inserted bilaterally (Fig. 4.1B and C), 16 penetrations reached MGBv (Fig. 4.1B), and 12 penetrations were located in MGBd and MGBm (Fig. 4.1C). The location of each recording site was identified by its response properties (based on comparisons with other species) and confirmed by histological analysis of the sections stained for Nissl substance.

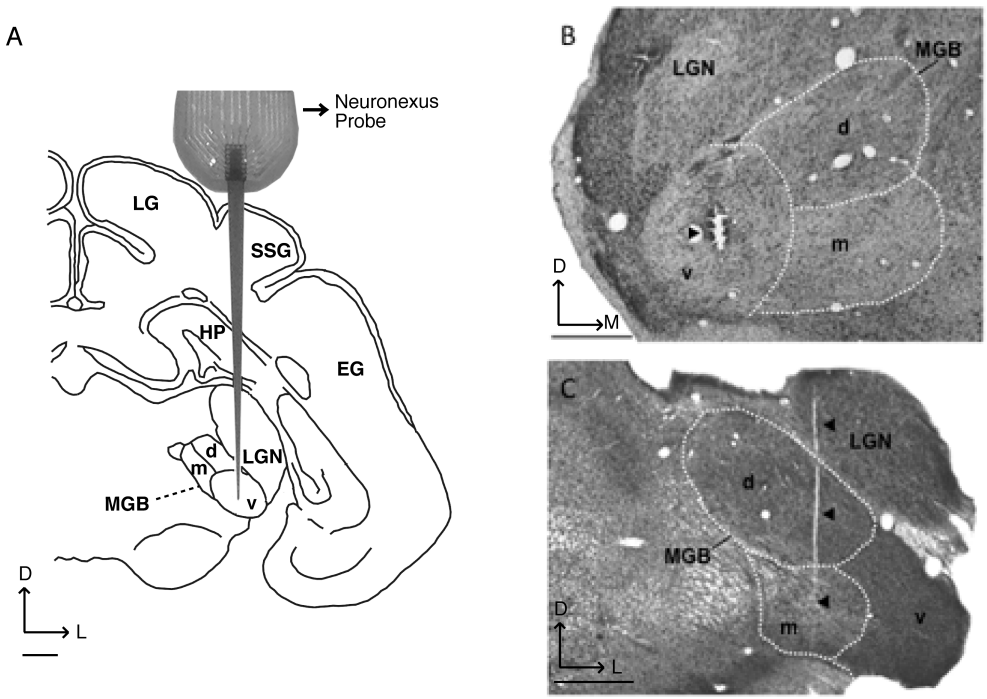

Figure 4.1 Experimental design.
(A) Schematic of recordings. Probe (Neuronexus, 16 recording sites, 100 µm apart) penetrated dorsoventrally through the cortex into LGN and MGB. (B) Electrode track (arrowhead) in the left ventral MGB. (C) Electrode track (arrowheads) in the right LGN and dorsal and medial MGB. D, dorsal; d, dorsal MGB; EG, ectosylvian gyrus; HP, hippocampus; L, lateral; LGN, lateral geniculate nucleus; LG, lateral gyrus; M, medial; m, medial MGB; MGB, medial geniculate body; SSG, syprasylvian gyrus; v, ventral MGB. Calibration bars = 1mm.

4.3.1. Responses to visual stimulation and BBN in the visual and auditory thalamus

BBN bursts (100 ms duration) at different intensities were presented either alone or together with constant intensity light flashes of the same duration from an LED (see Methods in Chapter 2 for details, Fig. 4.2). 46 units were identified in the LGN that responded exclusively to light (e.g. Fig. 4.2A and B), while units in the MGB (158 units) responded to the BBN stimulus. In the two examples of the MGBv units (Fig. 4.2C and D), there was no difference in response to BBN alone and BBN plus light. 15% of auditory evoked responses (24/158) showed monotonic rate-level functions, while 85% of the responses showed non-monotonic (Fig. 4.2C and D).

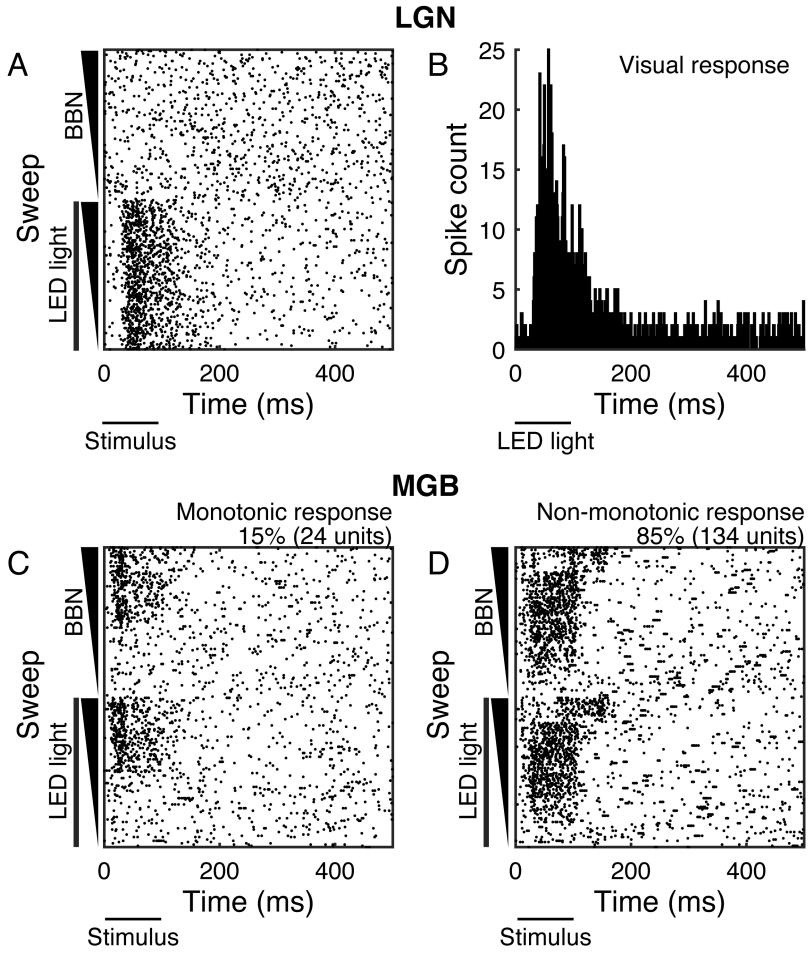

Figure 4.2 Examples of responses to visual and BBN stimulation in the visual and auditory thalamus.

(A, C, D) Rasterplots in the LGN (A) and the MGB (C, D). The line parallel to the y-axis indicates the light stimulus (100 ms flash from an amber LED). The triangular bar represents a 100 ms broadband noise (BBN) increasing in amplitude from 50 to 90 dB SPL in 10 dB steps every 10 sweeps with 0 dB SPL in the first ten. (B) PSTH example of responses to the visual stimulus in the LGN. (C, D) Examples of monotonic (C) and non-monotonic (D) auditory responses. Note that the responses to BBN combined with the visual stimulus in C and D were not different from those obtained to BBN alone. The stimulus length was 100 ms, as shown by the horizontal bar starting at time 0.

Onset responses were dominant

In the LGN, 96% of the evoked responses (44/46) to light were classified as onset, with a minimum response latency (when the response exceeded 20% of the difference between spontaneous and peak firing rates) of 17 ms with 25-75th percentile ranges of 7-42 ms, and a peak response latency (when the highest spike rate was evoked) of 71 ms with 25-75th percentile ranges of 60-83 ms (e.g. Fig. 4.2B). 57% of the units (26/46) also gave an offset response, with 2 units in the LGN showing exclusively offset responses. We did not find any segregation of these simple response properties in particular locations of the LGN.

Among 158 units assigned to the MGB, 71 were located in MGBv, while 37 and 48 units were in the MGBd and MGBm, respectively. The response patterns were classified into 5 groups following previous studies in the auditory thalamus (Calford and Webster 1981; Calford 1983) and auditory cortex (Bizley et al. 2005; Walker et al. 2011) (Fig. 4.3). 74% of the units (117/158) produced a significant response to BBN within the onset window (1-50 ms following the start of the sound presentation). A 'sustained' response pattern (e.g. Fig. 4.3A), which comprises an onset response plus subsequent spikes during the sound presentation (51-100 ms), was the most common response type in all MGB divisions (Fig. 4.3E). The firing of these units either gradually decayed or was maintained throughout sound presentation. Transient responses with a single onset peak ('transient single on,' e.g. Fig. 4.3B) were assigned to the units that produced a sharp onset response only. If a unit had multiple peaks at onset and offset (the latter response occurring in a window 1-50 ms after the end of the sound presentation), it was classified as 'transient multiple on/off' (e.g. Fig. 4.3C). 'Offset' refers to units that had an offset

response only (e.g. Fig. 4.3D). 'Others' were the units that did not match any of the criteria mentioned above, which also includes weak late onset responses and variable responses, as first described in cats by Calford and Webster (1981).

The proportion of units with different response patterns is distinctive for each division (Fig. 4.3E). In MGBv, more than 65% of units (45/71) showed onset only or combined onset and sustained responses. In MGBd, 26% of units (10/39) showed 'transient single on,' and 'offset' was also observed in 13 % of the units (5/39). In MGBm, 69% of the units (33/48) were 'sustained,' and no units gave an offset response.

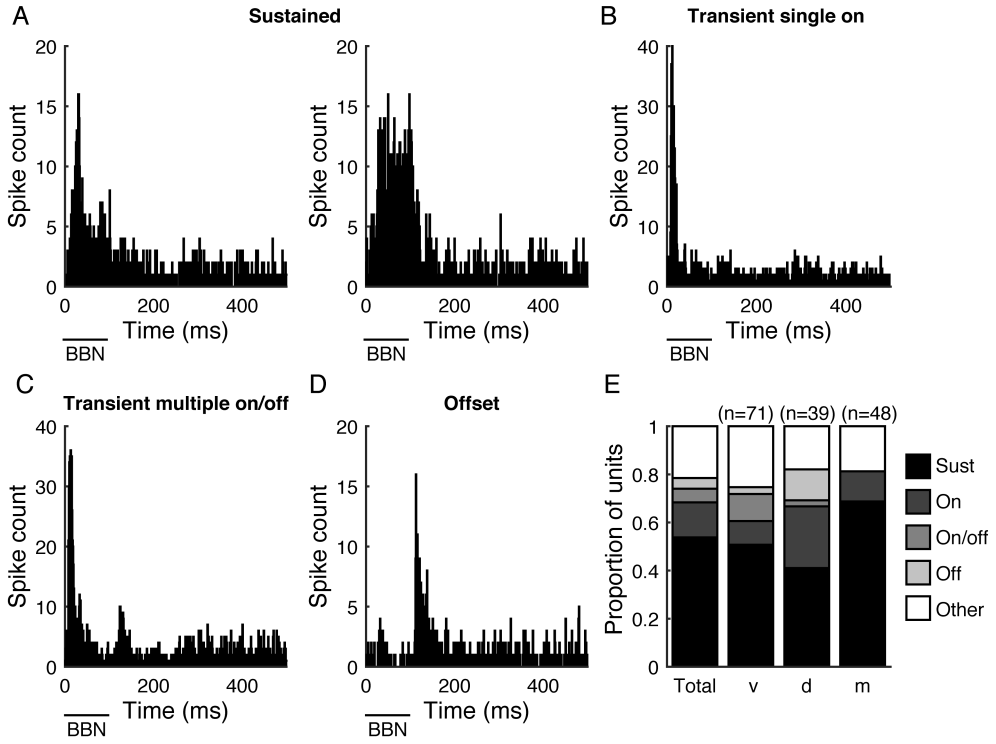

Figure 4.3 Response patterns to BBN in the auditory thalamus.
(A-D) PSTH examples of 'sustained' (A), 'transient single on' (B),'transient multiple on/off' (C), and 'offset' (D) response patterns. The 100-ms BBN stimulus is represented by the bar below each plot starting at time 0. (E) The proportion of units with different response patterns. Total was computed from the values for all three divisions. The number of units in each division (v, MGBv; m, MGBm; d, MGBd) is shown at the top of the bar. Response patterns are indicated by the grey scale for Sust, sustained; On, transient single on; On/off, transient multiple on/off; Off, offset; and Others. Others include all response patterns that could not be classified as A-D shown above.

Short response latencies were observed

Minimum and peak response latencies were computed for each recording location (MGBv, MGBd and MGBm) and response pattern (transient single on, transient multiple on/off, and sustained) (Fig. 4.4). Minimum and peak response latencies for the units with 'transient single on' in MGBv were shorter than those for neurons with other response patterns, with median values of 9 ms (7-9 ms 25-75th percentile range) and 13 ms (11-19 ms 25-75th percentile range), respectively (Fig. 4.4A and D). These latencies were shorter than those measured for units recorded in MGBd and MGBm (Fig. 4.4 B, C, E, F). For the units with 'sustained' responses, peak response latency was longer in MGBv due to the wider variability observed (Fig. 4.4D), while minimum response latency was the same in all divisions (Fig. 4.4A-C). Although minimum response latency tended to be shorter in the MGBv, the difference did not reach significance (P = 0.41, Kruskal-Wallis test on six groups classified by the three MGB divisions and two response patterns of 'transient single on' and 'sustained'). On the other hand, peak response latencies were statistically different ($P = 8\times10^{-8}$, Kruskal-Wallis test on the same six groups). Post hoc tests confirmed that peak latencies were significantly longer in the group of MGBv units with 'sustained' discharge patterns than for any of the other five subgroups (Tukey-Kramer, MGBv with 'sustained' vs MGBv with 'on' / MGBd with 'on' / MGBd with 'sustained'/ MGBm with 'on' / MGBm with 'sustained', P<0.05).

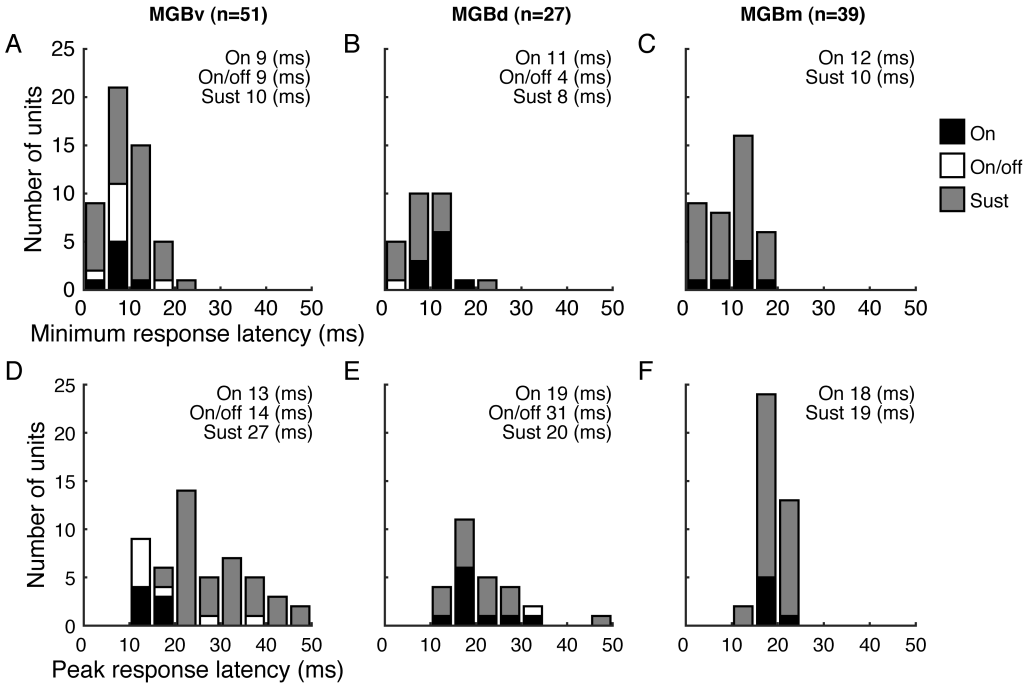

Figure 4.4 Response latencies to BBN in the auditory thalamus.
Histogram of minimum and peak response latencies for units recorded in MGBv (A, D), MGBd (B, E) and MGBm (C, F). The histogram bars for the units with 'transient single on' (On) response patterns are drawn in black, the bars for the units with 'transient multiple on/off' (On/off) response patterns are white, and the units with 'sustained' (Sust) response patterns are in grey. The median value for each case is shown at the right top corner. The number of units for each division is indicated at the top of column.

4.3.2. Responses to pure tones in the auditory thalamus

131 units in the MGB responded to pure tones with 71% of the units (93/131) responsive to both BBN and pure tones. Among the 131 tone-responsive units, 68 were located in the MGBv, 15 in the MGBd and 48 in the MGBm.

Onset responses in MGBv were also dominant

Pure tone response patterns were analysed from the PSTHs pooled at unit CFs in MGBv. 68% of the units (46/68) showed responded to stimulus onset, and the response patterns were similar to those obtained with BBN, although fewer offset responses were observed when pure tones were used as a stimulus. 79% of the units (37/47) produced the same firing pattern for both stimuli. With pure tone stimulation, the proportion of 'sustained' responses was 54%, and that of 'transient single on' was 12%, which is consistent with the proportions observed for BBN stimuli. On the other hand, the proportion of units that gave an offset response to pure tones was lower than with BBN.

Response latencies to pure tone stimuli were less variable

Minimum and peak response latencies to pure tones were calculated at the units' CF for each MGB division and response pattern. The histograms in Fig. 4.5 indicate that response latencies covered a smaller range with pure tones relative to the responses to BBN (compare Fig. 4.5 with Fig. 4.4A and D). There was a trend for shorter (minimum and peak) latencies in the responses to pure tones compared to those obtained using BBN, but these differences did not reach significance

(minimum latency, transient single on: $P = 0.20$, sustained: $P = 0.45$; peak latency, transient single on: $P = 0.08$, sustained: $P = 0.09$, Wilcoxon rank sum test).

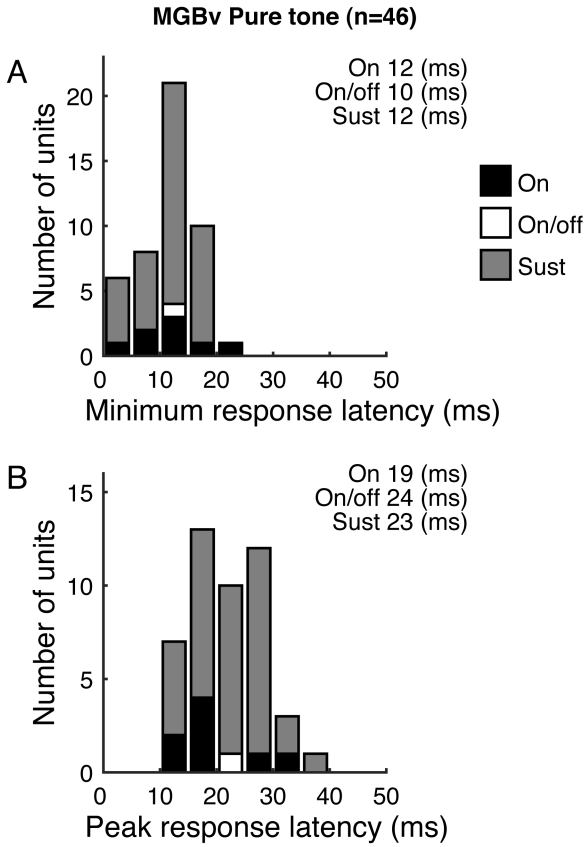

Figure 4.5 Response latencies to pure tones in MGBv.
Histogram of minimum (A) and peak (B) response latencies for 46 units. The format is the same as in figure 4.4.

A tonotopic gradient was observed in the MGBv

Frequency responses areas (FRAs) were computed for the units responding to pure tones in the MGBv. V-shaped (primary-like) FRAs are one of the main features of MGBv units in other species (Morel et al. 1987; Rouiller et al. 1989; Redies and Brandner 1991; Bordi and LeDoux 1994; Anderson et al. 2007). In the present study, we observed sharply tuned FRAs in the majority of units (84%, 57/68) located in the MGBv (e.g. Fig. 4.6A). At the borders of MGBv, 9 units had FRAs that were less well tuned compared with the more typical V-shaped units and these were not included in the subsequent analysis. In the MGBd, FRAs were broadly tuned (Fig. 4.6B), while neurons in MGBm typically showed multiple peaks in their tuning curves and broadly tuned FRAs (Fig. 4.6C).

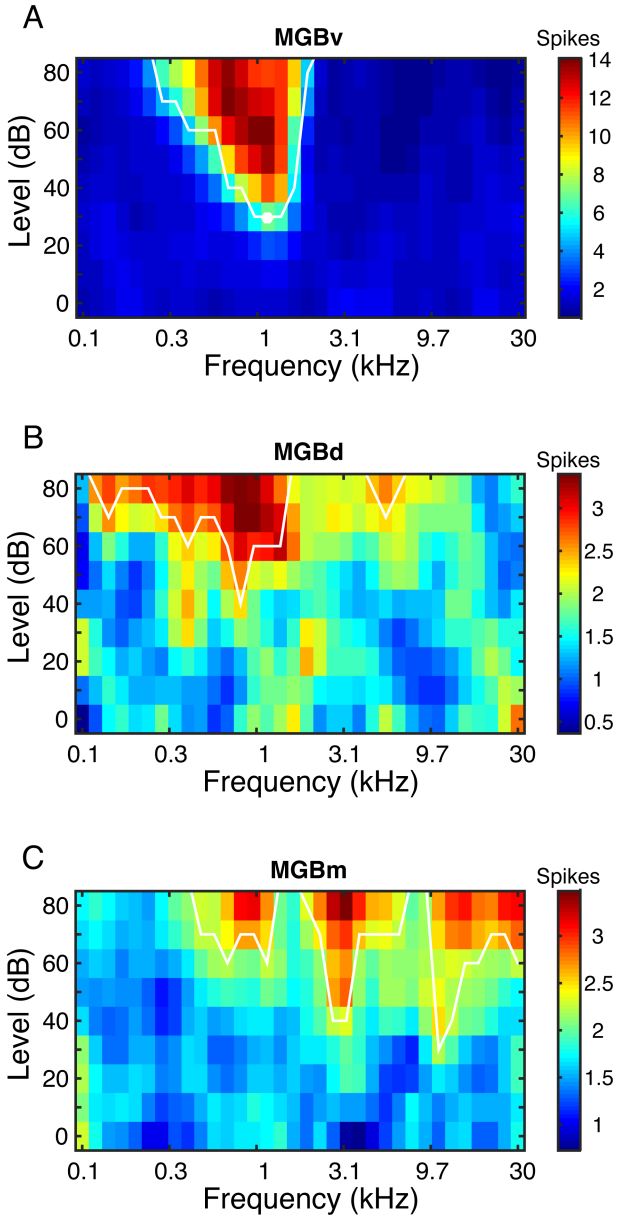

Figure 4.6 Examples of frequency response areas for the different divisions of auditory thalamus.
(A) Sharply tuned V-shaped FRA in MGBv. (B) Broadly tuned FRA in MGBd. (C) Multi-peaked FRA in MGBm. The white line indicates the tuning curve in each case. Characteristic frequencies (CF) are depicted by white dots. The colour scale shows the number of spikes evoked at each combination of level and frequency.

For the sharply tuned units in the MGBv, the threshold, CF and Q10 were analysed. Median threshold (lowest amplitude in dB SPL that evoked a significant response) was 60 dB SPL with 25-75th percentile ranges of 40-60 dB SPL, and CFs ranged from 170 Hz to 15.4 kHz. Median Q10 value (CF divided by the bandwidth at 10 dB above threshold) was 0.60 with 25-75th percentile ranges of 0.37-5.85. These values are comparable to previous reports in other species (Allon et al. 1981; Edeline et al. 1999), further indicating that ferret MGBv neurons have tuning properties that are typical of the auditory thalamus.

Examination of the location of units and their CFs showed that a tonotopic gradient is present in the MGBv. The CFs were grouped into 6 categories with the middle 4 categories having the same width of frequencies on a log scale from 0.4 to 5.3 kHz and the first and last categories including all frequencies lower or higher than this range, respectively (Fig. 4.7 and 4.8). Units with high CFs were located in the anterior part of the MGBv and units with low CFs were located in the posterior region (Fig. 4.7). In the example illustrated in figure 4.7A, the median CF calculated for units in the most anterior position (2.5 mm anterior to EG) was 5.5 kHz with 25-75th percentile ranges of 3.5-6.6 kHz. At a slightly more posterior position (antero-posterior, AP, coordinate 2.3 mm), the median CF was 1.1 kHz with 25-75th percentile ranges of 0.7-2.8 kHz (Fig, 4.7B). The CFs declined progressively as the location of the recording probe was shifted further posterior (Fig. 4.7C, D). Although a wide range of CFs was observed at each AP location, which, to some extent, reflected systematic changes with depth (e.g. Fig 4.7A, where CFs decreased from 7.5 kHz to 2.8 kHz as the recording probe was moved

from 6.3 mm to 8.3 mm below the cortical surface), a high to low frequency gradient was clearly present along the anterior-posterior axis of the ferret MGBv.

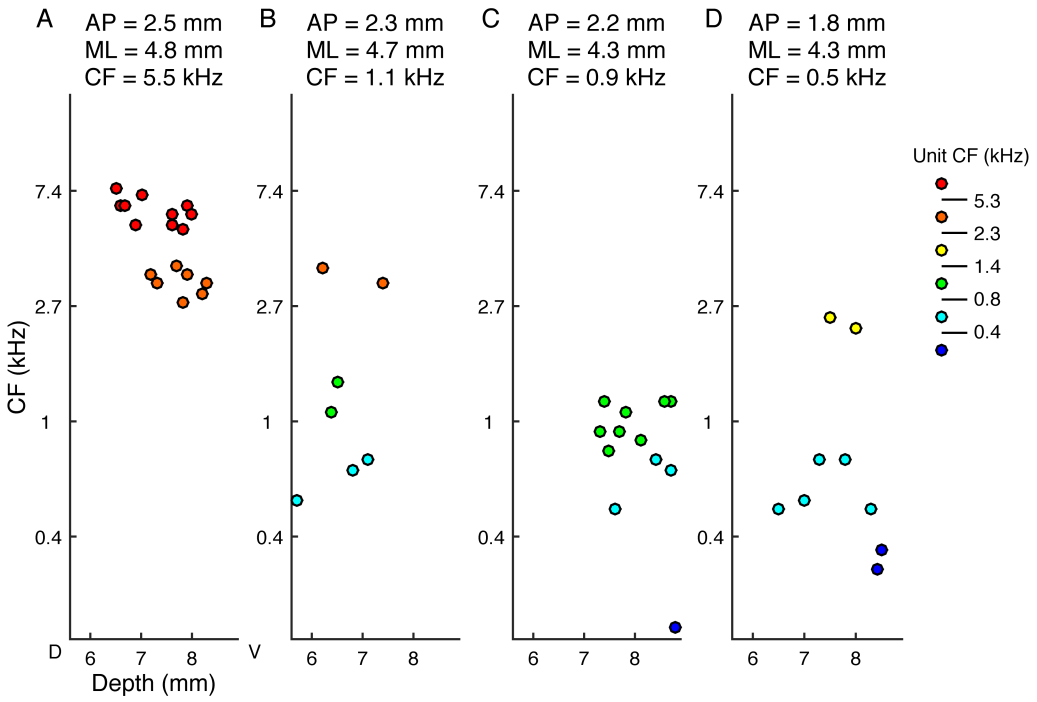

Figure 4.7 Variation in CF with the antero-posterior and dorso-ventral location of the recording sites in MGBv.
The antero-posterior distance from EG (AP) and the medio-lateral distance from the midline (ML) are shown at the top of each panel, together with the median value of unit CFs at this position. The dorso-ventral variation in CF is shown in each panel by plotting unit CFs as a function of depth. D, dorsal; V, ventral. Unit CFs are shown in different colours grouped into 6 categories with the middle 4 categories covering the same range of frequencies on a log scale from 0.4 to 5.3 kHz and the first and last categories comprising CFs < 0.4 kHz and > 5.3 kHz, respectively.

For each probe position, the median CF was calculated and plotted in Fig. 4.8 against both AP and medio-lateral (ML) coordinates, with the size of the circles being proportional to the number of units recorded. In addition to the AP gradient, the CFs varied across the ML dimension, with units in central regions being tuned to lower values than those on the lateral side.

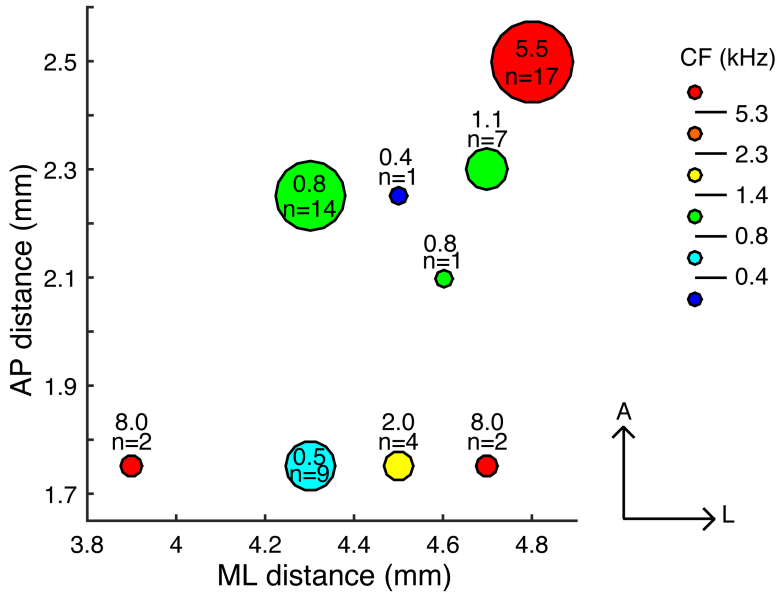

Figure 4.8 Tonotopic organization in MGBv.
A tonotopic gradient from high to low frequency is indicated by the variation in unit CF along the antero-posterior extent of this nucleus. The median CFs were calculated for each recording position defined by the antero-posterior distance from EG (AP) and the medio-lateral distance from the midline (ML) and plotted on the AP-ML grid. The number of units at each position is shown by the size of the circles. The median CFs are shown in different colours grouped into 6 categories, with the middle 4 categories covering the same range of frequencies on a logarithmic scale from 0.4 to 5.3 kHz and the first and last categories comprising CFs < 0.4 kHz and > 5.3 kHz, respectively. A, anterior; L, lateral; M, medial; P, posterior.

4.4. Discussion

The purpose of this study was to characterize the response properties of units recorded in the ferret MGB and to identify the position of its ventral division in the thalamus, so that this could be targeted reliably in the next part of the project. Consistent with previous studies in other mammalian species (Allon et al. 1981; Calford 1983; Rodrigues-Dagaeff et al. 1989; Rouiller et al. 1989; Redies and Brandner 1991; Bordi and LeDoux 1994; Edeline et al. 1999; Anderson et al. 2007), we have shown that ferret MGBv neurons tend to have short response latency, onset responses that often extend throughout the duration of the stimulus and occasionally produce what may be an offset response. As expected, most neurons had sharp, V-shaped FRAs, and displayed a high-to-low tonotopic gradient from the most antero-dorsal to the most postero-ventral part of the MGBv.

Response patterns

It has been reported that the peaked onset responses were dominant among mammalian MGB neurons (Calford 1983; Rodrigues-Dagaeff et al. 1989; Bordi and LeDoux 1994; Edeline et al. 1999), while our results show that a ‘sustained’ response is the most common type (Fig. 4.3A). However, a substantial number of ‘sustained’ responses have also been reported in awake cats (Aitkin and Prain 1974), indicating that the depth and type of anaesthesia as well as potential species differences have to be considered. This is further supported by studies showing that sustained responses dominate in awake squirrel monkeys (Allon et al. 1981) and that a greater proportion of ‘offset’ response are found in awake rats (Kalappa et al. 2014). Furthermore, in rats anaesthetised with chloral hydrate, fewer onset and

more rhythmic responses were reported in MGBv (Bordi and LeDoux 1994), compared to studies in cats under ketamine anaesthesia. On the other hand, it has been shown that the response properties that characterise each division of the MGB are comparable between awake and anaesthetised conditions (Edeline et al. 1999).

In this study, ferrets were anaesthetised with an i.v. infusion of ketamine, which is well-controlled lightly anaesthetised condition that may explain the preponderance of sustained responses. In addition, we have used multiunit recordings with Neuronexus probes, while the previous studies were usually single unit recordings with tungsten electrodes. We therefore cannot rule out the possibility that units with different temporal firing patterns may have contributed to the distribution of the responses that we observed.

Our results also showed that a proportion of units with 'sustained' responses is found in the MGBm while more transient onset and/or offset response patterns are commoner in the MGBd (Fig. 4.3E). These trends are consistent previous studies (Calford 1983; Bordi and LeDoux 1994; Edeline et al. 1999).

Response latency

Response latencies tend to be shorter in the MGBv for the units with 'transient single on' response patterns than in the MGBd and MGBm, although significant differences in response latency in the different divisions were not found (Fig. 4.4). Other studies have reported that MGBv neurons have the shortest latencies, and in some cases the differences were statistically significant (Calford 1983; Bordi and LeDoux 1994; Edeline et al. 1999). Furthermore, in our results, peak response latencies calculated at CF for the tone-responsive units in MGBv were less variable

than when BBN was used (compare Fig. 4.4D and Fig. 4.5B), suggesting that the onset peak is sharper for pure tones than for BBN.

The response latencies calculated here were shorter than those reported in ferret primary auditory cortex (A1) (Bizley et al., 2005, Fig 13C), the destination of MGBv thalamocortical projection neurons. This is consistent with the functional connectivity between these regions.

FRA shape

MGBv units typically had V-shaped tuning curves, those in MGBd were more broadly tuned, and those recorded in MGBm were heterogeneous with units displaying broadly tuned and multipeaked FRAs intermingled (Fig. 4.6). A sharply tuned V-shaped or primary-like tuning curve has been reported as a dominant feature in the MGBv, but is also observed in both the MGBd and MGBm (Morel et al. 1987; Rouiller et al. 1989; Redies and Brandner 1991; Bordi and LeDoux 1994; Anderson et al. 2007). In cats and guinea pigs, 50-60 % of MGBv neurons have been found to have V-shaped tuning curves (Morel et al. 1987; Anderson et al. 2007), whereas this figure was 84% in our sample. However, the relatively high proportion of sharply tuned units in ferrets may reflect our smaller sample size (n=131 for pure tones in total), compared to the previous studies (n>250 for each division), or to the bias in collecting data from the units with low and medium CFs and with little representation of high CFs.

CF and Q10

While ferrets can hear up to >30 kHz (Kelly et al. 1986), most of CFs obtained in this study were <15.4 kHz. In targeting the thalamus through the overlying cortex, we attempted to avoid blood vessels on the surface of the brain (see Chapter 2 for details), so this undersampling is perhaps inevitable. In addition, as the ferret MGB has a very flat shape in its dorso-ventral axis and is located at a very deep position in the thalamus, it is likely that we did not explore the full extent of the nucleus. Furthermore, the initial purpose of recording from the MGB in this thesis was not to map out its tonotopic organization, but to investigate responses to complex tones in MGBv neurons (Chapter 5). Thus, we made relatively few electrode penetrations in each animal, so that several sets of complex tone stimuli could be presented, rather than re-position the electrode sufficiently to fully characterize the tonotopic organization.

We calculated Q10 values for MGBv neurons to be median 0.60 with 25-75th percentile ranges of 0.37-5.85. Although broadly consistent with other studies, sharper tuning has been reported in guinea pigs, with a Q10 of 2.60 ± 0.25 (Edeline et al. 1999), and in squirrel monkeys (0.76 ± 0.85 below 8 kHz and 3.42 ± 2.92 above 8 kHz) (Allon et al. 1981). Bizley et al. (2005) reported that Q10 values in A1 and AAF of anesthetized ferrets ranged from 0 to 10, covering the range obtained in this study.

Tonotopic organization

A tonotopic gradient was observed in MGBv with CFs varying with the location of the recorded units. Although CFs varied along different anatomical axes, the

clearest gradient was for a high-to-low progression as the recording site was moved anterior to posterior (Fig. 4.7 and 4.8). The tonotopic organization in the lemniscal region of thalamus has been investigated in cats (Calford and Webster 1981; Calford 1983; Rodrigues-Dagaeff et al. 1989), guinea pigs (Redies and Brandner 1991), mice (Hackett et al. 2011) and Mongolian gerbils (Budinger et al. 2013). In keeping with our results, a high-to-low gradient from the anterior to posterior end of the MGBv has been found, except in gerbils where the gradient runs in the opposite direction (Budinger et al. 2013). Both parts of the MGBv, the pars ovoidea (OV) in the middle and the pars lateralis (LV), show a high to low gradient from dorso-medial to vento-lateral in cats, which is very similar to gradient found here in ferrets. On the other hand, in guinea pigs (Redies and Brandner 1991) a low-to-high CF progression from the dorso-medial to the ventro-lateral regions has been found, while in gerbils (Budinger et al. 2013) a low-to-high gradient extends from dorso-lateral to ventro-medial. These species differences presumably derive from differences in the shape and the orientation of the MGB. The ferret MGBv is relatively flat in the dorso-ventral dimension with flat laminae in the same dimension (Nodal et al. 2006). This anatomical study suggested that high frequency sounds should be represented antero-medially and low frequency sounds postero-laterally (see Appendix Fig. A.1). Our electrophysiological investigation supports the existence of a high-to-low gradient from anterior to posterior. The finding that CFs sometimes varied systematically with depth (e.g. Fig. 4.7A) can be attributed to the vertical electrode penetrations crossing different laminae in the MGBv. Since few penetrations were made at the same coronal plane in this study,

we have insufficient data to assess how CFs change across the medio-lateral extent of the thalamus.

Concluding remarks

The aim of this study was to characterize response properties in ferret MGB and identify the position of MGBv. The results show that ferret MGBv neurons have short response latencies and are sharply tuned and are tonotopically organized in much the same way as in other species.

Chapter 5

Responses to mistuned complex tones in the auditory thalamus

5.1. Abstract

Harmonicity in complex tones is an important cue for segregating and grouping different sounds as part of auditory scene analysis. It has previously been shown that neurons in the auditory cortex and in the inferior colliculus represent the spectral components and temporal patterns of harmonic and inharmonic complex tones. However, little is known about how thalamic neurons respond to complex tones with mistuning. Neurons in the ventral division of medial geniculate body (MGBv) are sharply tuned to sound frequency and sensitive to temporal modulation. In this study, responses to harmonic and mistuned complex tones were investigated in the MGBv. We use harmonic complex tones (HCTs) composed of 16 harmonics with a fundamental frequency, F_0 (200, 400 or 800 Hz), and mistuned complex tones (MCTs) with the 2^{nd}, 4^{th} or 8^{th} harmonic of the HCTs shifted to a higher frequency over a range from 0.05 to 12 %. Those parameters were chosen on the basis of previous psychoacoustic and electrophysiological

studies to include resolved or unresolved mistuned harmonic positions in MCTs. The degree of mistuning was equally distributed on a log scale, considering the shape of the mistuning detection psychometric function that we have measured in ferrets (Chapter 3).

The firing rates of MGBv neurons changed in a way that was dependent on the degree of mistuning and the F_0 of MCTs. Temporal response patterns distinctive to MCTs were also observed, which were phase locked to the periodicities created by the interactions between the mistuned harmonic and neighbouring harmonics. These results indicate that MGBv neurons can extract spectral and temporal information available in MCTs. This study is the first to investigate the auditory thalamus in ferrets using complex tones (HCTs and MCTs). It has also demonstrated that MGBv neurons are sensitive to MCTs. In addition, distinctive temporal response patterns of MGBv neurons to MCTs were observed even when the F_0 of the MCTs were high (800 Hz) and/or the mistuned harmonic was shifted by small degree (<3 %). Our results suggest that MGBv neurons may have an important role in the processing of complex tones.

5.2. **Introduction**

Harmonicity is one of the most important cues for segregating and grouping different sounds. In humans, mistuned partials can be heard as 'popped out' tones when their frequencies are close to a resolved low harmonic and as 'roughness' when they are close to an unresolved higher harmonics (Moore et al. 1985; Hartmann et al. 1990). It has been suggested that the perceptual 'pop out' can be observed in event-related brain potentials recorded from human listeners (Alain et

al. 2001; Alain et al. 2002) and by an increase in the firing rate of multi-units recorded in the primary auditory cortex, A1, of monkeys (Fishman and Steinschneider 2010).

The envelope and temporal fine structure of harmonic complex tones (HCTs) are altered when a mistuned harmonic is inserted into a HCT (mistuned complex tone, MCTs). Neural responses can be phase locked to the low frequency beats resulting from the way mistuned harmonics interact with neighbouring harmonics, and this is thought to be responsible for the perceptual 'roughness.' Distinctive temporal discharge patterns have been observed in the cochlear nucleus (CN) (Sinex 2008), in the inferior colliculus (IC) (Sinex et al. 2002; Sinex et al. 2005; Sinex and Li 2007) and in A1 (Fishman and Steinschneider 2010; Fishman et al. 2014).

Neurons in the CN tend to represent one or a small number of components of complex tones, although a small proportion have been found to produce distinctive temporal response patterns to MCTs like those observed in the IC (Sinex 2008). In the IC, neurons phase lock to the amplitude modulation of the MCTs regardless of the characteristic frequency (CF) of the neurons (CFs up to 5.9 kHz), with slightly higher firing rate in response to MCT than to HCTs (Sinex et al. 2005). In A1, responses to MCTs are enhanced when the frequency of the mistuned harmonic is close to the CF of the recorded neuron, and distinctive temporal responses to MCTs have been observed in units with low CFs (Fishman and Steinschneider 2010). MGBv and A1 neurons are sensitive to sound modulations (Miller et al. 2002), for example showing suppressed responses to fluctuating noise

in the presence of a weak tone (Las et al. 2005), but the responses of thalamic neurons have not been examined using MCTs.

Ferrets are a very suitable animal model for studying the perception of complex sound (Kalluri et al. 2008; Walker et al. 2009; Bizley et al. 2013b; Town et al. 2015). In Chapter 3, we have shown behaviourally that ferrets can detect mistuned harmonics and that their ability to do so is comparable to that of other animal species and superior to that of humans (Moore et al. 1985; Hartmann et al. 1990; Lohr and Dooling 1998; Klinge and Klump 2009; Klinge and Klump 2010).

In this study, HCTs and MCTs very similar to those used in the behavioural study described in Chapter 3 were used while recordings were performed in the MGBv of anaesthetised ferrets. We used F_0s of 200, 400 or 800 Hz, which are close to the values commonly used in the previous psychoacoustic and electrophysiological studies (Moore et al. 1985; Hartmann et al. 1990; Lohr and Dooling 1998; Sinex et al. 2005; Klinge and Klump 2009; Klinge and Klump 2010; Fishman and Steinschneider 2010). Three mistuned harmonic positions were chosen based on the resolvability of harmonics in a HCT to explore differences in the responses to resolved (2^{nd}) and unresolved (8^{th}) harmonics, with the 4^{th} harmonic also included since the resolvability is dependent on the F_0 (Moore and Gockel 2011) and the transition point of the resulting sensation reported to be the 4^{th} to 6^{th} harmonics in humans (Moore et al. 1985). The degree of mistuning was incremented on a log scale according to the shape of mistuning detection psychometric functions in ferrets (Chapter 3). Thus, the frequencies of mistuned harmonics used were 400 Hz (2^{nd} harmonic of the MCT with a 200 Hz F_0) to 6.4

kHz (8^{th} harmonic of the MCT with a 800 Hz F_0), which covers the most sensitive region of the ferret's hearing range (Kelly et al. 1986).

Our results support the relevance of MGBv neurons for extracting precise temporal information in sounds. We found that the firing rate of the neurons increased when the frequency of the mistuned harmonic for MCTs with a low F_0 (200 or 400 Hz) was close to the unit CF. Interestingly, the firing rate slightly decreased in response to MCTs with a high F_0 (800 Hz). However, temporal response patterns distinctive to MCTs were observed at every F_0 tested, suggesting that changes in firing rate alone are insufficient to indicate the ability of MGBv neurons to detect a mistuned harmonic.

5.3. **Results**

The basic properties of neurons recorded in the MGBv in response to BBN and pure tones were described in the previous chapter. Here, responses to HCTs composed of 16 harmonics with a 200, 400 or 800 Hz F_0 are presented. When MCTs were used, the 2nd, 4th or 8th harmonic was shifted to a higher frequency by 0.05, 0.2, 0.8, 3 or 12% (e.g. Fig. 5.1). Therefore, we used MCTs with three different F_0s (200, 400 and 800 Hz), three different mistuned harmonic positions (2^{nd}, 4^{th} and 8^{th}) and five mistuning shifts (0.05, 0.2, 0.8, 3 and 12%) to explore the effect of the fundamental frequency, the mistuned harmonic position, and the degree of mistuning on MGBv neurons (see Appendix Table A.1).

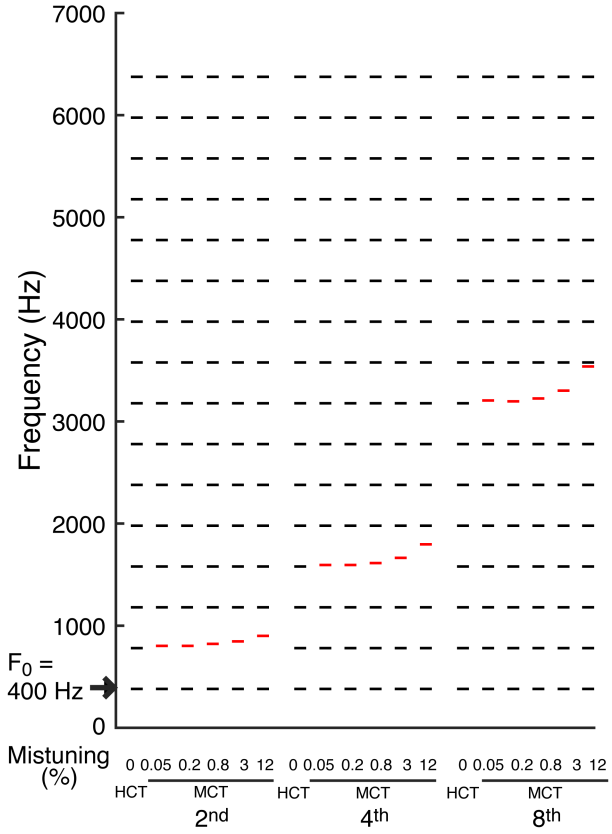

Figure 5.1 Examples of spectral components of complex tone stimuli.
Harmonic complex tones (HCT) comprised 16 harmonics with a 400 Hz fundamental frequency ($F_{0,}$ indicated by the arrow). For mistuned complex tones (MCT), the 2nd, 4th or 8th harmonic was shifted to a higher frequency by 0.05, 0.2, 0.8, 3 or 12% (shown from the left to the right in order). All harmonics are represented by the short horizontal lines, and the mistuned harmonics are highlighted in red. In this study, complex tones with a 200 or 800 Hz F_0 were also used and generated in the same way as the complex tones with a 400 Hz F_0.

Among the 57 units in the MGBv that presented sharp tuning curves (described in Chapter 4), 77% of the units (44/57) responded to complex tones (duration 350 ms). The response patterns were mainly 'sustained' with an onset peak (response window: peak 1-50 ms, sustained 51-350 ms, 68%, e.g. Fig.5.2A). Some units showed a single onset peak ('transient single on,' 9%, Fig. 5.2B), or with an accompanying offset component (response window 351-400 ms, 'transient multiple on/off,' 9%, e.g. Fig. 5.2C). Finally, two of the units showed an offset peak after a typical 'sustained' response pattern and were classified into 'sustained + off' (4%, e.g. Fig. 5.2D). Additionally, one unit presented an offset peak after the end of the tones, and the rest did not match to any of the response patterns mentioned above (7%, 3/44).

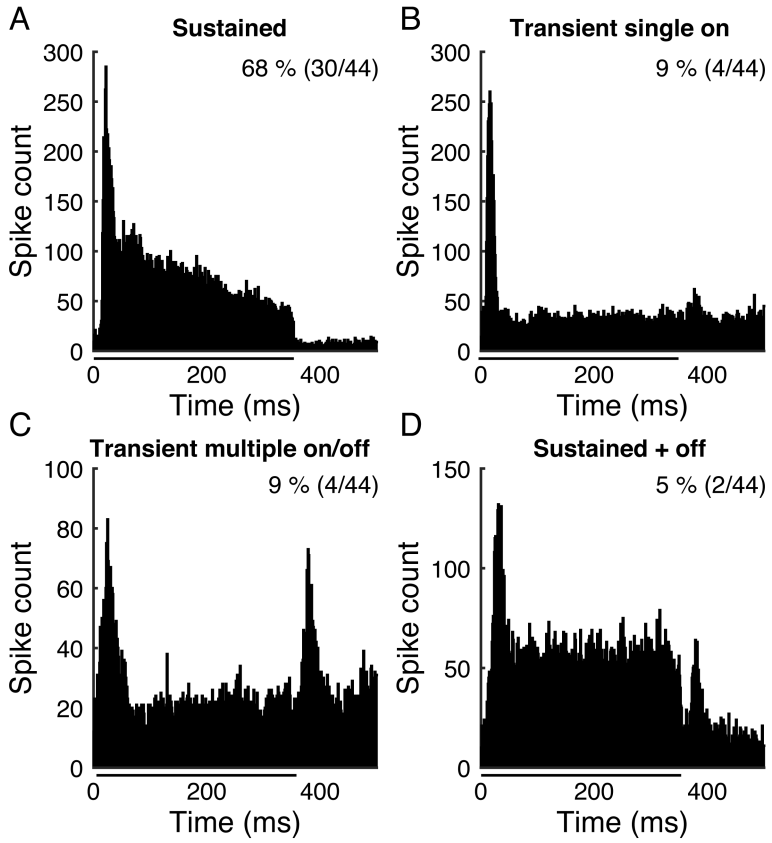

Figure 5.2 Examples of response patterns to complex tones in MGBv.
The majority of response patterns were 'sustained' (A). A minority produced a 'transient single on' pattern, as defined in Chapter 4 (B), 'transient multiple on/off' (C), or 'sustained+off' (D) response patterns. The proportion of each response pattern is shown in the right corner of each panel. The stimulus length was 350 ms shown by bar starting at time 0.

5.3.1. Effect of mistuning on firing rate

The firing rate of every recorded unit, excluding the four units with only offset or unclassified response pattern, was computed in the stimulus duration window (1-350 ms) for each stimulus combination grouped by F_0, mistuned harmonic position and mistuning shift.

Responses to MCTs with frequencies close to the unit CFs

One example of individual unit response is shown in figure 5.3, where complex tones (HCTs and MCTs) with a 200, 400 or 800 F_0 were presented. For MCTs, the harmonic at 1600 Hz (corresponding to the position 8^{th}, 4^{th} or 2^{nd} depending on the F_0 used) has been shifted to a higher frequency, from 0.05 to 12%, in each MCT stimulus used (Fig. 5.3A). Thus, in this example, the spectral distance between the mistuned harmonic (1,792 Hz for 12%) and the unit CF (1,091 Hz) is less than 0.7 octaves. After inspection of individual responses, we decided to use 0.7 octaves as a criterion to classify a response as close to unit CF. This follows the criterion used (0.5 octaves) in the previous study of A1 (Fishman and Steinschneider 2010). For the HCT with a 200 Hz F_0, the unit shows a 'transient multiple on/off' response pattern (Fig. 5.3B). However, when the 8^{th} harmonic of the HCT is shifted to a higher frequency by 12% (MCT, i.e. from 1600 Hz to 1792 Hz), it changes into a 'sustained' response pattern with an increased firing rate (Fig. 5.3C). Furthermore, the firing rate increases as the mistuning shift increases (0.05, 0.2, 0.8, and 3% in Fig. 5.3D).

This trend for increasing firing rate is also observed when HCTs and MCTs with a 400 Hz F_0 were presented. The unit shows a 'sustained' response

pattern to both the HCT and the MCT in which the 4th harmonic had been shifted to 1,792 Hz (12% mistuning) (Fig. 5.3E-F). The increased firing rate is observed at mistuning shifts > 0.2% (Fig. 5.3G).

The response pattern to complex tones with an 800 Hz F_0 is also 'sustained' for the same unit (Fig. 5.3H-I). Interestingly, however, the firing rate decreases when the 2nd harmonic was shifted to 1,792 Hz (12% mistuning). This decreasing trend is observed in all the cases with different degrees of mistuning (0.05-12%) (Fig. 5.3J). Since the unit CF of 1,091 Hz was close to the F_0 (800 Hz) in those cases, this may indicate that the unit responded well to the HCT and the firing rate decreased as the 2nd harmonic was shifted away from the CF.

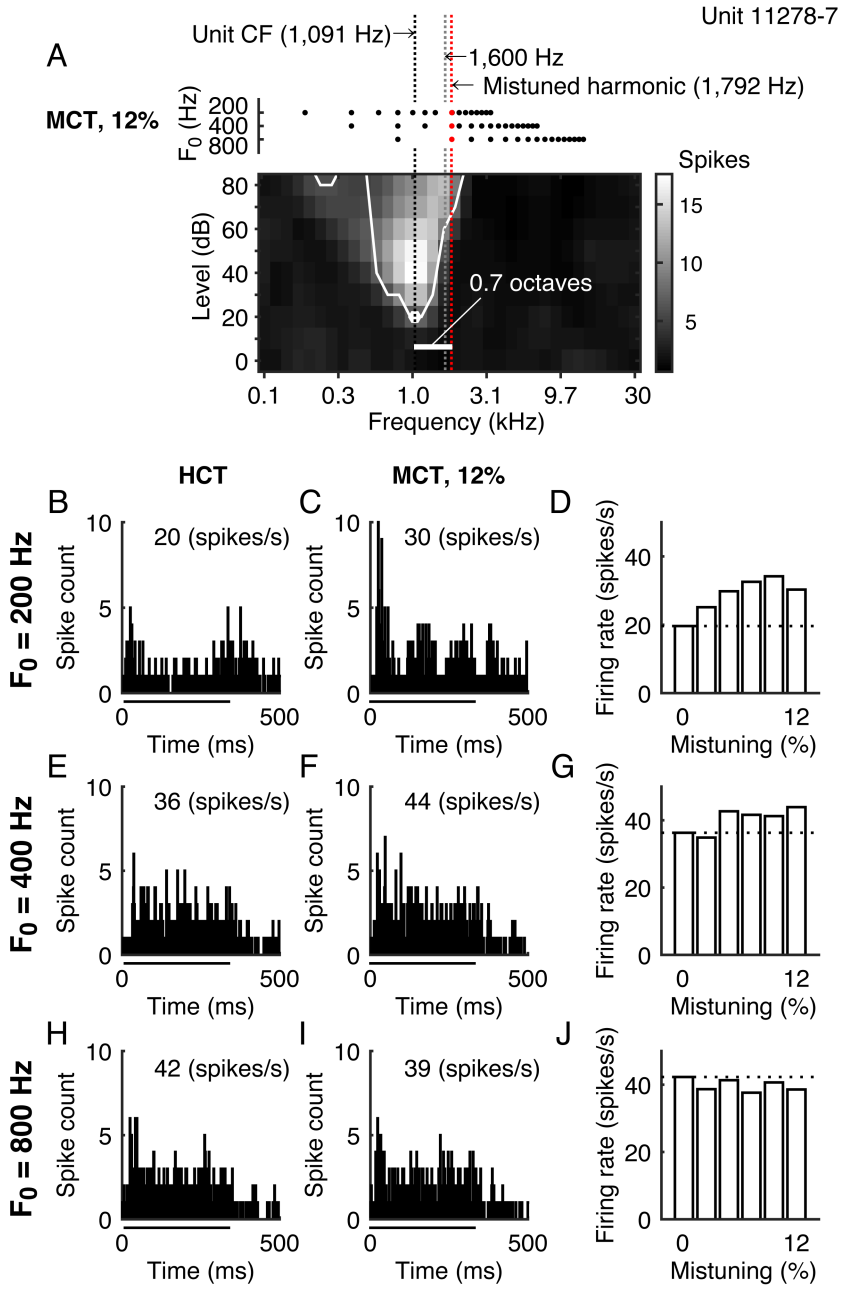

Figure 5.3 Example of firing rate change to different complex tones.
(A) Schematic of stimulus compositions and frequency response area. The characteristic frequency (CF) of the unit was 1,091 Hz, as indicated by the black dotted line. The mistuned harmonic (shown by the red dotted line) is shifted by 192 Hz (12%) from 1,600 Hz (shown by the grey dotted line) in the MCT. The spectral distance between mistuned harmonic and unit CF was 0.7 octaves and is indicated by the white thick horizontal line. The F_0 was 200, 400 or 800 Hz, and each harmonic is shown by the black dots at the upper part of the panel. The mistuned harmonics are highlighted in red. (B, E, H) The unit responded to each HCT with a 200 Hz F_0 (B), 400 Hz F_0 (E) or 800 Hz F_0 (H). The stimulus length was 350 ms shown by bar starting at time 0. The firing rate during the tone

presentation is shown in the upper-right corner of each panel. (C, F, I) The unit also responded to each MCT with a 200 Hz F_0 (C), 400 Hz F_0 (F) or 800 Hz F_0 (I). The degree of mistuning is 12% for the entire MCTs. (D, G, J) The firing rate increased with mistuning for the MCT with a 200 Hz F_0 (D) or 400 Hz F_0 (G) and decreased for the MCT with a 800 Hz F_0 (J). The degree of mistuning is indicated on x-axis from the left to the right: 0% (HCT), 0.05%, 0.2%, 0.8%, 3%, 12% mistuning. The horizontal dotted lines indicate the firing rate produced by the HCT.

Increase in firing rate when MCTs have a low F_0 and a large mistuning shift

The individual responses were pooled together across all penetrations when the spectral distance between the frequency of the mistuned harmonics and the unit CF was close (< 0.7 octaves). The majority of units (n = 38) were responsive to complex tones at every F_0, while only 4 units responded to only one or occasionally two particular F_0s.

With small individual variations, the responses to HCTs were very similar at every F_0 (One-way ANOVA; $F_{(2, 112)} = 2.7$, $P = 0.07$, Fig. 5.4A). Therefore, the change in firing rate when a harmonic is mistuned in a HCT was investigated by pairing responses to a MCT with the corresponding HCT and subtracting the firing rate of HCT from the MCT.

In order to understand the effect of the different degree of mistuning (mistuning shifts: 0.05, 0.2, 0.8, 3 and 12%), F_0 and mistuned harmonic position (2^{nd}, 4^{th} and 8^{th}), the difference of firing rate between MCT and HCT was computed for each case (Fig. 5.4B-C). Changes in the firing rate correlate with the degree of mistuning shift and depend on the F_0 (repeated measures ANOVA; mistuning, $F_{(4, 304)} = 7.7$, $P = 6.0\times10^{-6}$; mistuning × F_0, $F_{(8, 304)} = 2.3$, $P = 0.02$), but they are not dependent on mistuned harmonic position (mistuning × mistuned harmonic position, $F_{(8, 304)} = 1.2$, $P = 0.3$). Post hoc tests confirm the differences

between low and high F_0 (Tukey-Kramer; 200 Hz vs 800 Hz, P = 0. 0003; 400 Hz vs 800 Hz, P = 0.002; 200 Hz vs 400 Hz, P = 0.8).

The differences in firing rate (mean ± sem) between MCTs and HCTs stimuli are illustrated in figure 5.4B by the bars for each condition grouped by F_0 and mistuned harmonic position, with enhanced responses at low F_0 (200 and 400 Hz) and decreased responses at high F_0 (800 Hz). Based on trends observed in individual units, we conclude that firing rate increases when a mistuned harmonic is inserted in the HCT with a 200 or 400 Hz F_0, and the firing rate decreases when a mistuned harmonic is introduced in the HCT with a 800 Hz F_0 (two-tail paired *t* test; *P* values are shown in Fig. 5.4B).

To demonstrate that the degree of mistuning shift and the F_0 interact, firing rates of the recorded units were grouped by F_0 and by different degree of mistuning shift (Fig. 5.4C). The activity of the recorded neurons significantly increased for the MCTs with a 200 or 400 Hz F_0 when the degree of mistuning was $\geq$ 0.2 %, and decreased when the F_0 was 800 Hz, but in an inconsistent way with the degree of mistuning shift (two-tail paired *t* test; *P* values are shown in Fig. 5.4C).

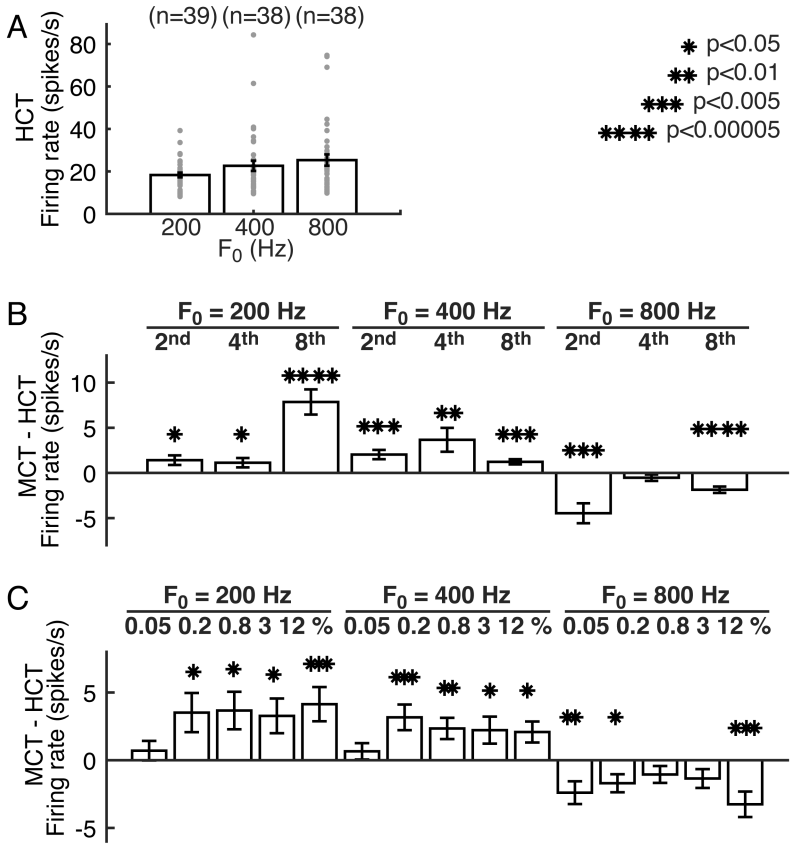

Figure 5.4 Change of firing rate to different complex tones when the frequency of mistuned harmonics was close to the unit CFs.

(A) There was individual variability in firing rate to the HCT with a 200, 400 and 800 Hz F_0 with trend for higher rates with increasing F_0 but no statistical significance. The bars indicate mean (± sem). The grey dots show the values for individual units. 40 units were analysed. The number of units responded to the HCT with an each F_0 is shown at the top of each bar. (B, C) The difference of firing rate was computed by subtracting the firing rate for the HCT from that of the MCT with the same F_0 for individual units. Mean firing rate increased in the MCT with a 200 or 400 Hz F_0 and decreased in the MCT with an 800 Hz F_0. In the MCT with a 200 or 400 Hz F_0, mean firing rate increased when the degree of mistuning was greater than 0.2%. The bars show the mean (± sem) for each stimulus condition grouped by F_0 and mistuned harmonic number (2^{nd}, 4^{th} or 8^{th}; B) or degree of mistuning (0.05%, 0.2%, 0.8%, 3% or 12%; C). The asterisks show the results of paired two-tail *t* tests between the responses to HCTs and MCTs. The number of asterisks represents *P* values as shown in the top right corner.

Units with low CFs show greater response differences between HCT and MCT stimuli

In order to demonstrate the effect of the CF of the recorded unit on the response to the HCTs and MCTs, the values of the firing rate to MCTs with 12% mistuning shift were plotted as a function of the firing rate to HCTs with the colour indicating the unit CF (Fig. 5.5). When MCTs used had a 200 or 400 Hz F_0, the values obtained increased greatly for CFs that range from 0.8 to 1.4 kHz (see green in Fig. 5.5A and B). On the other hand, the values for the MCTs with an 800 Hz F_0 were negative and uniformly distributed, indicating a firing rate decrease independent of CF (Fig. 5.5C). Overall, greater enhancement was observed at low CFs around 1 kHz, and this trend was also observed in the responses to MCTs with other degree of mistuning (0.2-3%).

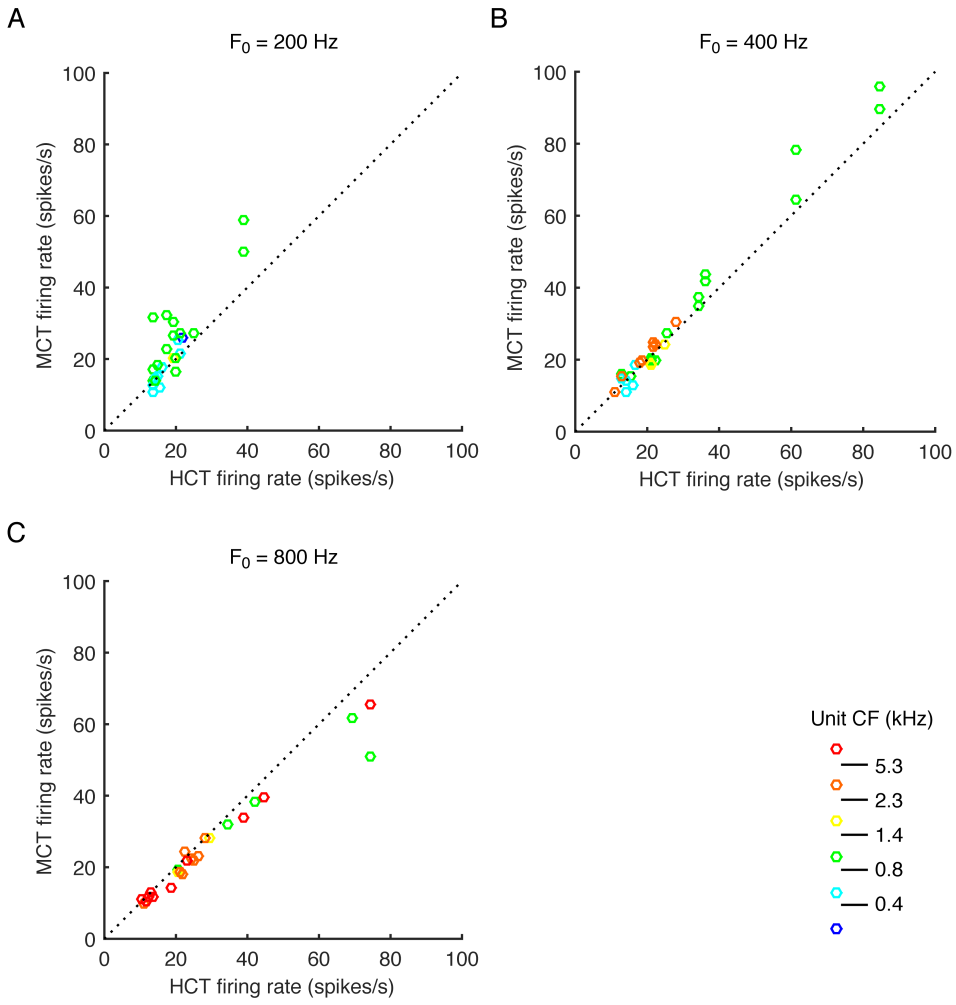

Figure 5.5 Effect of unit CF on the change in firing rate to mistuned complex tones. The firing rate for MCT (A, 200 Hz F_0; B, 400 Hz F_0; C, 800 Hz F_0) was plotted as a function of the firing rate for HCT when the frequency of mistuned harmonics was close to unit CFs. The figure shows the case of MCTs with 12% mistuning shift used. The most pronounced increase in firing rate occurred when the unit CF was low (0.8-1.4 kHz). Unit CFs are shown in different colours grouped into 6 categories with the middle 4 categories covering the same range of frequencies on a log scale from 0.4 to 5.3 kHz and the first and last categories comprising CFs < 0.4 kHz and > 5.3 kHz, respectively.

Enhanced responses are strong when the CF and the frequency of MCTs are close

In order to understand the effect of the spectral distance between the mistuned harmonic and the unit CF, and based on the fact that changes in the responses were observed even when each of these frequencies were not close, responses were categorised into three groups (Fig. 5.6A). The first group corresponds to a spectral distance between the frequency of mistuned harmonics and unit CF of less than 0.7 octaves; as previously mentioned this criterion was chosen based on inspection of individual responses (Group 1, 'Shift at CF'). The second group comprises the responses obtained when the frequency of the mistuned harmonics is > 0.7 octaves *below* the unit CF (Group 2, 'Shift at > 0.7 Oct *below* CF'), and the third group includes the data obtained when the frequency of the mistuned harmonics is > 0.7 octaves *above* the unit CF (Group 3, 'Shift at > 0.7 Oct *above* CF'). The firing rate was computed for each case and grouped by different F_0, and spectral distance.

The firing rate is dependent on the spectral distance between the frequency of the mistuned harmonic and the unit CF (repeated measures ANOVA; $F_{(8,\ 1360)} = 5.9$, $P = 2.0\times10^{-7}$). Post hoc tests revealed a strong effect on the responses when the frequency of the mistuned harmonic was close to unit CF (Tukey-Kramer; Group 1 vs Group 2, $P = 0.01$; Group 1 vs Group 3, $P = 0.0003$; Group 2 vs Group 3, $P = 0.69$).

In addition, the trend observed for the degree of mistuning shift and the F_0 is consistent with the results shown above when the frequency of the mistuned harmonic is close to unit CF (Group 1), with a significant effect of degree of mistuning ($F_{(4,1360)} = 13.1$, $P = 1.6\times10^{-10}$) and a significant interaction with the F_0

(mistuning × F_0, $F_{(8, 1360)} = 4.8$, $P = 6.8\times10^{-6}$). Post hoc tests also confirmed the presence of significant differences between low and high F_0 on the change in firing rate (Tukey-Kramer; 200 Hz vs 800 Hz, $P = 8.6\times10^{-9}$; 400 Hz vs 800 Hz, $P = 9.6\times10^{-10}$; 200 Hz vs 400 Hz, $P = 0.62$).

The differences in firing rate between MCT and HCT for each case, grouped by spectral distance between the mistuned harmonic and the unit CF at different F_0s, are shown in figure 5.6B (bars show the mean ± sem). This shows that larger changes in firing rate occurred when the spectral distance is close. These histograms also show that the response increase is larger for the MCTs with a 200 or 400 Hz F_0 when the mistuned harmonic is close to the unit CF, whereas the firing rate declines for the MCTs with an 800 Hz F_0 at all spectral distances (two-tail paired *t* test; *P* values are shown in Fig. 5.6B).

Firing rates were also computed for different degree of mistuning and F_0, and grouped by the spectral distance category. Consequently, differences in activity between MCTs and HCTs were plotted as a function of the degree of mistuning (Fig. 5.6C-D). As expected, the largest increase in firing rate occurred when the frequency of the mistuned harmonic was close to the unit CF (solid line in Fig. 5.6C), although enhanced responses were also observed for the MCTs with a 400 Hz F_0, when the frequency of the mistuned harmonic was above the CF (dashed line in Fig. 5.6C). The responses to the HCT and MCT were clearly distinct for a mistuning of just 0.2% (Tukey-Kramer, 0.2%, $P = 0.001$).

In contrast to the results obtained with the lower F_0 values, a lower firing rate was found for MCTs with an 800 Hz F_0, irrespective of the degree of mistuning (Fig. 5.6D). The only exception to this was observed for the largest

harmonic shift (12% mistuning), where a smaller reduction in response occurred when the frequency of the mistuned harmonic is below the unit CF (Tukey-Kramer, Shift at > 0.7 Oct *below* CF vs Shift at > 0.7 Oct *above* CF, $P = 0.005$). This last result seems to reflect the spectral distance between the mistuned harmonic and unit CF. As the degree of mistuning increases, a mistuned harmonic below unit CF will be shifted toward CF. On the other hand, if the mistuned harmonic is above CF, it is shifted progressively further away from CF as the degree of mistuning increases. This does not seem to be the case, however, for the MCTs with a low F_0 (Fig. 5.6D), where the increase in firing rate is dependent on the degree of mistuning *per se*. Thus, the response increases even when the mistuned harmonic is shifted away from CF as the degree of mistuning increases.

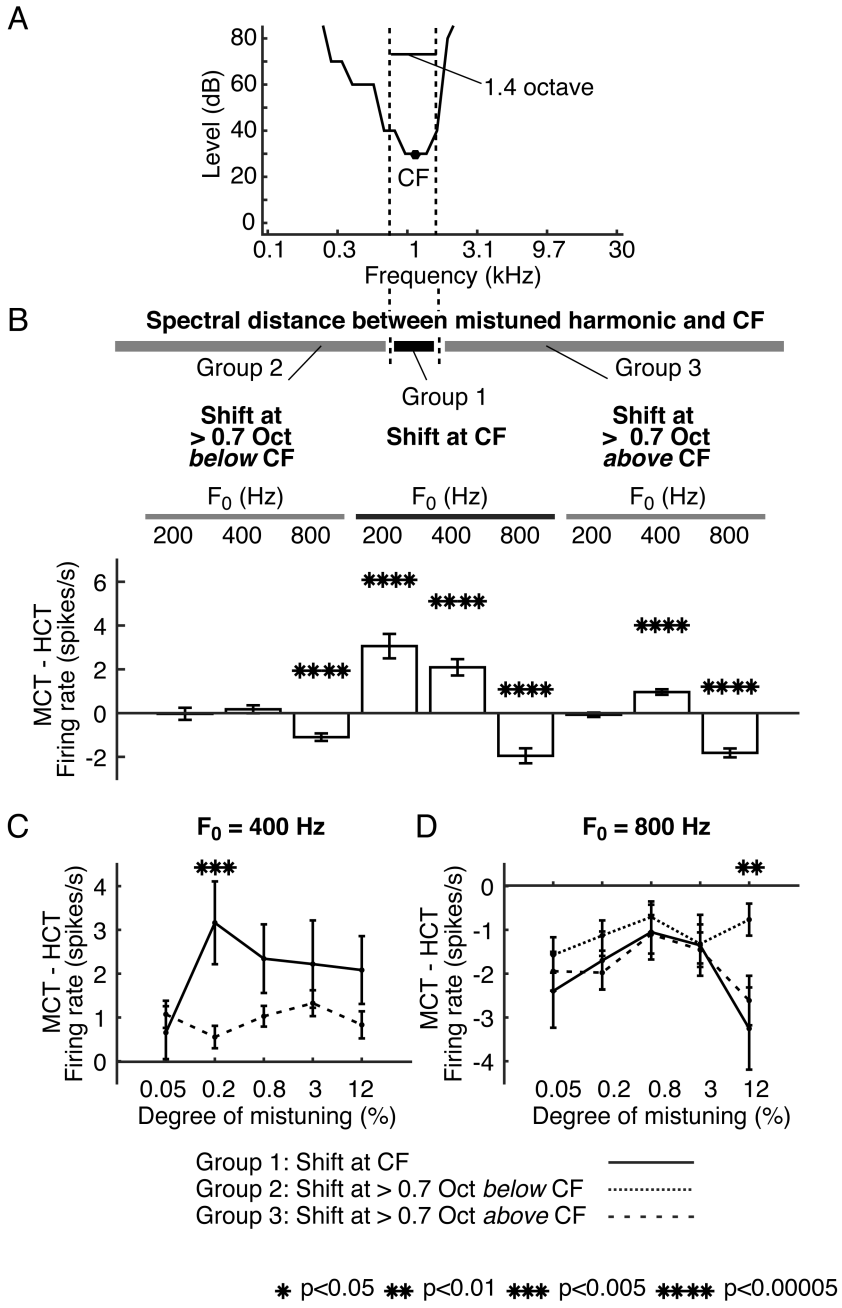

Figure 5.6 Effect of spectral distance between mistuned harmonic and unit CF on firing rate.

(A) Schematic of frequency response area to indicate the spectral distance between the frequency of the mistuned harmonic and the unit CF. The dotted lines indicate where the distance is 0.7 octaves. The black horizontal line indicates a range of 1.4 octaves. (B) The difference of firing rate between MCT and HCT was computed, and the mean (± sem) for each stimulus condition grouped by F_0 and mistuned harmonic number is shown by the bars. The difference was larger when the spectral distance was less than 0.7 octaves (Group 1, Shift at CF). When the mistuned harmonic was > 0.7 octaves *above* or *below* CF (Group2, Shift at > 0.7 Oct *below* CF; Group3, Shift at > 0.7 Oct *above* CF), the change

was smaller. For the MCTs with an 800 Hz F_0, a decreased firing rate was observed regardless of the spectral distance. (C, D) The difference of firing rate between MCT and HCT (mean ± sem) is plotted as a function of degree of mistuning. (C) When the F_0 was 400 Hz, the firing rate increased for the mistuned complex tones with 0.2 to 12% mistuning when mistuned harmonics are close to unit CF (Group1, solid line) compared with the responses obtained when mistuned harmonics are > 0.7 octave *above* unit CF (Group3, dashed line). (D) When the F_0 was 800 Hz, the change of firing rate was similar at different spectral distances and independent of the degree of mistuning. The dotted line indicates the values obtained when the mistuned harmonic was > 0.7 octaves *below* CF (Group 2). The coloured asterisks show the results of two-tail paired *t* test between HCTs and MCTs. The black asterisks show the results of Tukey-Kramer tests after repeated measures ANOVA. The number of asterisks represents the *P* values, as shown in the right bottom.

5.3.2. Effect of mistuning on temporal response pattern

To understand the effect of the F_0, the mistuned harmonic position, and the degree of mistuning shift on the temporal response patterns of MGBv neurons, a set of MCTs was presented (F_0, 200, 400 or 800 Hz; mistuned harmonic position, 2^{nd}, 4^{th} or 8^{th}; degree of mistuning shift, 0.05, 0.2, 0.8, 3 or 12%).

The MCTs elicited distinctive response patterns, which were apparent in the post stimulus time histogram (PSTHs) (e.g. Fig. 5.7). Temporal modulation is usually better observed in sustained responses, as the firing of the neurons can potentially phase lock to the periodicities of envelope and beating of sound. Thus, the temporal analysis was focused on the 32 units in the MGBv with 'sustained' or 'sustained + off' response pattern, excluding the onset component in the first 50 ms of the response. Among these, 22 units showed characteristic temporal response patterns to MCTs. Vector strength (VS) values were obtained and their significance assessed using Rayleigh statistics (Goldberg and Brown 1969; Lu and Wang 2000) (e.g. Fig. 5.7).

The stereotypical responses to MCTs observed in IC neurons (Sinex et al. 2002; Sinex et al. 2005) were phase locking to the periodicity of F_0 of the MCT

(F_0) and the beats created by the interaction between mistuned harmonic and next higher harmonic (*Beating*). Interestingly, it also showed synchronized responses to the envelope of the MCT or the periodicity corresponding to the degree of mistuning. Thus, the degree of mistuning shift in hertz was assigned to *Mistuning*. This modulation is thought to arise from the beats from two phase locked inputs of F_0 and *Beating*. Moreover, the temporal responses also showed the periodicity corresponding to the frequency difference of *Beating* and *Mistuning,* and we called this periodicity *Interaction* (see Chapter 2 Methods for further details). In addition, *Mistuning* usually corresponded to the periodicities of envelope, although *beating and interaction* represented it for some of cases (see Appendix).

Phase locking to mistuning is present in MGBv units

Responses to MCTs showed synchronized response patterns corresponding to the phase change due to mistuning. For example, when the MCT with a 200 Hz F_0, in which the 8th harmonic was shifted to 1,612 Hz (0.8%), was presented to a unit in the MGBv with a CF of 1,188 Hz, the resulting PSTH revealed synchronized responses with a periodicity of ~81 ms (Fig. 5.7A). The periodicity was confirmed by the presence of statistically significant synchronized responses at 10, 13, 23, 400 and 413 Hz (Rayleigh test, Fig. 5.7B). The largest peak was found at 13 Hz (VS = 0.46), which corresponds to the expected periodicity (81 ms) for 12 Hz *Mistuning*. This is the envelope periodicity of the MCT (see Appendix Fig. A.2). The peak at 23 Hz seems to correspond to half this value (43 ms), while peaks at 400 and 413 Hz are likely to be rectifier distortion products of the F_0. These half-length periodicities were observed due to the symmetric pattern from peak to

peak (or from valley to valley) in the periodic responses that can be recognized as another periodicity of peak to valley that is half the periodicity from peak to peak in the temporal analysis.

For the corresponding HCT with the same F_0, no specific temporal response pattern was observed (Fig. 5.7C), with only a weak onset and a strong offset response (small inset in panel C), but no peak in the plot of VS against frequency was observed that could indicate periodicity (Fig. 5.7D).

Another example unit is plotted in Fig. 5.7E, F, which shows a synchronized response pattern corresponding to the F_0 (200 Hz). The PSTH shows 5 ms periodic response (Fig. 5.7E), and the synchronized responses observed at 200 Hz were highly significant, which supports phase locking to the 200 Hz F_0. This unit also showed an 81 ms periodic temporal response pattern when the same MCT was presented (data not shown). Both of the unit CFs were 1,188 Hz.

These two examples are representative of the units recorded in the MGBv, and the results suggest that the temporal response patterns in MGBv neurons can be synchronized to *Mistuning* and can be specific to MCTs.

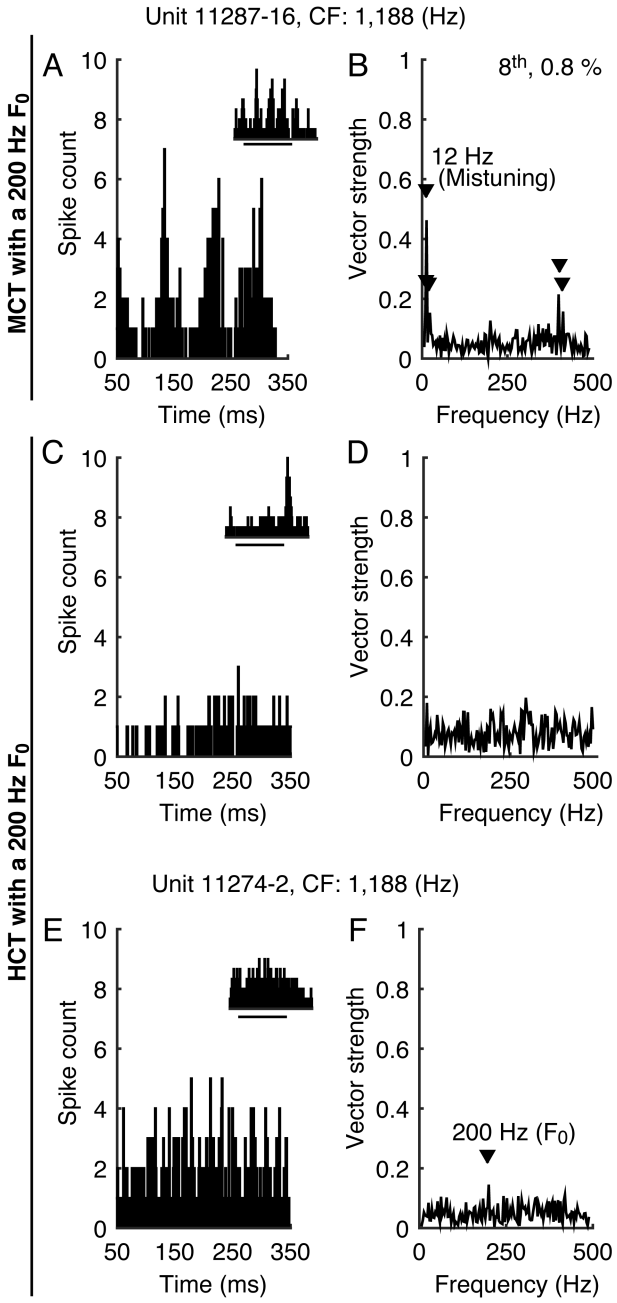

Figure 5.7 Examples of temporal response patterns to harmonic and mistuned complex tones.

(A, B) Synchronized response to the temporal structure of MCTs was observed. (A) The PSTH for the stimulus presentation time from 51 to 350 ms (sustained response window) indicates a response with a period of 81 ms. The small PSTH in the right corner shows the responses for the stimulus presentation from 1 to 350 ms and subsequent 150 ms of silence. The sustained response window is shown by the bar starting at time 50 under the small PSTH. (B) Vector strength values were computed from the PSTH. A statistically significant peak (Rayleigh test, $P < 0.001$, indicated by the downward-pointing triangle) was observed at 12 Hz, which corresponds to 81 ms periodicity and 0.8% mistuning (12

Hz). In the MCT, the 8th harmonic of the HCT with a 200 Hz F_0 was shifted to a higher frequency by 0.8%. (C, D) Although the firing of this unit was strongly modulated by the MCT, it did not response to the HCT with a 200 Hz F_0 in the sustained response window. The small PSTH shows weak onset and strong offset peaks. No significant peak was detected by the Rayleigh test. (E, F) A different unit showed phase locked response to the 200 Hz F_0 of the HCT. (E) The PSTH showed 5 ms periodic responses in the sustained response window. (F) A significant peak was observed at 200 Hz, which corresponds to the 5 ms periodicity and the 200 Hz F_0. Both units (A-D and E,F) had the same CF of 1,188 Hz.

Phase locking is also found for MCTs with high F_0 and small mistuning

Complex temporal response patterns were observed when the MCTs with a 400 Hz F_0 were used. For example, when the 2nd harmonic was shifted to 896 Hz (12%), the response showed statistically significant synchronized responses at 95 and 305 Hz (Fig. 5.8A). The peak at 305 Hz represented the *Beating* created by the interaction between the next harmonic and the mistuned harmonic (1200 - 896 = 304 Hz), and the peak at 95 Hz corresponded to the *Mistuning* (400 - 304 = 96 Hz). When the 4th harmonic of the HCT was shifted to 1792 Hz (12%) for the same recorded unit, the response showed statistically significant synchronized responses at 16, 190, 194, 207 and 400 Hz (Fig. 5.8B). The peak at 400 Hz is the F_0. The peak at 207 Hz corresponds to the *Beating* (2000 - 1792 = 208 Hz), and the peaks at 190 and 194 Hz represent the *Mistuning* (400 - 208 = 192 Hz). 16 Hz could be explained as the modulation between the *Beating* and *Mistuning* (208 – 192 = 16 Hz). The same kind of periodicity has been reported in the IC (Sinex et al. 2002; Sinex et al. 2005).

Phase locking to mistuning harmonics and beats were also observed when MCTs with a high F_0 (800 Hz) were used. When the 2nd harmonic was shifted to 1649 Hz (3%), we observed statistically significant synchronized

responses at 49 and 98 Hz (Fig. 5.8C). The peak at 49 Hz corresponds to the *Mistuning*, and the peak at 98 Hz represents the first harmonic of the *Mistuning* (49 Hz). The unit CF was 920 Hz. In addition, when the 4th harmonic was shifted to 3298 Hz (3%), the response showed statistically significant synchronized responses at 98 Hz (Fig. 5.8D). The peak at 98 Hz corresponds to the *Mistuning*. The unit CF was 1,188 Hz, and this is the same unit from figures 5.7A-D and 5.8A-B. Thus, this indicates that responses can synchronize to different periodicities regardless of F_0, mistuned harmonic position and even the periodicities created by the beats.

Furthermore, responses showed phase locking to small mistuning. When the 8th harmonic was shifted to 6,413 Hz (0.2%) in the HCT with an 800 Hz F_0, the statistically significant synchronized response were observed at 13 Hz (Fig. 5.8E). The peak at 13 Hz is phase-locking to the *Mistuning*. The unit CF was 1,091 Hz.

Finally, when the 8th harmonic was shifted to 7,168 Hz (12%) in the HCT with an 800 Hz F_0, the response showed statistically significant synchronization at 33 Hz (Fig. 5.8F). The peak at 33 Hz corresponds to the *Beating* (7,200 – 7,168 = 32 Hz). This is the same unit as the previous example.

These examples are representative of the recorded units in the MGBv. Our results indicate that phase locking to the beats and amplitude modulation in the envelope of MCTs can be observed even if F_0 is relatively high and the degree of mistuning small. Phase locking was widely found in different F_0s and mistuned harmonic positions and was clearly observed for HCTs with large degrees of mistuning (3 to 12%), although some units showed phase locking to 0.2 and 0.8% mistuning (e.g. Fig. 5.7 A-B and 5.8E). These temporal response patterns to small mistuning were observed, showing phase-locking to either the periodicities of

envelope or beating at least, in 25% of the units (8/32) recorded in our sample of MGBv neurons that showed sustained responses and potentially can synchronize to a specific periodicity.

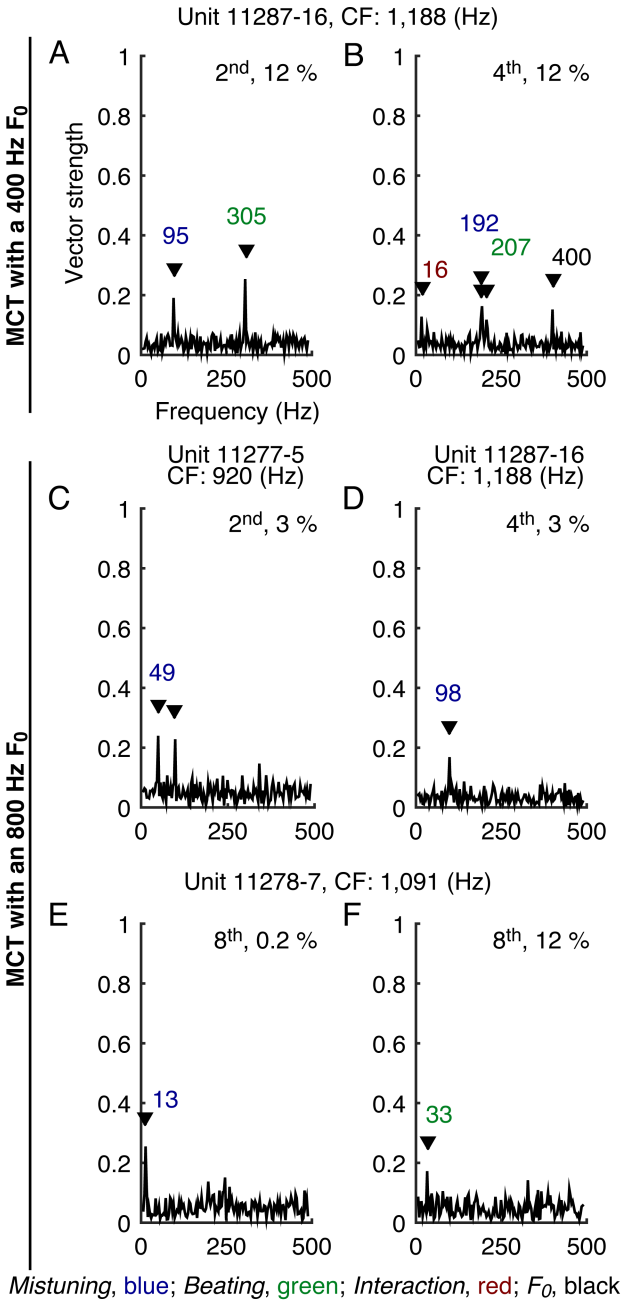

Figure 5.8 Examples of temporal response patterns to the mistuned complex tones with a high F_0 or small mistuning.
Periodic responses were analysed as in figure 5.7, and the results are presented in the same

format. (A, B) Complex periodic responses with beating were observed for the MCT with a 400 Hz F_0. (A) When the 2nd harmonic was shifted by 12%, periodic responses were observed with the peaks at 95 Hz corresponding to the *Mistuning* (shown in blue) and at 305 Hz corresponding to the *Beating* between the next (3rd) harmonic and mistuned harmonic (shown in green). (B) When the 4th harmonic was shifted by 12%, complex periodic responses were observed with peaks at 192 Hz (*Mistuning*), 207 Hz (*Beating*), 16 Hz, corresponding to the *Interaction* between the frequency of the beat and that of the mistuned harmonic (shown in red), and 400 Hz, corresponding to the F_0 (shown in black). (C, D, E, F) Periodic responses were observed for the MCT with a high F_0 (800 Hz). (C) When the 2nd harmonic was shifted by 3%, peaks were observed at 49 Hz (*Mistuning*) and 98 Hz, which is a half-length of the mistuning periodicity. (D) When the 4th harmonic was shifted by 3%, peaks were observed at 98 Hz (*Mistuning*). (E) Temporal response pattern observed for another unit for an MCT with small mistuning. When the 8th harmonic was shifted by 0.2 %, a peak was observed at 13 Hz (*Mistuning*). (F) When the higher (8th) harmonic was shifted by 12%, a peak was also observed at 33 Hz (*Beating*). The unit CFs are indicated at the top of each panel.

Phase locking to MCTs is present in low CF units

To visualize the temporal response patterns produced by different MCTs, the vector strength values were shown for all the significant peaks corresponding to expected periodicities of the F_0, envelope and beating (see Chapter 2 Methods and Appendix Table A.1) in figure 5.9. Phase locking was more likely to be observed in the units with low CFs. This was especially the case for units with CFs lower than 0.9 kHz, which tended to show phase locking for the MCTs with a 200 Hz F_0 (Fig. 5.9A). Units with 0.9-2 kHz CF showed phase locking to the envelope periodicities not only to the MCTs with a 200 Hz F_0, but also to those with a 400 or 800 Hz F_0 (Fig. 5.9B). The vector strength values suggest that the phase locking is stronger when the F_0 is 200 or 400 Hz. In the units with a CF above 2 kHz, phase locking to MCTs was rarely observed. For some cases, the phase locking to beating was observed when the frequencies of mistuned harmonics were from 400 to 1600 Hz (Fig. 5.9C).

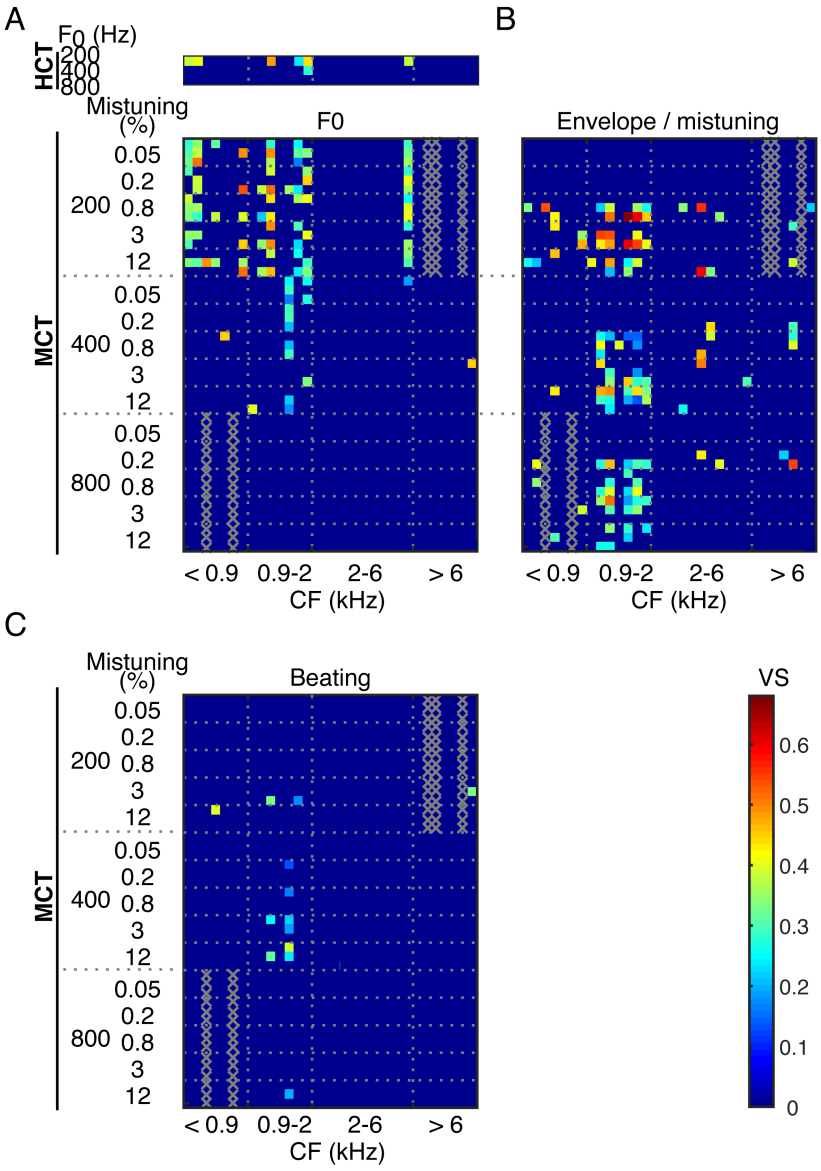

Figure 5.9 Effect of unit CF on temporal response patterns.
Phase locked responses were observed in units with low CFs. The vector strength values at the significant peaks corresponding to the periodicities of F_0 (A), envelope (B) and beating (C) (see Chapter 2 Methods and Appendix Table A.1) were shown by the colour scale. One column represents each unit, and the 32 units with sustained responses are displayed according to the unit CFs on the x-axis. The grey dotted vertical lines indicate grouping by the unit CFs. Responses to a set of complex tones are shown grouped by the F_0 (200, 400 or 800 Hz), the degree of mistuning (0.05, 0.2, 0.8, 3 or 12%) and the mistuned harmonic number (2^{nd}, 4^{th} or 8^{th}). The grey dotted horizontal lines indicate grouping by F_0 and the degree of mistuning. In each of these groups, the responses to the 2^{nd}, 4^{th} and 8^{th} mistuned harmonic position are lined up vertically in a column from top to bottom, respectively. The VS was also computed for each HCT and shown at the top of the panel A. The grey crosses indicate a lack of response to a specific F_0.

5.4. **Discussion**

This study demonstrated for the first time that MGBv neurons are sensitive to harmonic and mistuned complex tones (HCTs and MCTs). In A1, the firing rate of the MGBv neurons changed significantly when we switched from HCTs to MCTs and when they were tuned to the frequency of mistuned harmonic (Fishman and Steinschneider 2010). Distinct temporal response patterns were produced in response to the MCTs, regardless of the spectral distance between the mistuned harmonic and unit CF, as reported in the IC (Sinex et al. 2005). Our results also showed that the synchronized responses represent the beating and amplitude modulation in the envelope of MCTs with small mistuning (0.2-0.8%). This is consistent with previous studies that focused on the responses of neurons in other parts of the auditory pathway to large mistuning values (>3 %) (Sinex et al. 2002; Sinex et al. 2005; Fishman and Steinschneider 2010), indicating that MGBv is likely to be an important component of the IC-MGBv-A1 pathway in the processing of precise temporal information that contributes to auditory scene analysis.

Enhanced responses represent spectral information in mistuned harmonics

The firing rate of MGBv neurons in response to MCTs increases when the frequency of the mistuned harmonic is close (< 0.7 octaves) to the unit CF and when the F_0 was low (200 and 400 Hz) (Fig. 5.6B). In the IC, firing rates also increase for MCTs compared with HCTs (Sinex et al. 2005), however, it seems enhanced responses were not correlated with the unit CF (Sinex et al. 2002). Fishman and Steinschneider (2010) reported that response enhancement on A1 was

greater when the spectral distance between the mistuned harmonic frequency and the unit BF (best frequency instead of CF, representing the frequency with highest firing rate response instead of the frequency at which the neuron responds at lowest sound intensity) was less than 0.5 octaves. However, their experimental design was slightly different from the present study as the mistuned harmonic was fixed at the unit BF and the F_0 was shifted by 16 % upward or downward to generate mistuning.

In the present study, the firing rates to MCTs decreased when the F_0 was high (800 Hz) (Fig. 5.6B). This was also observed in A1 when the 3rd harmonic of the HCTs was at the unit BF and shifted upward or downward for the MCTs (Fishman and Steinschneider 2010), which is close to our strategy of generating a mistuned condition.

Our finding of both enhanced and reduced responses with MCTs may be understood from consideration of the fundamental frequency of the sounds used. Sinex and colleagues used relatively low F_0s around 200-250 Hz in the IC (Sinex et al. 2005). Fishman and colleagues used a wide range of F_0s from 125 to 1000 Hz in A1, and they showed enhanced responses to the MCTs with a low F_0 (around 200-350 Hz) in individual units (Fishman and Steinschneider 2010). Although the response changed in opposite directions for low and high F_0s, our finding that the magnitude of this change was greater when the mistuned harmonic and the unit CF/BF was close is consistent in MGBv and A1. The enhanced responses have been interpreted as a neural correlate of the perceptual 'pop out' experienced by human listeners (Moore et al. 1985; Hartmann et al. 1990; Alain et al. 2001; Alain et al. 2002; Fishman and Steinschneider 2010). In humans, a mistuned harmonic is

heard to pop out from the HCT if it is a low-frequency resolved tone (Moore et al. 1985; Moore et al. 1986). However, in our results, an increase in firing rate was observed when the 8th harmonic, which is assumed to be unresolved by cochlear filtering, was mistuned in HCTs with a 200 or 400 Hz F_0 (Fig. 5.4B). In addition, the spectral distance between mistuned harmonic and unit CF did not have a consistent effect on the reduction in firing rate correlated with the degree of mistuning (Fig. 5.6D). Thus, the firing rate change might not just reflect responses to the spectral composition of MCTs. Compared to the study in A1, increased firing rate in IC was only investigated with limited F_0s and mistuned harmonic positions, and the effect of spectral distance between unit CFs and the frequencies of mistuned harmonic needs to be examined further. In order to understand the differences in IC - MGBv - A1, comparison of responses in these stages using the same stimulus set and condition would be important.

Temporal periodicity cues of sound is represented in the responses by MGBv neurons

Phase locking corresponding to the periodicities of MCTs has been found in neurons recorded in the CN, IC and A1 (Sinex et al. 2002; Sinex et al. 2005; Sinex 2008; Fishman and Steinschneider 2010). Synchronized responses have been observed to the F_0, to the mistuning, and to the beating created by interactions between mistuned and neighbouring harmonics (Sinex et al. 2002; Sinex et al. 2005; Sinex 2008; Fishman and Steinschneider 2010). In the present study, phase locking to mistuning and beating was observed in the MCTs with different F_0s (200, 400 or 800 Hz). Although phase locking to all the MCTs with different F_0s was

observed in units with a CF of 0.9-2 kHz, units with CFs up to 6 kHz also showed phase locking to a part of the stimulus set (Fig. 5.9). Thus, the capacity to synchronize to some aspect of the stimulus periodicity is not limited by the upper limit of phase locking to tones in the ferret auditory nerve (Sumner and Palmer 2012). Our results agree with the previous study in the IC, where phase locking to MCTs with a 250 Hz F_0 was universally observed in neurons with CFs that ranged from 0.25 to 5.9 kHz (Sinex et al. 2005). In A1, temporal response patterns are more likely to be observed in low BF neurons, leading to the suggestion that cortical neurons possess dual mechanisms for representing mistuned sounds involving the detection of low frequency components on the basis of temporal cues by neurons with low BFs and detection of high frequency components using spectral cues by neurons with high BFs (Fishman and Steinschneider 2010).

In the MGBv, however, temporal response patterns synchronized to the MCTs were observed in the example unit that increased its firing rate in response to MCTs (e.g. Fig. 5.3B-D). Furthermore, the firing rate decreased for the MCTs with a high F_0, while the units showed distinctive temporal response patterns. This suggests that the basis for detecting mistuning in MGBv is not clearly segregated into spectral and temporal cues dependent on the frequency of mistuned harmonics. In our experiments, firing rate was slightly higher for the HCT with a high F_0 (Fig. 5.4A), probably because the units recorded were biased to low CFs around 1 kHz, which might therefore show better responses to the HCT with a F_0 of 800 Hz. We speculate that the firing rate of MGBv neurons may be modulated so that they have precise temporal response patterns and that corticothalamic projections from A1 to the MGBv might contribute to this (Ryugo and Weinberger 1976; Villa et al. 1991;

He 1997; He et al. 2002). Phase locking to pure tones has been observed up to 520 Hz in guinea pig MGBv (Wallace et al. 2007), which is a sufficient range to represent the temporal periodicity cues of MCTs. On the other hand, the upper limit of phase locking is lower at 250 Hz in AC of the same species (Wallace et al. 2002), where both temporal and rate coding are used for representing stimulus periodicities (Langner 1992; Lu et al. 2001; Wang et al. 2008). In addition to transmitting fine temporal information to A1, MGBv may partially transform these signals into the rate code used by the cortex.

Implications for psychoacoustic tests using MCTs

The present study shows that both spectral and temporal information is represented in the responses of ferret MGBv neurons. Changes in firing rates were greater when the spectral difference between mistuned harmonic and unit CF was small, and temporal response patterns were synchronized with the beating and amplitude modulations that characterise MCTs.

It seems likely that, like other animal species, ferrets rely largely on temporal information, since their auditory nerve fibres are relatively broadly tuned and similar to smaller animals with a short cochlea (Fay 1992; Klinge et al. 2010; Sumner and Palmer 2012), while behavioural studies suggest that they use temporal periodicity cues in unresolved harmonics to discriminate HCTs (Walker et al. 2014). However, they do seem to have a capacity to use spectral information. We found that the mistuning detection threshold was 0.8 ± 0.1 Hz in ferrets when the F_0 was 400 Hz and the 4^{th} harmonic was shifted to a higher frequency (Chapter 3). In percentage terms, this threshold is equivalent to approximately 0.05%

mistuning. The psychometric curve of *d'* against mistuning showed that maximal performance was found for mistuning of 3 Hz (Fig. 3.2A), which corresponds to 0.2% mistuning. The range of mistuning where we observed an increase in firing rate of MGBv neurons to the MCTs with a 400 Hz F_0 is consistent with the behavioural thresholds.

Synchronized responses were observed in the MGBv for 0.2 to 12% mistuning of the stimulus. One unit showed phase locking to the periodicity around 400 Hz when the 4^{th} harmonic was shifted by 0.8 Hz (0.05%), while it did not have any specific periodicity in its response to the HCT. Therefore, the temporal modulations in the neural responses are also found for harmonic shifts close to the thresholds measured behaviourally. As discussed above, if temporal information is changed into a rate code toward higher levels of the auditory pathway, it would seem that the threshold for mistuning detection in ferrets is likely based on the temporal periodicity cues of the responses that has a subcortical origin.

The ability to detect a mistuned harmonic is thought to depend on the degree of mistuning, the F_0 and the mistuned harmonic position (Moore et al. 1985; Moore et al. 1986; Hartmann et al. 1990; Lohr and Dooling 1998; Klinge and Klump 2009; Klinge and Klump 2010). A psychoacoustic study in humans has shown that the ability of listeners to detect a mistuned harmonic improves with increasing F_0 and harmonic number, whereas another study showed that this matches the frequency range over which neural synchrony observed in the cat auditory nerve fibres (Moore et al. 1985; Hartmann et al. 1990). We found that MGBv neurons increased their firing rate in response to MCTs with a low F_0, whereas the opposite occurred for MCTs with a high F_0 (Fig. 5.6B-C and Fig. 5.8).

Moreover, distinctive temporal response patterns were observed even when the F_0 of the MCT was high (Fig. 5.8 and 5.9), indicating that the neurons are sensitive to harmonic mistuning in HCTs with a high F_0.

Sensitivity to mistuned harmonics has been examined previously in gerbils, which have a similar low frequency hearing range to ferrets (Ryan 1976; Kelly et al. 1986). Moreover, gerbils seem to rely primarily on temporal fine structure for mistuning detection (Klinge and Klump 2009). Their thresholds were better when the same harmonic was mistuned in an HCT with a F_0 of 800 Hz compared to an HCT with a 200 Hz F_0 and indistinguishable when the frequency of the mistuned harmonics was matched (e.g. comparing thresholds for detecting a mistuned 8^{th} harmonic in an HCT with a 200 Hz F_0 and a mistuned 2^{nd} harmonic in an 800 Hz F_0 HCT – i.e. a 1,600 Hz tone in each case) (Klinge and Klump 2010). If ferrets also rely on temporal periodicity cues for mistuning detection, as suggested by our MGBv data, we would expect them to show a comparable behavioural ability to gerbils to detect a mistuned harmonic in an HCT with a high F_0.

Finally, as already mentioned, our recordings were dominated by units with low CFs. Although the CF range was appropriate to cover the frequencies of mistuned harmonics from 400 Hz to 6,4 kHz and to examine the effect of different F_0s and degrees of mistuning, it was inevitable that units with CFs around 1 kHz may have overrepresented the trends observed in this study. To build up the findings presented here, neurons with a broader range of CFs should be explored using HCTs and MCTs with different parameter values for the F_0, mistuned harmonic positions and degree of mistuning.

Concluding remarks

The aim of this study was to investigate how thalamic neurons respond to MCTs. By exploring responses to various MCTs composed with different F_0s changing mistuned harmonic number and degree of mistuning, we revealed the following six points. First, MGBv neurons are sensitive to MCTs. Second, relative to HCTs, firing rate increased for the MCTs with a low F_0. Third, firing rate decreased in the MCTs with a high F_0. Fourth, the increased firing rate was greater when the spectral distance of the mistuned harmonic frequency and unit CF is close. Fifth, phase locked responses to the temporal periodicity cues of MCTs were prominent for units with low CFs (0.9-2 kHz), but were also observed in units with CFs up to 6 kHz.

MGBv neurons represent spectral and temporal information in MCTs. As in A1, firing rate was strongly affected when MCTs were presented to neurons that were tuned to the mistuned harmonic frequency. Like the IC, MGBv neurons also phase locked to the MCTs independently of CF. Our results therefore suggest that MGBv is not just a relay in the auditory pathway, but represents an important stage in the processing of complex tones.

Chapter 6

The role of A1-MGBv corticothalamic feedback in mistuning detection

6.1. Abstract

Recent evidence suggests that corticothalamic feedback can sharpen the spectral receptive fields of thalamic neurons and modulate the temporal precision of their responses. In this chapter, the role of corticothalamic feedback in the perception of spectral modulations was investigated using a mistuning detection task with complex sounds. The behavioural effects of selective elimination of neurons projecting from A1 to MGBv were evaluated in adult ferrets trained to carry out a mistuning detection task. Bilateral injections of fluorescent microbeads conjugated with a light-sensitive chromophore, chlorin e_6, were made in MGBv. After allowing sufficient time for the beads to be transported to the cortical cell bodies, apoptosis was induced by infrared (λ = 670 nm) laser illumination of A1. Mistuning detection was measured using a positive conditioned go/no-go behavioural paradigm. The selective elimination of the A1-MGBv pathway by chromophore-targeted laser photolysis was performed once the animals had been

trained, and mistuning detection was tested before and after bilateral laser illumination of A1. The cell densities of NeuN-positive layer VI neurons were measured using the optical fractionator stereological probe in the auditory cortex. A reduction in cell density by 30% in A1 relative to controls was observed, suggesting that A1-MGBv neurons had been eliminated. The corticothalamic lesion resulted in poorer mistuning detection performance, as indicated by decreased *d'* values, a shift of the psychometric curves towards higher frequencies, and a threshold increase. The results support a role for A1-MGBv corticothalamic feedback in the accurate discrimination of complex auditory stimuli.

6.2. **Introduction**

Investigating how the auditory system processes complex sounds is important to understand auditory perception. Mistuning detection has been used to study auditory processing perception in humans (Moore et al. 1985; Hartmann et al. 1990) and non-human species (Lohr and Dooling 1998; Klinge and Klump 2009; Klinge and Klump 2010). These studies have shown that animal models including gerbils, starlings, zebra finches, and budgerigars, have better frequency difference limens in sine phase harmonic complex tones (HCTs) than humans. Switching from sine to random phase HCTs results in reduced sensitivity to mistuning in animals but not in humans, suggesting that animals rely more on temporal cues to process complex sounds (Lohr and Dooling 1998; Klinge and Klump 2009; Klinge et al. 2010; Klinge and Klump 2010). It has been proposed that this may be due to the relatively shorter cochlea in animals compared to humans (Klinge et al. 2010).

We have demonstrated (Chapter 3) that ferrets are able to detect mistuning in a HCT, with a threshold close to that reported for other animals species (Lohr and Dooling 1998; Klinge and Klump 2009; Klinge and Klump 2010). Furthermore, ferrets seem to use temporal periodicity cues in unresolved harmonics for pitch discrimination (Walker et al. 2014), while the neurophysiological data presented in Chapter 5 suggest that a combination of changes in firing rate and temporal firing patterns allows mistuned harmonics to be detected.

In addition to being an obligatory relay station for transmission of information to the cortex, the auditory thalamus is likely to have a far more complex role in hearing. Recent evidence suggests that it is involved in the processing of rapidly modulating sounds like speech (Miller et al. 2002; Las et al. 2005). In Chapter 5, we have shown that MGBv neurons show synchronised responses to the periodic waveform envelopes of mistuned complex tones (MCTs) by distinct temporal response patterns, as has previously been described in IC neurons (Sinex et al. 2005). Moreover, changes in firing rate of MGBv neurons when the mistuned harmonic was close to the CFs, reflecting the spectral composition of MCTs, were observed that are similar to the responses reported in A1 neurons (Fishman and Steinschneider 2010). Therefore, MGBv neurons are sensitive to both the spectral composition and temporal structure of complex sounds, and therefore represent an intermediate stage of processing between the IC and the cortex.

The descending corticothalamic projections from layer VI in A1 to the MGBv is one of the largest feedback pathways in the auditory system (Rouiller and

Welker 1991; Ojima 1994; Bajo et al. 1995; Prieto and Winer 1999), with a key potential role in modulating the receptive field properties and temporal firing patterns of thalamic neurons. Indeed, changes in response properties, such as sharpened tuning curves, shifts in best frequency, and changes in latencies or in sound source sensitivity, have been observed in both thalamic and collicular neurons in response to local stimulation or inactivation of A1 (Yan and Suga 1996; Zhang et al. 1997; Ma and Suga 2001; Yan and Ehret 2002; Ma and Suga 2007; Luo et al. 2011). Furthermore, stimulation and cooling in the cortex have demonstrated that A1 activity modulates the spontaneous and driven firing rate in MGBv neurons (Ryugo and Weinberger 1976; Orman and Humphrey 1981; Villa et al. 1991; He 1997; He et al. 2002; Yu et al. 2004).

Acute cortical inactivation can disrupt the ability to discriminate tone frequencies (Talwar et al. 2001; Jaramillo and Zador 2011), suggesting that cortical activity is essential for the accurate perception of sounds. However, the behavioural effects depend on the techniques used for inactivation (acute versus chronic or reversible versus non-reversible). For example, cortical ablation has been shown to have little effect on frequency discrimination behaviour using pure tones, but impairs frequency modulated tone discrimination (Ohl et al. 1999; Ono et al. 2006).

It is difficult with these approaches to target specific neuronal populations. Chromophore-targeted laser photolysis, which selectively induces apoptosis in labelled cells (Macklis 1993; Magavi et al. 2000), provides an alternative and more selective method for targeting populations of interest and can be combined with behaviour (Bajo et al. 2010). We therefore set out to use this

technique to target A1-MGBv corticothalamic projection neurons by making retrograde tracer injections of fluorescent microbeads in MGBv, which are fluorescent nanospheres (100-300 nm) conjugated with chlorin e_6 (Madison et al. 1990). After conjugated microbeads were transported from the terminals in the MGBv to the cell bodies, infrared laser illumination at the absorption spectra (λ = 670 nm) was applied to A1, focusing on layer VI where the A1-MGBv corticothalamic cells originate. The laser illumination induces apoptosis due to formation of radicals from singlet oxygen production (Sheen and Macklis 1994). This technique has previously been shown to selectively eliminate about two third of targeted pathways in corticogeniculate (Eyding et al. 2003) and corticocollicular (Bajo et al. 2010) neurons.

Mistuning detection behaviour (described in Chapter 3) was combined with chromophore-targeted laser photolysis to selectively eliminate the corticothalamic projection neurons. The hypothesis was that the corticothalamic feedback modulates the receptive fields and temporal precision of thalamic neurons in a dynamic and task-specific manner. Therefore, the loss of corticothalamic neurons may cause a change of tuning properties and lower the temporal resolution of MGBv neurons, and consequently impair performance in a mistuning detection task.

6.3. **Results**

Eight adult ferrets were trained in the mistuning detection task. In three of them, corticothalamic neurons were selectively eliminated by chromophore-targeted laser photolysis (lesion animals). Five more were used as control animals. The

experimental design is shown in figure 6.1. The animals were first trained on a mistuning detection task using the go/no-go behavioural paradigm described in Chapter 3. HCTs with 16 harmonics of 400 Hz F_0 were used for the reference stimulus, and the 4^{th} harmonic of the HCT was shifted to a higher frequency by 0.1 to 192 Hz for the mistuned target tones (MCTs).

After initial training, chlorin e_6 conjugated red- and green-fluorescent microbeads were injected in the left and right MGBv, respectively, in the lesion animals (n = 3). We used three types of controls. First, active conjugated microbeads were injected in a different location, outside MGBv (n = 3, with one case injected in the visual thalamus, LGN, and two other cases in caudal MGB and hippocampus). Second, the injection was in the right place (MGBv) but used inactive unconjugated microbeads (n = 1). Third, PBS was injected in the MGBv (n = 1). Infrared laser illumination was applied to the A1 bilaterally in order to induce selective apoptosis in the three lesion animals and all the control animals.

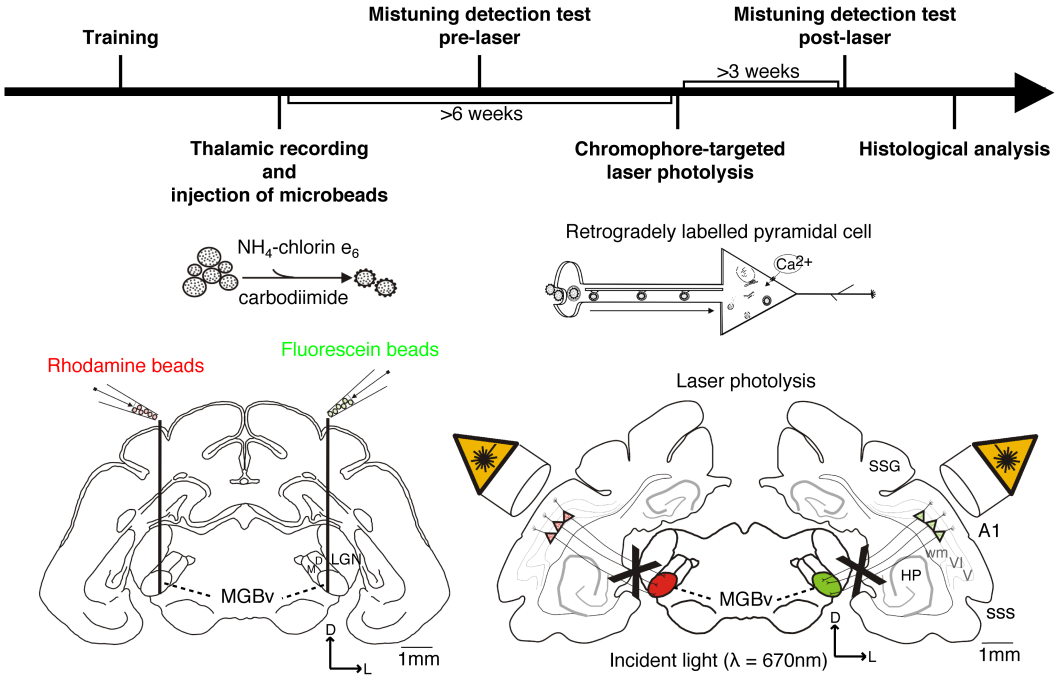

Figure 6.1 Experimental design.
Corticothalamic projection neurons were selectively eliminated by chromophore-targeted laser photolysis. The technique comprises neural recording guided injections of chlorin e_6 conjugated to fluorescent microbeads in the MGBv and subsequent infrared (λ = 670 nm) laser illumination of the middle ectosylvian gyrus (MEG) where primary auditory fields (A1 and AAF) are located to induce apoptosis of the retrogradely-labelled cells. Rhodamine and fluorescein microbeads were injected into left and right MGBv, respectively, and laser light was applied bilaterally over MEG. A1, primary auditory cortex; D, dorsal; d, dorsal MGB; HP, hippocampus; LGN, lateral geniculate nucleus; L, lateral; m, medial MGB; MGBv, the ventral division of medial geniculate body; SSG, syprasylvian gyrus; sss, suprasylvian sulcus; V, layer V; VI, layer VI; wm, white matter.

6.3.1. Effect of corticothalamic lesion on mistuning detection

6.3.1.1. Detection sensitivity

The thresholds obtained before the injection of microbeads were not significantly different from those in pre-laser test (two tailed unpaired *t*-test: $P = 0.28$). Thus, the surgical intervention to inject microbeads did not affect the behavioural performance of the animals. The behavioural performance was again compared before and after laser illumination (pre- and post-laser) using signal detection theory. Lesion animals showed reduced sensitivity to mistuning and increased thresholds by 5.8 ± 2.3 Hz (mean ± sem), while control animals did not have altered thresholds for mistuning detection (-0.08 ± 0.09 Hz).

Psychometric functions and response biases for each animal were plotted as a function of mistuning on a log scale (Fig. 6.2), by calculating the sensitivity index (*d'*) and λ_{center} for response bias. The *d'* values were smoothed based on a model-free estimation (Zychaluk and Foster 2009), since lesion animals showed fluctuating *d'* values in the post-laser period. The estimated thresholds were comparable to those obtained by psychometric functions fitted to a cumulative Gaussian distribution (*t*-test for the differences: $P = 0.37$, n = 15).

In lesion animals, *d'* values decreased after selective corticothalamic lesion, with the psychometric functions shifted towards higher frequencies. In one of the cases (F1205), the threshold increased from 7.8 (pre-laser) to 17.8 Hz (post-laser, Fig. 6.2A). The response bias for this animal was consistent between pre- and post-laser periods, showing almost no bias above threshold (Fig. 6.2B). In another case (F1209, Fig. 6.2C), the threshold also increased from 7.8 (pre-laser) to

13.5 Hz (post-laser), however, the animal seemed to find the task more difficult after the corticothalamic lesion and was less reliable in waiting at the trigger spout for the target tones presentation. This change in behaviour was reflected in an overall decrease of *d'* and λ_{center} values in the post-laser period (Fig. 6.2C,D). In the third lesion animal (F1430), the threshold increased from 0.9 (pre-laser) to 2.9 Hz (post-laser), similar to the previous cases, but in this animal no response bias was observed in either pre- or post-laser periods (Fig. 6.2E,F).

Despite individual differences in thresholds and response bias trends, these results indicate that impaired behavioural performance consistently results from corticothalamic lesion, with decreased *d'* values and increased thresholds.

In control animals, the thresholds did not change between pre- and post-laser periods, and small increases in *d'* values above threshold was observed. In three of them, the thresholds fell slightly (F1433, 1.0 to 0.6 Hz; F1223, 1.4 to 1.2 Hz; F1325, 0.8 to 0.7 Hz; Fig. 6.2G,K,O), while the others showed slight increases (F1225, 1.3 to 1.5 Hz, Fig. 6.2M) or exactly same threshold in pre- and post-laser periods (F1444, 0.4 Hz, Fig. 6.2I). Control cases all showed a bias toward go responses (Fig. 6.2H,J,L,N,P), as we observed for the animals described in Chapter 3 (Fig. 3.2B).

The psychometric functions in control cases were generally shifted upwards in the post-laser period for mistuning values above threshold, suggesting that there may have been a learning effect on the animals' performance. However, this did not affect the thresholds measured for a *d'* of 1 (Fig. 6.2G, I, K, M,O).

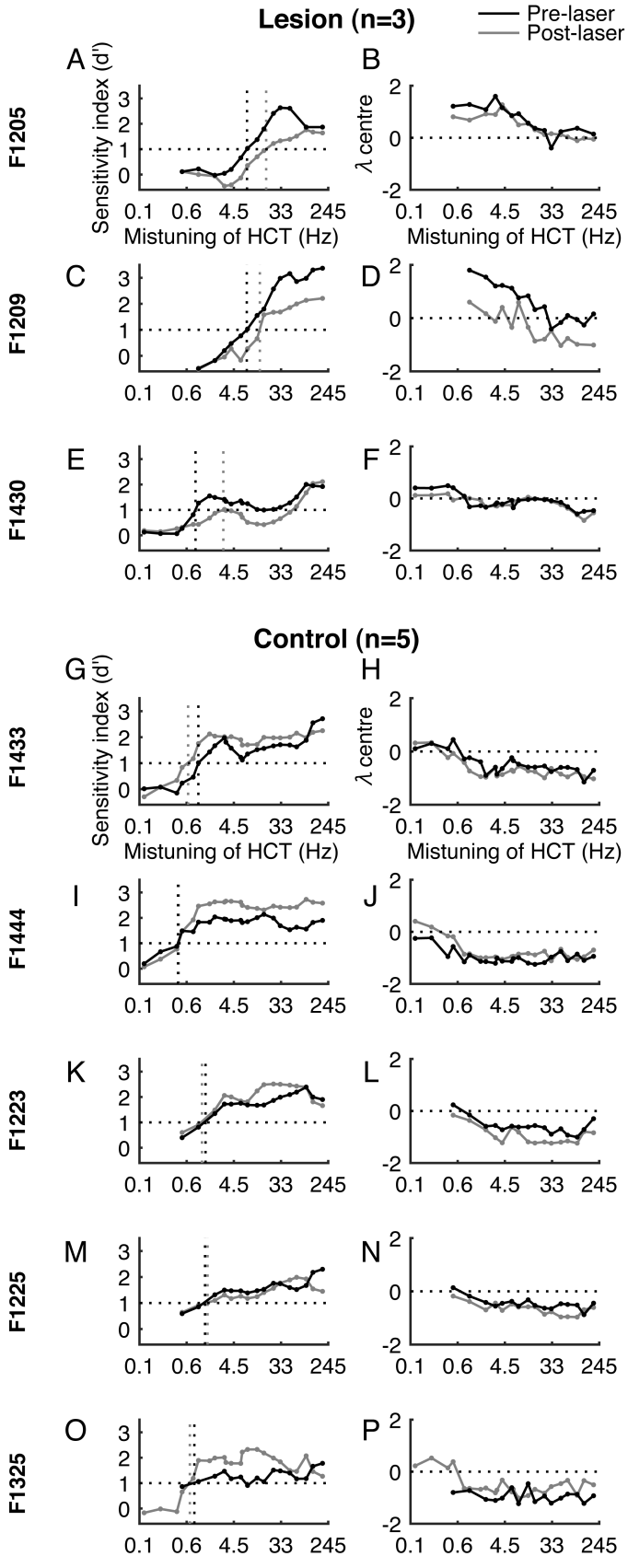

Figure 6.2 Mistuning detection performance of individual animals. Behaviour of the three lesion (A-F) and five control (G-P) animals. Black shows performance in the pre-laser period, and grey shows post-laser performance. (A, C, E, G, I, K, M, O) Sensitivity index (*d'*) was calculated and plotted a function of mistuning of HCT on a log scale. The horizontal dashed lines are drawn as a reference for the threshold criteria *d'*=1, and the orthogonal dashed lines indicate thresholds for each period tested. (B, D, F, H, J, L, N, P) λ_{center} was calculated and plotted to investigate response bias. Negative values indicate bias to go responses and positive values bias to no-go responses. The dashed line (λ_{center} = 0) is shown as a reference for zero bias.

The *d'* values followed a cumulative Gaussian distribution dependent on the degree of mistuning (Fig. 6.3A, B), as previously shown in Chapter 3 (Fig. 3.2A). Individual differences were larger in the lesion group, reflected by larger sem values (grey areas, Fig. 6.3). This greater variability may arise from varying levels of corticothalamic cell loss in each case.

For the lesion group as a whole, the threshold increased by 5.8 ± 2.3 Hz (mean ± sem), with a decrease in the sensitivity indicated by the psychometric function shifting towards higher frequencies (right) and downward (Fig. 6.3A). In the control group, the difference in thresholds between pre- and post-laser periods was minimal (-0.08 ± 0.09 Hz, mean ± sem) (Fig. 6.3B) and significantly smaller than the threshold change in the lesion group (two tailed unpaired *t*-test for comparison of the difference of thresholds between pre- and post-laser in lesion and control group: $P = 0.01$, Fig. 6.4A).

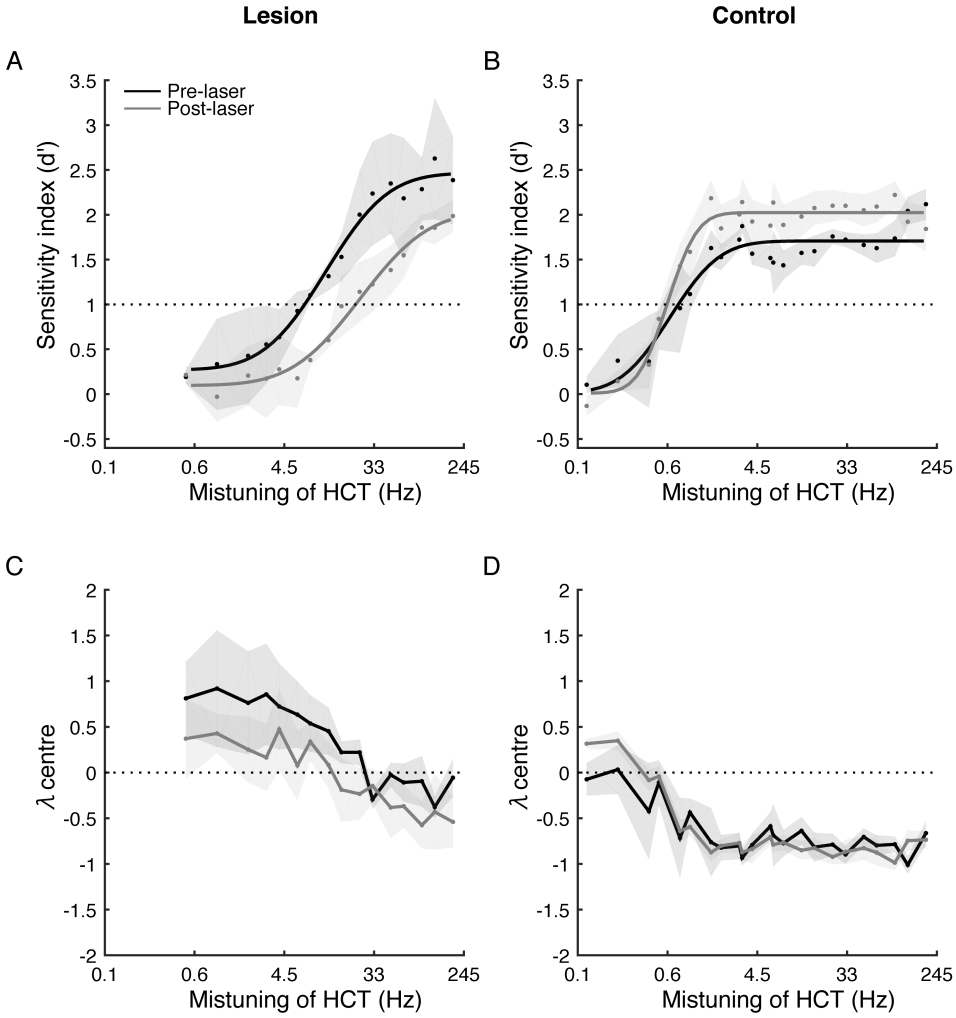

Figure 6.3 Mistuning detection was impaired in the post-laser period for the lesion group.

Mistuning detection performance of the lesion (n=3) and control (n=5) group. Black lines and dots show the performance in the pre-laser period and grey lines and dots show the post-laser performance. The areas shadowed in grey indicate the standard error of the mean (sem). (A, B) The mean of *d'* values was calculated and plotted as a function of mistuning of HCT (on a log scale) for lesion (A) and control (B) groups. A cumulative Gaussian distribution was used to fit the psychometric functions. The horizontal dashed lines are drawn as a reference for the threshold criteria of *d'* = 1. (C, D) The mean of λ_{center} values was calculated and plotted for lesion (C) and control (D) groups. The dashed horizontal line at zero indicates no bias.

The pooled data from the control animals confirms that their *d'* values were higher above threshold in the post-lesion period (Fig. 6.3B), supporting a learning effect on their sensitivity to mistuning. The mean threshold (± sem) in the post-laser period was 0.9 ± 0.2 Hz, almost identical to the value (0.8 ± 0.1 Hz) reported in Chapter 3.

That corticothalamic lesions reduce sensitivity for detecting mistuned harmonics is supported by the mean difference of *d'* values between pre- and post-laser periods. This difference was -0.4 ± 0.1 in the lesion group, which is opposite to the positive value of 0.3 ± 0.1 (mean ± sem) for the control group (two tailed unpaired *t*-test: P= 0.007, Fig. 6.4B).

Because individual lesion animals showed distinct patterns of response bias (Fig. 6.2B, D, F), the λ_{center} values (mean ± sem) also indicated large variability in the lesion group compared to controls (Fig. 6.3C,D). Animals in the lesion group were less biased to go responses, suggesting a more conservative judgement in the task. On the other hand, the consistent bias to move to the reward spout reported in Chapter 3 was clear in the control group, both in the pre- and post-laser testing periods (Fig. 6.3D). Comparison of the pre- vs post-laser mean difference in λ_{center} values showed no significant difference in the way the response bias changed between lesion and control groups (two tailed unpaired *t*-test: P = 0.22, Fig. 6.4C).

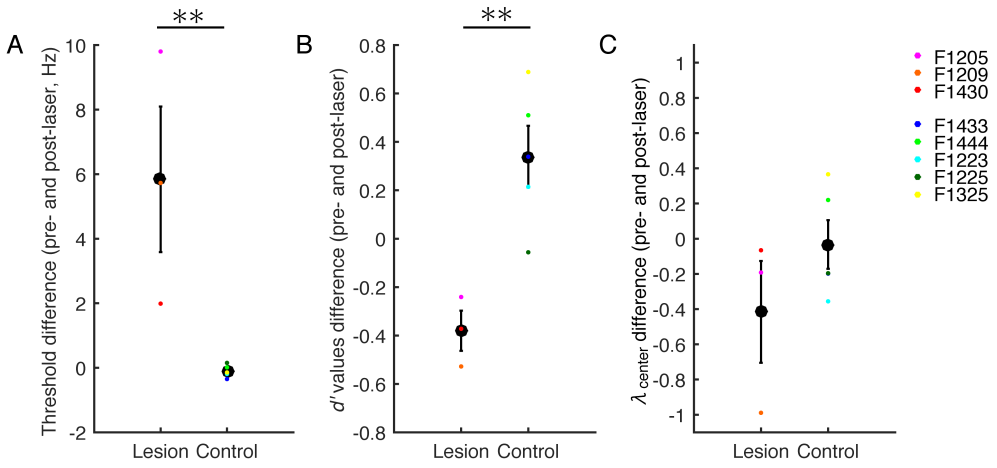

Figure 6.4 Corticothalamic neuron lesions result in lower sensitivity and higher mistuned detection thresholds.

Differences between pre- and post-laser performance were computed for threshold (A), mean difference of *d'* values (B), and mean difference of λ_{center} values (C). Large black circle indicate mean ± sem. Coloured dots represent data from individual animals. *T*-tests revealed significant differences in the value of threshold and sensitivity between the lesion and control groups (threshold: $P = 0.01$; *d'*: $P = 0.007$) but not in response bias (λ_{center}, $P = 0.22$). $^{**}P < 0.01$.

As described in the Methods (Chapter 2), training the animals on the mistuning detection task included a phase where an intensity difference was introduced between the reference and target tones. This intensity difference was removed for measurement of the mistuning detection thresholds. Re-learning sessions that included intensity difference cues were provided at the three stages of this experiment (training, pre-laser and post-laser). No difference in correct response rates was found between the lesion and control groups or at these three time points (two-way ANOVA; groups, $F_{(1,17)} = 1.15$, $P = 0.30$; time, $F_{(2,17)} = 0.47$, $P = 0.63$). Thus, the ability to detect target MCTs using intensity difference cues remained intact after injection of the microbeads and laser illumination. Instead, the deficit in the lesion group was apparent only for mistuning detection when no other cues were available.

Because training can improve performance in auditory tasks (Bao et al. 2004; Polley et al. 2006; Keating et al. 2014) and deficits observed following cortical lesions can recover over time (Heffner and Heffner 1986; Kavanagh and Kelly 1988), we examined whether any learning occurred on the mistuning detection task. The sensitivity and thresholds were compared for the data obtained in the first and second half of the pre- or post-laser periods by computing the mean difference of *d'* values. Although two of the three lesion cases and two of the five control animals had slightly better *d'* values in the second half of the testing periods, suggesting a learning effect, this difference was not significant (repeated measures ANOVA; time (first or second half), $F_{(1,12)} = 3.71$, $P = 0.08$; time × groups, $F_{(3,12)} = 1.81$, $P = 0.20$).

6.3.1.2. Reaction time

Reaction time from go trials was calculated as the time from the first target tone onset until the animal breaks contact with the trigger spout. The histograms of reaction times were not normally distributed, presenting two peaks that correspond to the two target tones presented and another peak to missed responses (Miss, incorrect responses in go trials). Therefore, the median values were computed to represent the trend of reaction time responses. Reaction times were then obtained for four groups classified by the experimental case (lesion or control) and the time course of the procedure (pre- or post-laser) (Fig. 6.5).

We anticipated that reaction times would be longer in the post-laser period for the lesion group, since larger mistuning thresholds are likely to be associated with slower responses (Chapter 3) and missed responses. As predicted, one lesion animal (F1430) showed longer reaction times in the post-laser period, and the second lesion animal (F1205) did not change its reaction times in pre- and post- laser. In contrast, reaction times were shorter in the post-laser period in the third lesion animal (F1209), although the shift in response bias towards go responses following the lesion may be responsible for this (Fig. 6.2D). Control animals showed a small reduction in reaction time in the post-laser period.

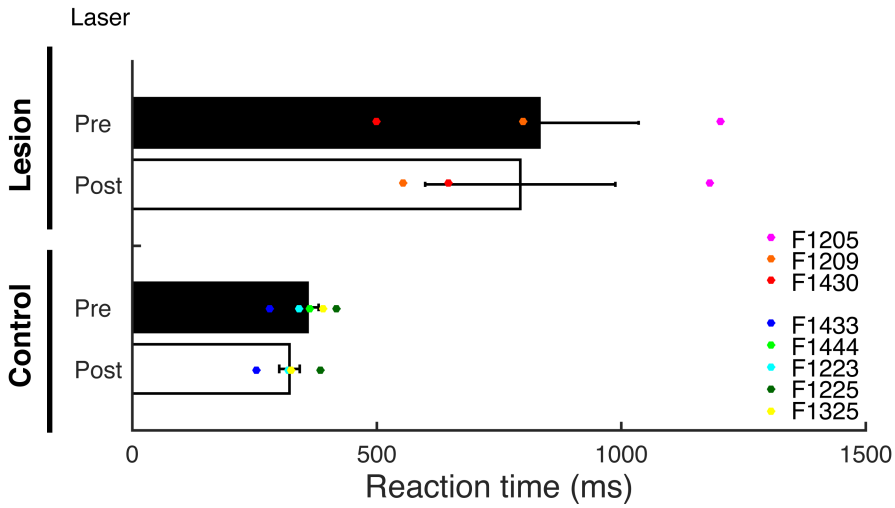

Figure 6.5 Reaction time differences between lesion and control groups.
Bars indicate the mean (± sem) of reaction time for each case grouped by procedure (lesion or control) and testing period (black, pre-laser; white, post-laser). Different colour dots represent the values of individual animals.

Reaction times did not differ significantly between lesion and control groups, and there was no effect of time course of procedure (repeated measures ANOVA; pre- and post-laser periods, $F_{(1,6)} = 0.8$, P=0.39; lesion and control groups, $F_{(1,6)} = 0.0007$, $P = 0.98$). Since it was shown that reaction time is dependent on the degree of mistuning (Chapter 3, Fig. 3.4), the different target MCTs were divided into two groups according to the shape of their psychometric functions while balancing the number of trials in each case (small: < 3 Hz; large: 3 to 8 Hz) in order to examine the effect of degree of mistuning for control animals.

Since shorter reaction times were observed in the post-laser period for the control group, we grouped the data by time course (pre- and post-laser) and degree of mistuning (small and large). There were significant differences between large mistuning post-laser group and the small mistuning group in pre- and post-laser periods (one way ANOVA, $F_{(3,16)} = 7.10$, $P = 0.003$; post hoc tests, Tukey-Kramer,

$P < 0.05$). In other words, responses became faster for supra-threshold stimuli in the post-laser period, whereas, this was not the case for below threshold mistuning values.

6.3.2. Identification of injection sites

Histological analysis of the injection sites in the thalamus was conducted once animals completed the behavioural testing. The injection sites were identified by the presence of fluorescence (neurons or aggregates of multiple neurons) that contained the injected microbeads (Fig. 6.6 asterisks). In one lesion case (F1205), a clear injection site was observed in the MGBv in the left hemisphere, while the injection seemed to have caused some degeneration in the MGBv in the right hemisphere. In another lesion case (F1209), the injection site on the left side was more medial in the MGBv, close to the dorsal division (MGBd), while on the right side, the injected microbeads were placed dorsal to the MGB itself.

In each case, retrogradely labelled fluorescent cells were observed in the ipsilateral auditory cortex (AC) and in the inferior colliculus (IC). In one control case (F1225), the injection sites were placed bilaterally in the visual thalamus (LGN), and labelled cells were observed in the ipsilateral visual cortex. In another control case (F1223), the left injection site was located in the caudal end of the MGBv and spread into the rostral IC, with labelled cells in rostral IC and in the AC. The injection site on the right side was placed between the cortex and thalamus. Anatomical confirmation of the injection sites for the rest of the lesion (F1430) and the control (F1325, F1433, F1444) cases is planned to be performed following thesis submission.

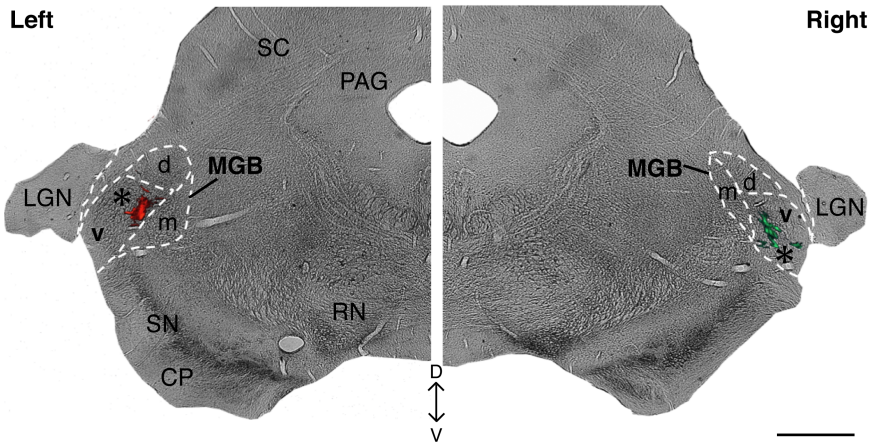

Figure 6.6 Injection sites of microbeads in the auditory thalamus of one animal.
Red and green fluorescent microbeads were injected in left and right MGBv, respectively. The injection sites are indicated by asterisks. CP, cerebral peduncles; D, dorsal, d, dorsal MGB; LGN, lateral geniculate nucleus; m, medial MGB; MGB, medial geniculate body; PAG, peri-aqueductal grey matter; RN, red nucleus; SC, superior colliculus; SN, substantia nigra; V, ventral; v, ventral MGB. Calibration bars = 1 mm.

6.3.3. Corticothalamic cell loss

Loss of corticothalamic cells by chromophore-targeted laser photolysis was evaluated by the proportion of fluorescent labelled cells in AC and by the cell density in layer VI of AC.

The number of retrogradely labelled fluorescent cells in the AC was counted (in every 5th section), and the number of cells in each region, anterior (AEG), middle (MEG, were A1 is located) and posterior ectosylvian gyrus (PEG), were divided by the total number of counted cells for each case (F1205, F1209, F1223) to calculate the proportion of cells labelled in each region (Fig. 6.7A). MEG, PEG and AEG comprise the auditory cortex in the ferret, with MEG containing the primary fields (core), PEG containing the secondary areas (belt) and AEG containing the higher-level areas (e.g. Bajo et al. 2007; Bizley et al. 2015).

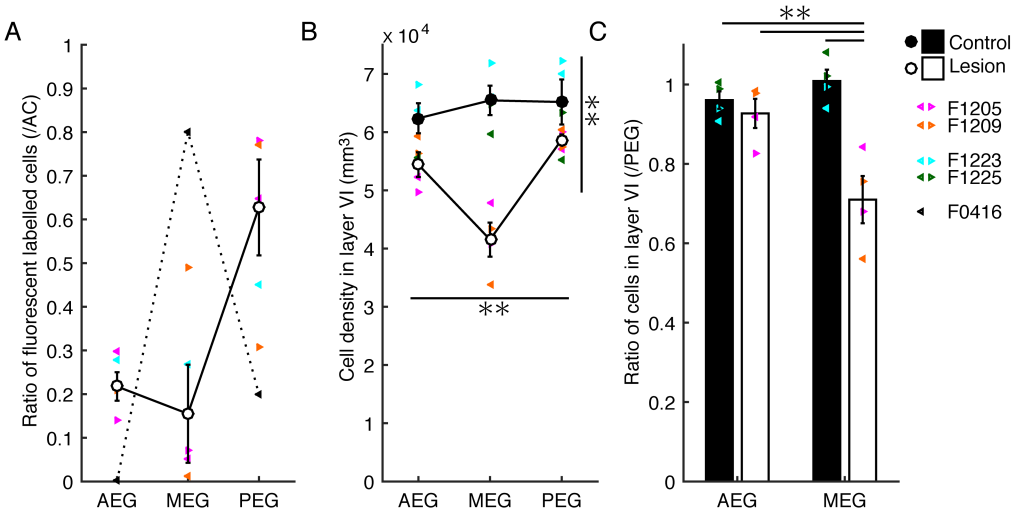

Figure 6.7 Corticothalamic cell loss after chromophore-targeted laser photolysis in the A1-MGBv pathway.
Different colours indicate the values of individual animals (left-pointing triangles, left hemisphere; right-pointing triangles, right hemisphere). Error bars indicate sem. (A) The ratio of labelled cells in AEG, MEG and PEG to the total number of cells in AC. White circles indicate the mean in the lesion animals. Black is a control case that received an injection of BDA in the left MGBv. (B) Cell density values in layer VI of AEG, MEG and PEG. White circles indicate the mean of lesion cases, while black circles represent the mean of control cases. Cell density in MEG in the lesion group was significantly different from the same region in the control group and from other auditory cortical regions in both control and lesion group (Scheffé, $P<0.05$) indicated by asterisk. (C) The ratio of cell density in AEG and MEG to PEG was calculated and is shown by the histogram bars (mean ± sem). Black indicates control group, and white shows lesion cases. The ratio for the MEG in lesion cases was reduced compared with control cases (Tukey-Kramer, $P<0.01$, indicated by asterisks).

A previous case (F0416, provided by Dr. Nodal), with the tracer biotinylated dextran amine (BDA) injected in the centre of the MGBv has been used as a control template to calculate the ratio of neurons labelled in each region of the auditory cortex. This control case (F0416) showed that 85% of neurons projecting to MGBv were labelled in the MEG, demonstrating the strong descending connectivity between A1 and MGBv.

In lesion animals (F1205 and F1209), the ratio of MEG labelling was only 0.01-0.07 for three out of four thalamic injections (right and left MGBv were injected), with a higher ratio of labelled cells in PEG and AEG (Fig. 6.7A). In the right hemisphere of F1209, the ratio in MEG was higher than in the other lesion cases, consistent with the injection site being placed dorsal to the MGBv. In one of the control animals (F1223) with an injection in the caudal end of MGBv, the ratio of labelled neurons in the MEG was 0.27, the same as in AEG (0.28). These data suggest that the reduced ratio in the MEG of lesion animals that have injection sites in the right place is indicative of a selective loss of retrogradely labelled cells in the MEG following laser illumination.

Neurons in the ferret cortex were also visualized by immunohistological staining of NeuN (neural protein), and the cell densities in layer VI of the AC (e.g. Fig. 6.8A) were obtained in four cases (F1205, F1209, F1223 and F1225) by unbiased stereological estimation of number of cells and cortical volumes using the optical fractionator probe with StereoInvestigator software. The population size was estimated by setting the parameters to obtain a coefficient of error of <0.05 with a 100×100 μm counting window. Cell densities in layer VI of the MEG in lesion cases were reduced compared to controls, while no differences were

observed in PEG or AEG (Fig. 6.8B, C). The cell density in layer VI of AEG, MEG and PEG was obtained for each animal and each hemisphere (Fig. 6.7B) and was significantly different between lesion and control groups and cortical regions, but not between left and right hemispheres (repeated measures ANOVA; groups, $F_{(2,10)} = 10.6$, $P = 0.003$; regions, $F_{(2,10)} = 8.20$, $P = 0.007$; hemispheres, $F_{(2,10)} = 0.12$, $P = 0.89$), and the interaction between groups and cortical regions ($F_{(2,14)} = 6.43$, $P = 0.01$) was significant. Post hoc tests revealed that cell density in MEG of the lesion groups was significantly different from the same region in the control group and from any other regions of both control and lesion groups (Scheffé, $P<0.05$). The results show that corticothalamic cells in layer VI of AC were selectively eliminated in the MEG of the lesion group.

No difference in cell densities in the three regions of AC (MEG, PEG and AEG) was found in the control group, and there was no difference in the values for PEG between lesion and control groups. Therefore, cell densities of AEG and MEG were normalized by the values of PEG to evaluate cell loss (Fig. 6.7C). The ratio for MEG in the lesion group was reduced by 0.3 compared to the control group (Tukey-Kramer, $P<0.01$), suggesting that ~30% of cells were eliminated by chromophore-targeted laser photolysis.

Histological and stereological analyses support that the fact that animals showing behavioural impairment had selective corticothalamic cell loss. The results indicate that corticothalamic feedback is important for normal mistuning detection.

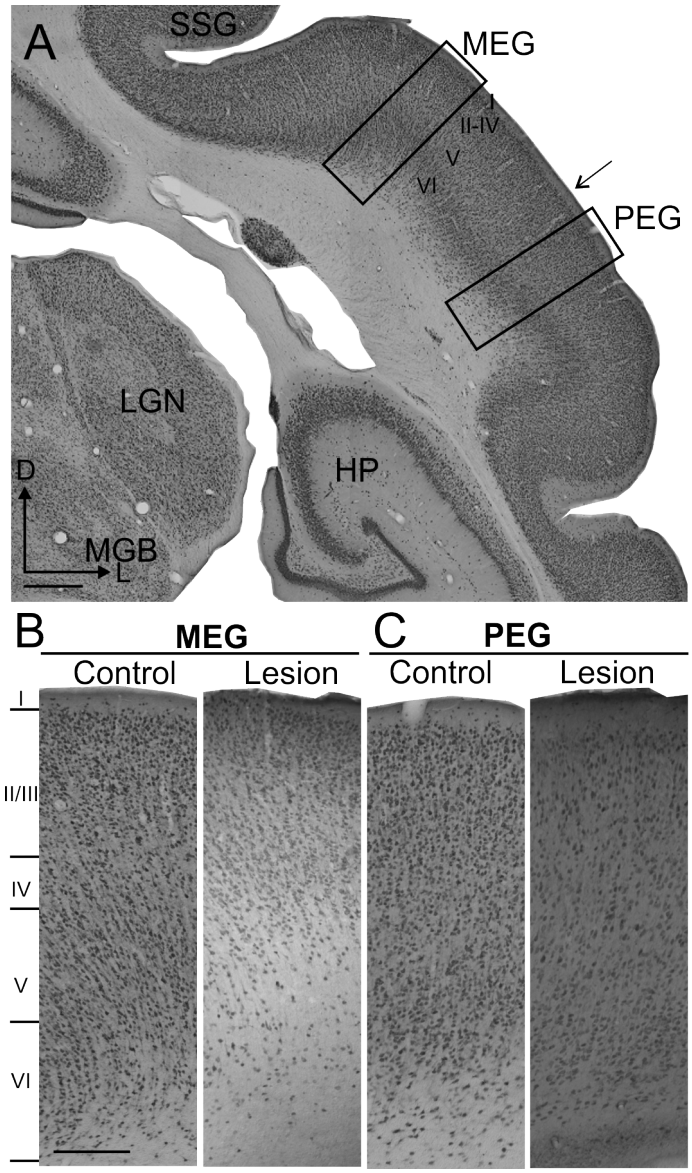

Figure 6.8 Coronal sections at the level of the auditory cortex showing the appearance of the cortical layers in lesion and control animals.

The brain sections were immunostained using NeuN antibody. (A) Layers in the right cortex of a control case. The black square indicates the area shown at higher magnification for the control case in panels B and C. Calibration bars = 1 mm. (B) The number of cells in layer VI of the middle ectosylvian gyrus (MEG) was reduced in a lesion case compared with a control one. Calibration bars = 0.25 mm. (C) There was no difference in the number of cells in layer VI of the posterior ectosylvian gyrus (PEG) in control and lesion cases. D, dorsal; I, HP, hippocampus; layer I; II, layer II; IV, layer IV; L, lateral; LGN, lateral geniculate nucleus; MEG, middle ectosylvian gyrus; MGB, medial geniculate body; PEG, posterior ectosylvian gyrus; SSG, syprasylvian gyrus; V, layer V; VI, layer VI.

6.4. Discussion

Using chromophore-targeted laser photolysis that induces apoptosis only in the targeted cells, we attempted to eliminate the major feedback projection from A1 to MGBv bilaterally. Mistuning detection was tested before and after this selective elimination to explore the role of corticothalamic neurons. Performance on this task was impaired after the feedback connection was lesioned, whereas no deficits were found in a series of control animals, supporting a role for corticothalamic feedback in mistuning detection.

The effect of lesion

We measured the behavioural consequences of corticothalamic lesions on mistuning detection thresholds and reaction times. Compared to control animals, thresholds were increased significantly (Fig. 6.3), although the effect on reaction times showed considerable individual variability (Fig. 6.5).

Lesions of the auditory cortex, including A1, result in impairments in vocalization discrimination or impaired behaviour in frequency modulated tone detection (Heffner and Heffner 1986; Kavanagh and Kelly 1988; Ohl et al. 1999), while reversible inactivation of A1 disrupts the ability to discriminate tone frequency (Talwar et al. 2001; Jaramillo and Zador 2011). The present study shows that selective bilateral elimination of corticothalamic projection neurons increases mistuning detection thresholds, while their ability to discriminate tones on the basis of intensity difference cues is not impaired. It is possible that the selective elimination of layer VI corticothalamic cells not only perturbs the balance of excitation and inhibition in the cortical circuits, but also the loop linking the MGB,

the thalamic reticular nucleus (TRN) and the AC, given the close relation between the three structures (Jones 1975; Stratford et al. 1996).

The effect of learning

We found that control ferrets exhibited an improvement in sensitivity for detecting a mistuned harmonic between pre- and post-laser periods (Fig. 6.3B and 6.4B), while recovery from the initial effects of cortical lesions have been reported (Heffner and Heffner 1986; Kavanagh and Kelly 1988). However, in the present study, no clear improvement in performance was observed for animals with corticothalamic lesions when their performance was compared between the first and second half of the post-laser testing period. This is possibly because cortical ablations in previous studies extended beyond A1, were not layer specific and animals were tested after a longer recovery time.

In contrast to the lesion animals, mistuning detection ability clearly improved in control animals. They showed improved sensitivity above threshold, while the threshold itself was consistent between pre- and post-laser periods (Fig. 6.3B). Training-induced changes in A1 response properties have been described in a number of studies (Kilgard and Merzenich 1998; Kilgard et al. 2001; Bao et al. 2004; Polley et al. 2006; Schnupp et al. 2006; Huetz et al. 2009), so it seems likely that neuronal sensitivity to mistuning would have improved in our control ferrets over the course of training.

Furthermore, reaction times above threshold mistuning values were shorter in control animals in the post-laser period (Fig. 6.5). It is interesting to note that cortical electrical activation has been shown to induce centripetal or centrifugal

response latency shifts, for example, in cochlear nucleus (CN) neurons (Luo et al. 2008), and the direction of response latency change in A1 neurons was variable and dependent on the acoustic composition of stimuli (Kilgard et al. 2001). Reaction time is also shortened by practice (Ando et al. 2002), and requires the cooperation of cortical and other complex related neural circuits, such as the cholinergic nucleus basalis and GABAergic interneurons (Liu et al. 2011; Schreiner and Polley 2014). Since our ferrets were trained to respond to target tones as soon as possible to receive a reward, we can speculate that the learning effect, expressed by better sensitivity and shorter reaction times, can be achieved by adjusting receptive fields and/or responses to the relevant signal in MGBv and/or cortical neurons.

Experimental design

Chromophore-targeted laser photolysis is a technique for selectively eliminating targeted population of neurons without damaging other non-targeted neurons, glia or axons (Macklis 1993; Magavi et al. 2000). It has been shown that non-targeted cortical layers that comprise non-labelled neurons were preserved by focusing the infrared laser light at the targeted cortical layer that includes the labelled neurons (Bajo et al. 2010).

In the present study, the ability of the ferrets to discriminate complex tones on the basis of intensity difference cues was preserved throughout the surgical interventions (i.e. no-manipulation, after injections of microbeads into MGBv, and after laser illumination to induce corticothalamic lesion). This contrasts with the effects of large auditory cortical lesions or acute inactivation of A1 basic spectral discrimination abilities (Heffner and Heffner 1986; Kavanagh

and Kelly 1988; Talwar et al. 2001), sound localization or experience-dependent spatial plasticity (Nodal et al. 2010; Nodal et al. 2012). Two animals in our cohort had higher thresholds in the pre-laser compared to post-laser period, which may be due to relatively short training and testing period used or, in one case, to the unilateral lesion in the thalamus. However, other animals trained before the pre-laser period had consistent thresholds before and after injections of the microbeads and all control animals had similar thresholds in the pre- and post-laser periods, suggesting that the surgical interventions *per se* did not affect the animals' behaviour. Furthermore, our study was based on a longitudinal comparison; we compared each animal's performance individually before and after the corticothalamic lesion. For example, we still see the effect of the lesion in animals with slightly higher thresholds and can explain this as a consequence of loss of corticothalamic function.

Selective elimination of corticothalamic neurons

The amount of corticothalamic cell loss induced by chromophore-targeted laser photolysis in the present study is comparable to previous reports (Eyding et al. 2003; Bajo et al. 2010). With the same approach 27 ± 4% of corticothalamic neurons were reported to be eliminated in layer VI of the primary visual cortex (Eyding et al. 2003). In the present study, cell density in layer VI was reduced bilaterally by ~30% compared to control cases (Fig. 6.7C), indicating the same ratio of reduction for A1-MGBv corticothalamic cells.

Corticothalamic cells make up about 50% of neurons in layer VI of A1 (Prieto and Winer 1999), in agreement with studies in visual cortex (McCourt et al.

1986; Eyding et al. 2003). Therefore, a ~30% loss of layer VI neurons in the primary auditory (our results) and visual (Eyding et al. 2003) cortices corresponds to ~60% loss of the corticothalamic neurons. This value is close to the previously reported corticocollicular cell loss in ferret A1 using the same technological approach, which was sufficient to generate a learning deficit in a sound localization task (Bajo et al. 2010). In summary, chromophore-targeted laser photolysis produced a similar degree of corticofugal cell loss in our study to that reported in previous work, which in each case clear physiological or behavioural changes were produced (Eyding et al. 2003; Bajo et al. 2010).

Although the corticothalamic lesions produced significantly raised mistuning detection thresholds, the animals were still able to perform the task. This may reflect the contribution of the remaining neurons in the corticothalamic pathway, as well as other circuits in the auditory system.

The role of corticothalamic feedback

Corticothalamic neurons have mainly small distal terminals with thin axons and convergent endings (Rouiller and Welker 1991; Ojima 1994; Bajo et al. 1995; Winer et al. 1999; Bartlett et al. 2000; Llano and Sherman 2008), activate metabotropic glutamate receptors (Godwin et al. 1996; Vidnyanszky et al. 1996) and show an excitatory effect with small EPSPs (Granseth 2004; Lee and Sherman 2008; Lee and Sherman 2009). These types of terminals are considered to be 'modulators' (Sherman and Guillery 2011; Sherman and Guillery 2013) and control properties of MGBv neurons by affecting their overall excitability, the voltage gated conductance and synaptic potentials. This is consistent with the

effects of focal electrical stimulation and cooling of A1, which suggest that corticothalamic projections modulate the receptive fields of thalamic neurons (Zhang and Yan 2008; Luo et al. 2011) and control their firing patterns (Ryugo and Weinberger 1976; Orman and Humphrey 1981; Villa et al. 1991; He 1997; He et al. 2002; Yu et al. 2004).

In order to detect mistuned harmonics from a HCT, spectral and temporal cues are used (Goldstein 1973; Houtsma and Smurzynski 1990; Meddis and Hewitt 1991a; Meddis and Hewitt 1991b). We showed in Chapter 5 that ferret MGBv neurons represent the temporal periodicity created by the interaction between the mistuned harmonic and neighbouring harmonics, supporting that ferrets can use temporal cues to detect MCTs. We would therefore predict that enhanced temporal precision in tonic firing patterns by corticothalamic feedback may play a role in mistuning detection. At the same time, changes in MGBv neuron firing rate were also observed when we switched from HCTs to MCTs (Chapter 5). If corticothalamic modulation alters receptive field bandwidth and other response properties (reviewed in Suga 2012), this might contribute to the response changes that facilitate the detection of mistuned harmonics.

When neurons fire tonically, the firing pattern can represent the envelope of the stimulus (Sherman 2001; Sherman and Guillery 2013) and is potentially suitable for precise phase locking to the envelope and temporal fine structure of MCTs. It has been proposed that, in cooperation with TRN neurons, the principal cells in the MGBv detect novel stimuli when their spontaneous rate is low, and that corticothalamic feedback increases the firing rate once those signals have been detected (Crick 1984; Sherman 2001). If the firing rate of MGBv neurons is

modulated as a result of corticofugal feedback when MCTs are detected, this change in the firing rate may help to establish precise temporal response patterns in the MGBv.

Concluding remarks

The present results are the first to show that corticothalamic feedback is important at a behavioural level. Our finding that corticothalamic feedback is required for normal mistuning detection, suggests that this descending pathway may play an important role in auditory scene analysis.

Chapter 7

General discussion

7.1. **Overview**

In this thesis, the role of A1-MGBv corticothalamic feedback has been investigated using a wide range of experimental approaches. A behavioural go/no-go paradigm was developed and used to measure the ability of ferrets to discriminate a mistuned complex tone (MCT) containing a single mistuned harmonic from a harmonic complex tone (HCT) in ferrets. Electrophysiological recordings were used to investigate the functional organization of the ferret auditory thalamus and, in particular, to explore how neurons in the ventral division of medial geniculate body (MGBv) respond to different HCTs and MCTs. The behavioural mistuning detection test was then combined with chromophore-targeted laser photolysis to selectively eliminate corticothalamic projection neurons (A1 to MGBv) and to investigate the role of corticothalamic feedback in complex sound processing.

7.2. **The ferret as an animal model for mistuning detection**

Mistuning detection has been used to study the mechanisms of complex sound processing based on the harmonicity and/or periodicity of acoustic stimuli in

auditory scene analysis. We have shown that ferrets are able to detect mistuned harmonics using a go/no-go task, and that their detection thresholds are comparable to those of other species.

To understand how the auditory system processes complex sounds, various models have been proposed as part of human psychoacoustic studies. These include the concept of 'harmonic sieves' (Goldstein 1973), temporal models based on the temporal excitation pattern on the basilar membrane (Licklider 1951; Meddis and Hewitt 1991a; Meddis and Hewitt 1991b), and a template model that emphasizes the importance of local harmonic regularity (Lin and Hartmann 1998).

The recent prevalent view, however, is that both of place and temporal models can contribute in a complementary manner to explain harmonicity processing in low and high frequency domains (Houtsma and Smurzynski 1990). On the other hand, small animals, such as gerbils (Klinge and Klump 2009; Klinge and Klump 2010), zebra finches and budgerigars (Lohr and Dooling 1998), mainly rely on the temporal fine structure to decode complex sounds. This potential difference in coding strategy between those small animals and humans may reflect the relatively short cochlea in the animals, which might limit the availability of place coding (Fay 1992; Klinge et al. 2010). The threshold for MCTs in ferrets (Chapter 3) are very close to those reported for these animal species and an order of magnitude smaller than that of humans (Moore et al. 1985; Hartmann et al. 1990; Lohr and Dooling 1998; Klinge and Klump 2009). Therefore, it is tempting to speculate from the behavioural data alone that ferrets mainly rely on temporal periodicity cues to process MCTs. In addition, other data from our lab (Walker et al.

2014) also suggest that ferrets use temporal periodicity cues in unresolved harmonics for pitch discrimination.

Specific comment about the behavioural paradigm used in this project is warranted. Ferrets are very active and curious species, and it is not easy to train them to maintain contact with the trigger spout while listening to reference HCTs until the target MCT is played. This is the main reason for the long training time, the variability of the data and the necessity to introduce correction trials after the first group of animals had been tested. It also explains not only the variability of the data, but also differences in strategy seemingly adopted by different animals in the same group (Chapter 6). However, and despite these differences, the longitudinal nature of our experimental design enabled us to unequivocally conclude that the A1-MGBv corticothalamic pathway is important for normal mistuning detection in ferrets.

We looked for neural correlates of mistuning detection by recording from the auditory thalamus. MGBv is located between the auditory midbrain and the auditory cortex, comprising a part of the core, central lemniscal pathway. Therefore, its position, the complex circuitry, and the exquisite tonal tuning of its neurons make the MGBv an attractive candidate in harmonic complex sound processing. Moreover, it receives extensive cortical feedback, which is known to modulate its response properties.

It has been demonstrated at various levels of the auditory pathway that neurons show increased firing rates to MCTs compared to HCTs and distinctive temporal response patterns that are phase locked to the envelop and temporal fine structure of MCTs (Sinex et al. 2002; Sinex et al. 2005; Sinex 2008; Fishman and

Steinschneider 2010). In Chapter 5, we showed that the increase in excitation and the distinct temporal patterns of neurons recorded in the MGBv are dependent on the degree of mistuning.

Spectral enhancement in the neural responses was, however, only observed with MCTs with a low fundamental frequency (F_0), while temporal information in MCTs was represented by the synchronized phase locked responses regardless of F_0. Thus, the responses to MCTs with a low F_0 provided evidence for the use of both spectral and temporal cues, and the temporal responses of MGBv neurons seem to define the mistuning detection thresholds.

These results therefore further suggest that ferrets use temporal cues for mistuning detection. In order to expand the use of this species in the study of complex sound perception, further investigation with a larger set of MCTs with different F_0s and mistuned harmonic positions will allow to understand the global patterns of mistuning detection in ferrets. For example, it would be interesting to explore the performance of ferrets in a mistuning detection task using MCTs with a high F_0, as MGBv neuron responses to MCTs with an 800 Hz F_0 did not show an increase in firing rate but did exhibit distinctive temporal response patterns (Chapter 5). Moreover, randomising the phase of the different tone components of the HCT would be a useful way of assessing the animal's dependence of temporal cues.

In the present electrophysiological study, we have not found a clear effect of mistuned harmonic position. The use of smaller mistuning shifts should be explored, given that behavioural studies in small animals have demonstrated threshold differences smaller than 1 Hz (Lohr and Dooling 1998; Klinge and

Klump 2009; Klinge and Klump 2010). Finally, combining behavioural and physiological studies in the same animal would be essential to identify the neural correlates for specific MCT perception and to understand the neural circuits involved in complex sound processing.

7.3. **The auditory thalamus as a linchpin in the processing of complex sounds**

We investigated the functional organization of the ferret auditory thalamus. Neurons in the MGBv were sensitive to tonal stimuli, showing short response latencies and sharply tuned frequency response areas (FRAs), while MGBd neurons were less sensitive to pure tones and the FRAs were broadly tuned. MGBm neurons were heterogeneous with broadly tuned or multipeaked FRAs. The response properties observed in the present study agree with previous studies in other species (cat: Rouiller et al. 1979; Rouiller et al. 1981; Calford 1983; Morel et al. 1987; Rodrigues-Dagaeff et al. 1989, guinea pig: Redies and Brandner 1991; Edeline et al. 1999; Wallace et al. 2007; Anderson et al. 2007, marmosets: Bartlett and Wang 2007; Bartlett and Wang 2011, mouse: Hackett et al. 2011, rat: Bordi and LeDoux 1994; Kimura et al. 2009, squirrel monkey: Allon et al. 1981). Thus, it supports the organization of auditory thalamus is well conserved among mammalian species.

Despite similar MGB general organization, tonotopic gradients in MGBv are more variable among species. In ferrets, a high-to-low gradient was observed from the most antero-dorsal to the most postero-ventral part of the MGBv (Chapter 4). That gradient resembles the organization described in cats (Calford and Webster 1981; Calford 1983; Rodrigues-Dagaeff et al. 1989). This adds to the similarities

that have been reported in the central auditory system between these species (Moore et al. 1983; Kelly et al. 1986; Phillips et al. 1988), although it should be noted that the frequency gradients of the two fields that comprise the primary auditory cortical areas of ferrets (Versnel et al. 2002; Nelken et al. 2004; Bizley et al. 2005) and cats (Knight 1977; Reale and Imig 1980) are quite different. Moreover, the response properties of ferret auditory nerve fibres are closer to those present in smaller animals (Sumner and Palmer 2012).

The tonotopic gradient in the MGBv of other species, such as guinea pigs (Redies and Brandner 1991) and gerbils (Budinger et al. 2013), has a somewhat different direction, with a low-to-high CF progression from dorsal to ventral, although mice (Hackett et al. 2011) more closely resemble cats and ferrets in this respect. The species differences may just derive from the differences of the shape and the orientation of the isofrequency lamina, and inter-species differences in tonotopic gradient orientation do not necessarily imply functional differences in MGBv but rather reflect anatomical differences.

The ferret thalamus seems to be a flatter version of the cat thalamus with a smaller dorso-ventral dimension. The cat MGB approximates a spherical ball while the ferret MGB seems to be more like a rugby ball in shape. This difference in gross anatomy might determine the folding and orientation of the isofrequency laminae, which in any case seem to follow the curvature of the MGB's latero-posterior shape.

To fully investigate the tonotopic organization in the ferret MGBv, a large set of electrode penetrations using different angles need to be made. Furthermore, it has recently been shown in cats that the middle part of MGBv

projects to the narrowly tuned central region of A1, and the anterior part of MGBv connects to dorsal A1, supporting a posterior to anterior segregation in this species (Read et al. 2011). This therefore needs to be explored in the ferret too. Although thalamocortical and corticothalamic pathways have been studied anatomically in ferrets in our group (part of the results were shown in Appendix Fig. A.1, from Nodal et al. 2006), anatomical studies to explore the detailed connectivity between each division of MGB and different cortical areas will be required to understand the functional organization of ferret auditory thalamus.

We found that MCTs elicited distinctive temporal firing patterns in the responses of ferret MGBv neurons tuned to low frequencies. This result agrees with the responses observed in IC neurons (Sinex et al. 2005). In A1, the change in firing rates was larger when the mistuned harmonic was closer to the neuron's best frequency, and this has been interpreted as a neural correlate of the 'pop out' sensation produced by a mistuned harmonic (Fishman and Steinschneider 2010). However, in the MGBv, the change in the firing rate is not due to the spectral enhancement and was observed when the firing rate was relatively low in responses to the HCTs (Chapter 5).

Thalamic neurons are sensitive to temporal modulation (Rouiller et al. 1981; Bartlett and Wang 2011) and show phase locked responses to stimulus periodicities, such as those in conspecific vocalizations in the guinea pig (Wallace et al. 2007). However, responses to complex tones in the thalamus have not previously been studied. Indeed, to my knowledge, Chapter 5 is the first investigation of responses to a large set of complex tones in the MGBv. We showed that MGBv neurons with low CFs can synchronize to components (<500 Hz) of the complex tones

irrespective of their F_0s. Other studies have shown that thalamic neurons are sensitive to rapidly modulated sounds (Miller et al. 2002) and can adapt to fluctuating noise in the presence of low level tones (Las et al. 2005).

It has been argued that temporal information is gradually transformed into a rate code at higher levels of the auditory pathway (Wang et al. 2008). Nevertheless, both spike rate of ferret AC neurons may contribute to pitch discrimination behaviour (Bizley et al. 2010). While two distinct populations of rate- and temporal-coding neurons coexist in the AC (Lu et al. 2001), these two coding types are exhibited by the same thalamic neurons (Bartlett and Wang 2007). Indeed, our data show that neurons with low CFs respond to MCTs with distinct temporal patterns and also show firing rate changes (Chapter 5), supporting the existence of mixed responses in the thalamus, which could be an important stage in the transformation of temporal coding to rate coding.

7.4. **The role of corticothalamic feedback**

To investigate the role of corticothalamic feedback, we combined the mistuning detection behaviour task with selective elimination of corticothalamic neurons by chromophore-targeted laser photolysis. Given the evidence that cortical feedback can alter the response properties of neurons in the thalamus (and other levels of the auditory pathway), we had the following hypotheses. First, corticothalamic feedback may sharpen the receptive fields of MGBv neurons, as happens in the visual thalamus (Jones et al. 2012), and assist in the discrimination of mistuned harmonics. Second, the feedback modulates the firing patterns in the recipient neurons, helping them to synchronize to the temporal structure of MCTs. As

discussed, it is likely that ferrets rely primarily on temporal periodicity cues for mistuning detection. Thus, impaired performance in mistuning detection after selective corticothalamic lesion supports that the corticothalamic feedback modulates temporal precision in thalamic neurons.

Manipulation of neural circuits has been used to study the neural networks involved in particular behaviours. For example, pharmacological inactivation or ablation of the auditory cortex impairs tone discrimination abilities (Ohl et al. 1999; Talwar et al. 2001; Ono et al. 2006; Zhang and Yan 2008; Jaramillo and Zador 2011). These approaches do not show, however, whether the behavioural impairments reflect the involvement of the cortex itself or its influence on other brain regions. On the other hand, manipulation of cortical activity by focal electrical simulation or cooling has demonstrated that A1 activity modulates firing patterns and spontaneous firing rate in MGBv (Ryugo and Weinberger 1976; Orman and Humphrey 1981; Villa et al. 1991; He 1997; He et al. 2002; Yu et al. 2004), suggesting that behavioural changes resulting from cortical lesions may be due primarily to a loss of corticofugal modulation.

However, the approaches mentioned were not able to target specific neuronal populations. We therefore chose to use chromophore-targeted laser photolysis, which selectively induces apoptosis in labelled cells without damaging other non-targeted neurons, glia and axons (Macklis 1993; Magavi et al. 2000). Using this technique, we were able to selectively eliminate a substantial proportion of corticothalamic projection neurons, which resulted in raised thresholds for mistuning detection (Chapter 6). Although this approach allowed us to target a specific pathway, there are limitations in the technique: the effects of

chromophore-targeted laser photolysis are irreversible, and it is difficult to control precise timing.

Ideally, the activity of corticothalamic neurons should be altered reversibly with high temporal precision in order to investigate how this feedback affects sound processing in the MGBv and behavioural performance in tasks such as mistuning detection. Optogenetics is a technique that has been developed over the past decade, which potentially allows the activity of a specific population of neurons to be controlled reversibly with millisecond precision (Fenno et al. 2011). It was applied in rat AC targeting the projections to the striatum to investigate the change of ability in frequency discrimination tasks when the pathway was selectively activated or silenced (Znamenskiy and Zador 2013; Xiong et al. 2015), and it is now becoming available in ferrets (Bajo et al. 2013). Alternatively, we could use designer receptor exclusively activated by designer drugs (DREADDs), a chemogenetic approach to reversibly manipulate specific neural types with a wider timeframe (minutes to hours) (Sternson and Roth 2014). In any case, temporally precise reversible manipulations targeting corticothalamic neurons will be essential for further studying the role of corticothalamic feedback.

Furthermore, *in vitro* and *in vivo* electrophysiological studies have elucidated the general mechanisms of corticothalamic feedback, including the involvement of collateral projections to the thalamic reticular nucleus (TRN) (Jones 1975). Therefore, MGBv neurons receive both of excitatory and inhibitory inputs (Fig. 7.1). If cortical and thalamic neurons had similar receptive fields, the MGBv neuron would be excited by reciprocally connected corticothalamic feedback (reviewed in Suga and Ma 2003). If the receptive fields in connected

cortical and MGBv neurons do not match, the effect will be broadly inhibitory. As a consequence, the receptive fields of MGBv neurons and their tuning properties are altered in a lateral inhibition manner, which is also observed in the somatosensory (Temereanca and Simons 2004) and visual (reviewed in Cudeiro and Sillito 2006) thalamus.

Moreover, as it has been suggested that the firing patterns in the thalamus are modulated by cortical activity (Sherman 2001; Sherman and Guillery 2013), recent studies have indicated that corticothalamic feedback may be important for controlling the gain of responses in the thalamus and the cortex. Cortical and thalamic neurons are generally suppressed by corticothalamic neurons via inhibitory inputs from the intracortical GABAergic circuits and the TRN (Olsen et al. 2012; Bortone et al. 2014). However, thalamic neurons can be reciprocally facilitated by corticothalamic inputs dependent on the cortical activity (Crandall et al. 2015). The auditory thalamus and cortex (MGB and A1) showed suppressed responses to the fluctuated background noise, suggesting corticothalamic feedback might be involved (Las et al. 2005). Perhaps this mechanism is far more complicated than the one proposed above that corticothalamic feedback contributes to the synchronized responses observed in the MGBv by facilitating the firing of these neurons. Cortical activity (not only of the A1 but also probably in the higher cortical fields) and attention (O'Connor et al. 2002; McAlonan et al. 2008) may determine which signals should be enhanced and supressed in MGBv neurons to achieve precise sound processing. Further studies are necessary to understand these mechanisms at the perceptual level while examining the microcircuits at the physiological level.

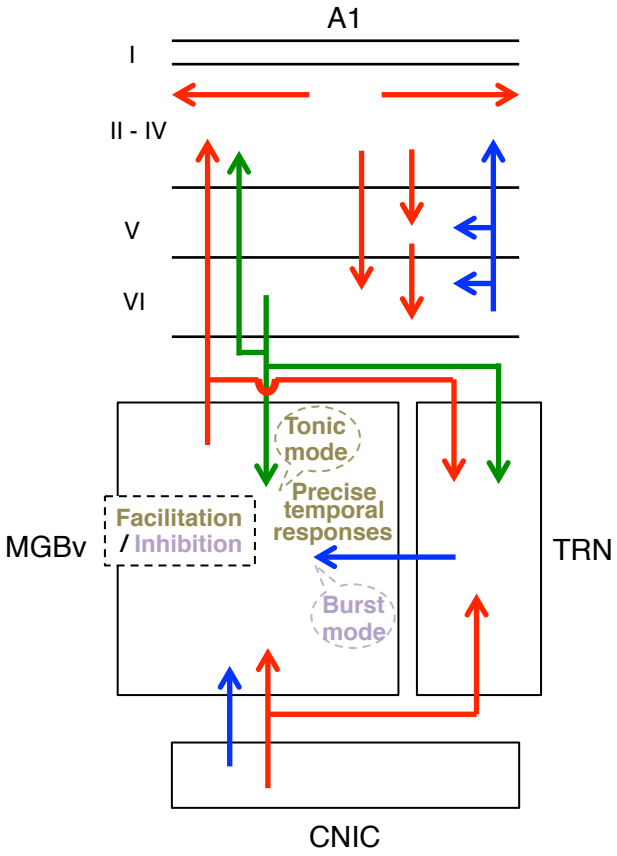

Figure 7.1 Model of role of corticothalamic feedback
In the feedforward ascending pathway, auditory information from the periphery is transmitted to the primary auditory cortex (A1) via the central nucleus of inferior colliculus (CNIC) and the ventral division of medial geniculate body (MGBv). These are excitatory inputs (red). MGBv neurons receive descending feedback projections from corticothalamic neurons (green), which enable the neurons to transition into tonic mode (brown). They also innervate the thalamic reticular nucleus (TRN), which provides inhibitory inputs (blue) to MGBv and decreases spontaneous rate (burst mode, purple). Other inhibitory inputs from the IC to the MGBv and intracortical circuits are also shown in blue.

7.5. Conclusions

In this thesis, the role of corticothalamic feedback has been studied in a mistuning detection behavioural task, combining selective elimination of corticothalamic neurons by chromophore-targeted laser photolysis. We have shown that corticothalamic feedback is essential for detecting temporal modulation of sounds. Since rapid temporal fluctuation is a characteristic of speech (e.g. Moore 2008) and fluctuating signals are important cues for segregate different sounds from background noise (Nelken et al. 1999; Las et al. 2005), our results suggests that corticothalamic feedback, one of the principal and hitherto poorly understood descending pathway in the auditory system, is important for auditory scene analysis.

Appendix

A.1. Beads conjugation

The photolysis technique was developed previously by Macklis and colleagues (Macklis 1993; Magavi et al. 2000). Fluorescent microbeads (red and green Retrobeads IX, Lumafluor Inc., Durham NC) were conjugated to chlorin e_6 monoethylene diamine monoamide disodium salt (C40890, Frontier Scientific Inc., Logan UT) activated with N-cyclohexyl-N′-(2-morpholinoethyl) carbodiimide methyl-p-toluenesulfonate (C106402, Sigma-Aldrich, Steinheim, Germany). 0.1 M glycine buffer (pH = 8) was added after 65 min to stop the reaction, and a pellet was produced by high-speed centrifugation (48,000 rpm) for 80 min at +4°C and suspended with double distilled water and phosphate buffer saline (PBS) at the end.

A.2. Nissl staining

Nissl staining is a classical method to visualize nucleic acid using the principle that a basic dye binds to negatively charged nucleic acids. Slides with brain sections were dipped through graded alcohol, 95-100 % EtOH, to chloroform/100% EtOH (1:1) solution, and back through graded alcohol, 95-70 % EtOH. Sections were

rehydrated with double distilled water and stained for 5-7 min in 0.5 % cresyl violet (wt/vol) solution (cresyl violet acetate, 61123, Fluka, Buchs, Switzerland). The solution was agitated and filtrated before using. Once stained, it was rinsed in double distilled water and dipped through graded alcohol, 70-95 % EtOH. Differentiation was performed by 1 % glacial acetic acid in 95 % EtOH solution for 5 min. Then, sections were fully dehydrated by passing through graded alcohol, 95-100 % EtOH, and Xylenes. Slides were coverslipped with mounting medium (QPath Coverquick 2000, VWR International, Fontenary-sous-Bois, France).

A.3. NeuN staining

NeuN staining was performed to visualize neuronal nuclei. Sections were washed in 0.1 M phosphate buffer saline (PBS) and permeated in 0.4% Triton in PBS. After rinsing with PSB, they were placed in 5% normal horse serum (S2000, Vector Laboratories Inc., Burlingame, CA) to block non-specific reaction. The first antibody (MAB377, monoclonal mouse antibody to NeuN, 1:500, Millipore, Temecula, CA) was applied to the sections for 3 days at +5°C on a shaker. The sections were washed in PBS and 0.1 % Triton in PBS, and the second antibody (biotinylated antibody to mouse IgG, Vector Laboratories Inc.) was applied for 2 hours at the room temperature. After consecutive rinsing with 0.1 % Triton in PBS and pure PBS, the reaction product was visualized by avidin biotin complex (PK6100 VECTASTAIN Elite ABC kit, Vector Laboratories Inc.) using 3,3'-diaminobenzine (SK4100 DAB peroxidase substrate kit, Vector Laboratories Inc.) in the presence of 0.003 % H_20_2 in 0.1 M PB. The sections were mounted on

double subbed slides and coverslipped with non-aqueous mounting medium (361254D, DEPEX mounting medium GURR, VWR International, Dorset, UK).

A.4. Anatomical study of tonotopic organization in ferret MGBv

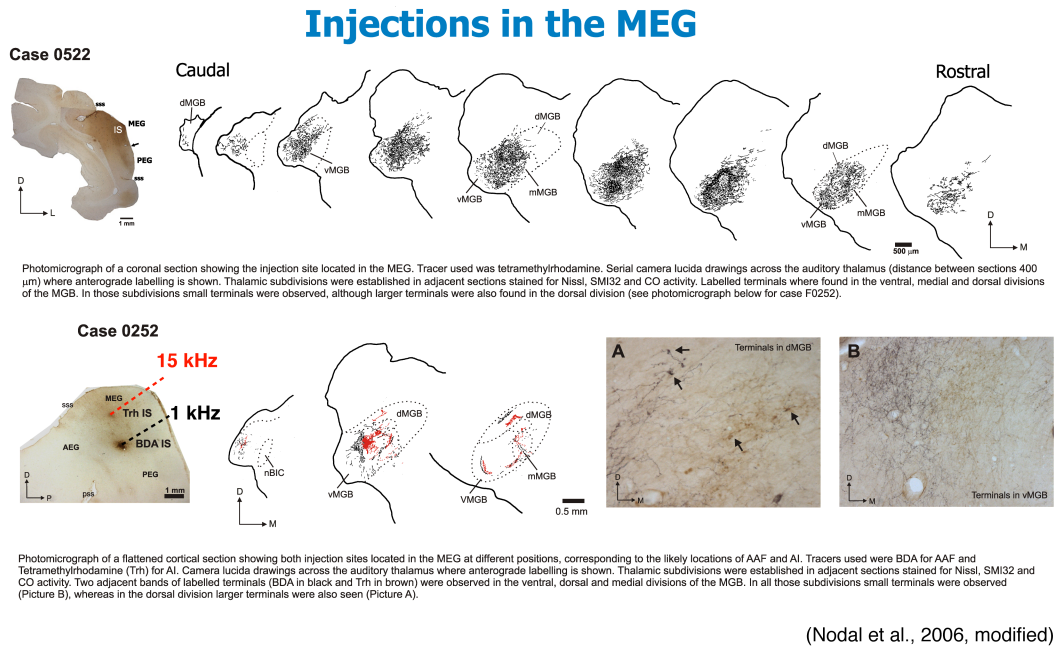

(Nodal et al., 2006, modified)

Figure A.1 Anatomical study of tonotopic organization in ferret MGBv.

A.5. Estimated periodicities

Mistuned complex tones			Estimated periodicities							
Stimulus parameters			(Hz)				(ms)			
F0 (Hz)	Shift	Mistuning (%)	*F0*	*Beating*	*Mistuning*	*Interaction*	F0	Beating	Mistuning	Interaction
200	2	0.05	200.0	199.8	0.2	199.6	5.0	5.0	5000.0	5.0
200	2	0.2	200.0	199.2	0.8	198.4	5.0	5.0	1270.3	5.0
200	2	0.8	200.0	196.9	3.1	193.8	5.0	5.1	322.7	5.2
200	2	3	200.0	187.8	12.2	175.6	5.0	5.3	82.0	5.7
200	2	12	200.0	152.0	48.0	104.0	5.0	6.6	20.8	9.6
200	4	0.05	200.0	199.6	0.4	199.2	5.0	5.0	2500.0	5.0
200	4	0.2	200.0	198.4	1.6	196.9	5.0	5.0	635.2	5.1
200	4	0.8	200.0	193.8	6.2	187.6	5.0	5.2	161.4	5.3
200	4	3	200.0	175.6	24.4	151.2	5.0	5.7	41.0	6.6
200	4	12	200.0	104.0	96.0	8.0	5.0	9.6	10.4	125.0
200	8	0.05	200.0	199.2	0.8	198.4	5.0	5.0	1250.0	5.0
200	8	0.2	200.0	196.9	3.1	193.7	5.0	5.1	317.6	5.2
200	8	0.8	200.0	187.6	12.4	175.2	5.0	5.3	80.7	5.7
200	8	3	200.0	151.2	48.8	102.4	5.0	6.6	20.5	9.8
200	8	12	200.0	8.0	192.0	-184.0	5.0	125.0	5.2	-5.4
400	2	0.05	400.0	399.6	0.4	399.2	2.5	2.5	2500.0	2.5
400	2	0.2	400.0	398.4	1.6	396.9	2.5	2.5	635.2	2.5
400	2	0.8	400.0	393.8	6.2	387.6	2.5	2.5	161.4	2.6
400	2	3	400.0	375.6	24.4	351.2	2.5	2.7	41.0	2.8
400	2	12	400.0	304.0	96.0	208.0	2.5	3.3	10.4	4.8
400	4	0.05	400.0	399.2	0.8	398.4	2.5	2.5	1250.0	2.5
400	4	0.2	400.0	396.9	3.1	393.7	2.5	2.5	317.6	2.5
400	4	0.8	400.0	387.6	12.4	375.2	2.5	2.6	80.7	2.7
400	4	3	400.0	351.2	48.8	302.4	2.5	2.8	20.5	3.3
400	4	12	400.0	208.0	192.0	16.0	2.5	4.8	5.2	62.5
400	8	0.05	400.0	398.4	1.6	396.8	2.5	2.5	625.0	2.5
400	8	0.2	400.0	393.7	6.3	387.4	2.5	2.5	158.8	2.6
400	8	0.8	400.0	375.2	24.8	350.4	2.5	2.7	40.3	2.9
400	8	3	400.0	302.4	97.6	204.9	2.5	3.3	10.2	4.9
400	8	12	400.0	16.0	384.0	-368.0	2.5	62.5	2.6	-2.7
800	2	0.05	800.0	799.2	0.8	798.4	1.3	1.3	1250.0	1.3
800	2	0.2	800.0	796.9	3.1	793.7	1.3	1.3	317.6	1.3
800	2	0.8	800.0	787.6	12.4	775.2	1.3	1.3	80.7	1.3
800	2	3	800.0	751.2	48.8	702.4	1.3	1.3	20.5	1.4
800	2	12	800.0	608.0	192.0	416.0	1.3	1.6	5.2	2.4
800	4	0.05	800.0	798.4	1.6	796.8	1.3	1.3	625.0	1.3
800	4	0.2	800.0	793.7	6.3	787.4	1.3	1.3	158.8	1.3
800	4	0.8	800.0	775.2	24.8	750.4	1.3	1.3	40.3	1.3
800	4	3	800.0	702.4	97.6	604.9	1.3	1.4	10.2	1.7
800	4	12	800.0	416.0	384.0	32.0	1.3	2.4	2.6	31.3
800	8	0.05	800.0	796.8	3.2	793.6	1.3	1.3	312.5	1.3
800	8	0.2	800.0	787.4	12.6	774.8	1.3	1.3	79.4	1.3
800	8	0.8	800.0	750.4	49.6	700.9	1.3	1.3	20.2	1.4
800	8	3	800.0	604.9	195.1	409.8	1.3	1.7	5.1	2.4
800	8	12	800.0	32.0	768.0	-736.0	1.3	31.3	1.3	-1.4

Mistuning (Hz) = Mistuning (%) / 100 x *F0* (Hz) x Shift
Beating (Hz) = *F0* (Hz) x (Shift+1) - [F0 (Hz) x Shift + *Mistuning* (Hz)]
Thus, *Mistuning* (Hz) is also calculated as *F0* (Hz) - *Beating* (Hz)
Interaction (Hz) = *Beating* (Hz) - *Mistuning* (Hz)

Table A.2 Estimated periodicities in responses to MCTs
Shift indicates mistuned harmonic position. F_0 was defined as the frequency of the F_0 of the stimuli, and *Beating* is the difference in frequency between mistuned harmonic and next higher harmonic. *Mistuning* corresponds to the degree of mistuning shift in hertz, which is the frequency difference of F_0 and *Beating*. Then, *Interaction* was calculated as the frequency difference of *Beating* and *Mistuning* (also see Chapter 2 Methods).

A.6. Example of envelope of a MCT

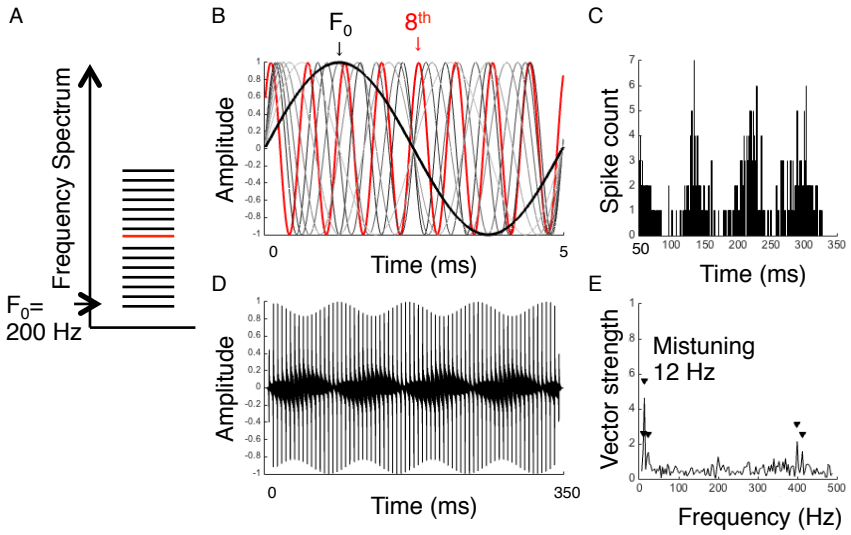

Figure A.3 Example of envelope of a MCT
(A) Schematic of sound stimulus. Mistuned complex tones (MCT) comprised 16 harmonics with a 200 Hz fundamental frequency (F_0, indicated by the arrow), and the 8th harmonic was shifted to a higher frequency by 0.8%. All harmonics are represented by the short horizontal lines, and the 8th mistuned harmonics is highlighted in red. (B) Individual harmonic components of the MCT are shown for one cycle of F_0. F_0 is shown in black. 8th harmonic is highlighted by red. Other harmonic components are shown in grey. (C) The PSTH for the stimulus presentation time from 51 to 350 ms (sustained response window) indicates a response with a period of 81 ms. (D) Envelope of the MCT for the 350 ms tone duration. (E) Vector strength values were computed from the PSTH. A statistically significant peak (Rayleigh test, $P < 0.001$, indicated by the downward-pointing triangle) was observed at 12 Hz, which corresponds to 81 ms periodicity and 0.8% mistuning (12 Hz). C and E were shown as figure 5.7A,B.

A.7. Correct response rate

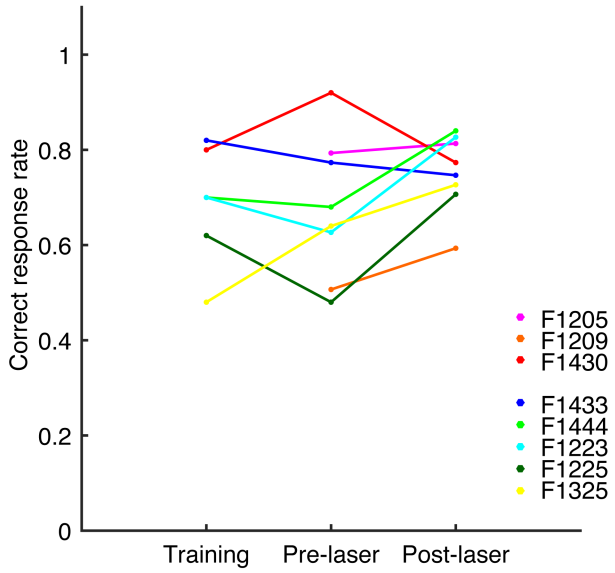

Figure A4 Correct response rate in the different training and re-training periods. The proportion of correctly answered trials in the training phase, where animals detect complex tones with intensity difference cues. The training phase precedes microbeads injection, pre- and post-laser testing period. Different colours represent each individual animal.

A.8. Reaction time in pre- and post-laser periods for two examples.

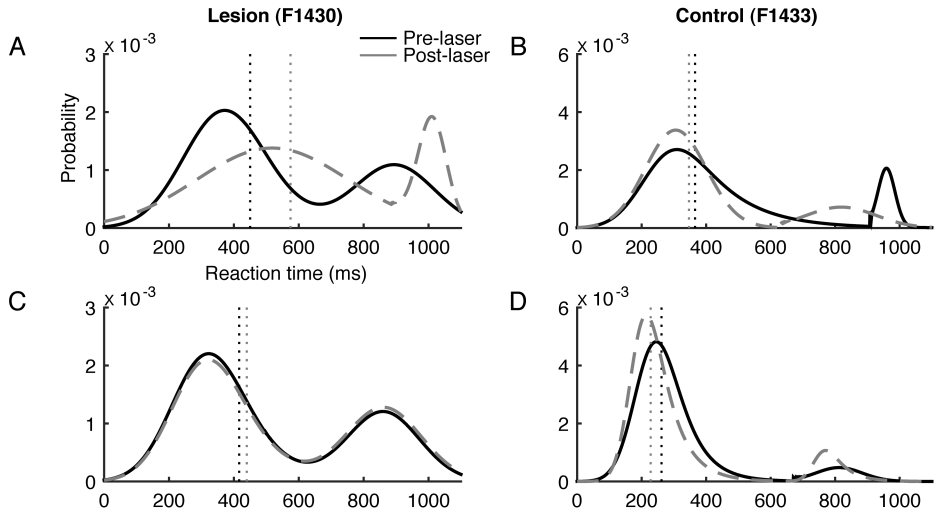

Figure A.5 Reaction time in pre- and post-laser periods for two examples of lesion and control animals.
Fitted reaction time for pre-laser (black) and post-laser (grey long-dashed). The vertical dashed lines indicate median of reaction time for pre- and post- laser, respectively. It was drawn for different degrees of mistuning (A and B, small, < 3 Hz; C and D, large, 3-8 Hz). (A, C) a lesion animal (F1430). (B, D) a control animal (F1433).

References

Aitkin LM, Prain SM (1974) Medial geniculate body: unit responses in the awake cat. J Neurophysiol 37:512–521.

Aitkin LM, Webster WR, Veale JL, Crosby DC (1975) Inferior colliculus. I. Comparison of response properties of neurons in central, pericentral, and external nuclei of adult cat. J Neurophysiol 38:1196–1207.

Alain C, Arnott SR, Picton TW (2001) Bottom-up and top-down influences on auditory scene analysis: evidence from event-related brain potentials. J Exp Psychol Hum Percept Perform 27:1072–1089. doi: 10.1037//0096-1523.27.5.1072

Alain C, Schuler BM, McDonald KL (2002) Neural activity associated with distinguishing concurrent auditory objects. J Acoust Soc Am 111:990–995. doi: 10.1121/1.1434942

Allon N, Yeshurun Y, Wollberg Z (1981) Responses of single cells in the medial geniculate body of awake squirrel monkeys. Exp Brain Res 41:222–232. doi: 10.1007/BF00238879

Anderson L a, Linden JF (2011) Physiological differences between histologically defined subdivisions in the mouse auditory thalamus. Hear Res 274:48–60. doi: 10.1016/j.heares.2010.12.016

Anderson L a., Wallace MN, Palmer a. R (2007) Identification of subdivisions in the medial geniculate body of the guinea pig. Hear Res 228:156–167. doi: 10.1016/j.heares.2007.02.005

Ando S, Kida N, Oda S (2002) Practice effects on reaction time for peripheral and central visual fields. Percept Mot Skills 95:747–751. doi: 10.2466/pms.2002.95.3.747

Ashmore J (2008) Cochlear outer hair cell motility. Physiol Rev 88:173–210. doi: 10.1152/physrev.00044.2006

Bajo VM, Korn C, Reynolds K, et al (2013) Behavioural and neural effects of silencing the auditory cortex in adult ferrets using optogenetics. In: Society for Neuroscience Abstracts. Washington, DC, pp 877–878

Bajo VM, Moore DR (2005) Descending projections from the auditory cortex to the inferior colliculus in the gerbil, Meriones unguiculatus. J Comp Neurol 486:101–16. doi: 10.1002/cne.20542

Bajo VM, Nodal FR, Bizley JK, et al (2007) The ferret auditory cortex: Descending projections to the inferior colliculus. Cereb Cortex 17:475–491. doi: 10.1093/cercor/bhj164

Bajo VM, Nodal FR, Moore DR, King AJ (2010) The descending corticocollicular pathway mediates learning-induced auditory plasticity. Nat Neurosci 13:253–60. doi: 10.1038/nn.2466

Bajo VM, Rouiller EM, Welker E, et al (1995) Morphology and spatial distribution of corticothalamic terminals originating from the cat auditory cortex. Hear Res 83:161–74. doi: 10.1016/0378-5955(94)00199-Z

Bao S, Chang EF, Woods J, Merzenich MM (2004) Temporal plasticity in the primary auditory cortex induced by operant perceptual learning. Nat Neurosci 7:974–981. doi: 10.1038/nn1293

Bartlett EL (2013) The organization and physiology of the auditory thalamus and its role in processing acoustic features important for speech perception. Brain Lang 126:29–48. doi: 10.1016/j.bandl.2013.03.003

Bartlett EL, Stark JM, Guillery RW, Smith PH (2000) Comparison of the fine structure of cortical and collicular terminals in the rat medial geniculate body. Neuroscience 100:811–28.

Bartlett EL, Wang X (2011) Correlation of neural response properties with auditory thalamus subdivisions in the awake marmoset. J Neurophysiol 105:2647–2667. doi: 10.1152/jn.00238.2010

Bartlett EL, Wang X (2007) Neural representations of temporally modulated signals in the auditory thalamus of awake primates. J Neurophysiol 97:1005–17. doi: 10.1152/jn.00593.2006

Bizley JK, Bajo VM, Nodal FR, King AJ (2015) Cortico-cortical connectivity within ferret auditory cortex. J Comp Neurol 000:000–000. doi: 10.1002/cne.23784

Bizley JK, King AJ (2008) Visual–auditory spatial processing in auditory cortical neurons. Brain Res 1242:24–36. doi: http://dx.doi.org/10.1016/j.brainres.2008.02.087

Bizley JK, Nodal FR, Bajo VM, et al (2007) Physiological and anatomical evidence for multisensory interactions in auditory cortex. Cereb Cortex 17:2172–89. doi: 10.1093/cercor/bhl128

Bizley JK, Nodal FR, Nelken I, King AJ (2005) Functional organization of ferret auditory cortex. Cereb Cortex 15:1637–53. doi: 10.1093/cercor/bhi042

Bizley JK, Walker KM, King AJ, Schnupp JW (2013a) Spectral timbre perception in ferrets: discrimination of artificial vowels under different listening conditions. J Acoust Soc Am 133:365–376. doi: 10.1121/1.4768798

Bizley JK, Walker KMM, King AJ, Schnupp JWH (2010) Neural ensemble codes for stimulus periodicity in auditory cortex. J Neurosci 30:5078–5091. doi: 10.1523/JNEUROSCI.5475-09.2010

Bizley JK, Walker KMM, Nodal FR, et al (2013b) Auditory cortex represents both pitch judgments and the corresponding acoustic cues. Curr Biol 23:620–625. doi: 10.1016/j.cub.2013.03.003

Bleeck S, Ingham NJ, Verhey JL, Winter IM (2008) Rebound depolarization in single units of the ventral cochlear nucleus: A contribution to grouping by common onset? Neuroscience 154:139–146. doi: 10.1016/j.neuroscience.2008.03.020

Boehnke SE, Phillips DP (2005) The relation between auditory temporal interval processing and sequential stream segregation examined with stimulus laterality differences. Percept Psychophys 67:1088–1101. doi: 10.3758/BF03193634

Bordi F, LeDoux JE (1994) Response properties of single units in areas of rat auditory thalamus that project to the amygdala - II. Cells receiving convergent auditory and somatosensory inputs and cells antidromically activated by amygdala stimulation. Exp Brain Res 98:275–286. doi: 10.1007/BF00228415

Bortone DS, Olsen SR, Scanziani M (2014) Translaminar inhibitory cells recruited by layer 6 corticothalamic neurons suppress visual cortex. Neuron 82:474–85. doi: 10.1016/j.neuron.2014.02.021

Brand A, Behrend O, Marquardt T, et al (2002) Precise inhibition is essential for microsecond interaural time difference coding. Nature 417:543–547. doi: 10.1038/417543a

Brawer JR, Morest DK, Kane EC (1974) The neuronal architecture of the cochlear nucleus of the cat. J Comp Neurol 155:251–300. doi: 10.1002/cne.901550302

Bregman A (1990) Auditory Scene Analysis: The Perceptual Organization of Sound. The MIT Press, Cambridge, MA

Bregman AS, Campbell J (1971) Primary auditory stream segregation and perception of order in rapid sequences of tones. J Exp Psychol 89:244–249. doi: 10.1037/h0031163

Briggs F, Usrey WM (2008) Emerging views of corticothalamic function. Curr Opin Neurobiol 18:403–407. doi: 10.1016/j.conb.2008.09.002

Budinger E, Brosch M, Scheich H, Mylius J (2013) The subcortical auditory structures in the mongolian gerbil: II. Frequency-related topography of the connections with cortical field AI. J Comp Neurol 521:2772–97. doi: 10.1002/cne.23314

Buell TN, Hafter ER (1991) Combination of binaural information across frequency bands. J Acoust Soc Am 90:1894–1900. doi: 10.1121/1.401668

Calford MB (1983) The parcellation of the medial geniculate body of the cat defined by the auditory response properties of single units. J Neurosci 3:2350–2364.

Calford MB, Aitkin LM (1983) Ascending projections to the medial geniculate body of the cat: evidence for multiple, parallel auditory pathways through thalamus. J Neurosci 3:2365–2380.

Calford MB, Webster WR (1981) Auditory representation within principal division of cat medial geniculate body: an electrophysiology study. J Neurophysiol 45:1013–1028.

Carandini M, Churchland AK (2013) Probing perceptual decisions in rodents. Nat Neurosci 16:824–831. doi: 10.1038/nn.3410

Cariani P a, Delgutte B (1996a) Neural correlates of the pitch of complex tones. I. Pitch and pitch salience. J Neurophysiol 76:1698–1716.

Cariani P a, Delgutte B (1996b) Neural correlates of the pitch of complex tones. II. Pitch shift, pitch ambiguity, phase invariance, pitch circularity, rate pitch, and the dominance region for pitch. J Neurophysiol 76:1717–1734.

Carr CE, Konishi M (1988) Axonal delay lines for time measurement in the owl's brainstem. Proc Natl Acad Sci U S A 85:8311–8315. doi: 10.1073/pnas.85.21.8311

Chase SM, Young ED (2008) Cues for Sound Localization Are Encoded in Multiple Aspects of Spike Trains in the Inferior Colliculus. J Neurophysiol 99:1672–1682. doi: 10.1152/jn.00644.2007

Cherry EC (1953) Some Experiments on the Recognition of Speech, with One and with Two Ears. J Acoust Soc Am 25:975. doi: 10.1121/1.1907229

Chowdhury S a., Suga N (2000) Reorganization of the frequency map of the auditory cortex evoked by cortical electrical stimulation in the big brown bat. J Neurophysiol 83:1856–1863.

Christison-Lagay KL, Gifford AM, Cohen YE (2014) Neural correlates of auditory scene analysis and perception. Int J Psychophysiol 95:238–245. doi: 10.1016/j.ijpsycho.2014.03.004

Crandall SR, Cruikshank SJ, Connors BW (2015) A corticothalamic switch: controlling the thalamus with dynamic synapses. Neuron 86:768–82. doi: 10.1016/j.neuron.2015.03.040

Crick FC (1984) Function of the thalamic reticular complex : The searchlight hypothesis Neurobiology. Proc Natl Acad Sci U S A 81:4586–4590. doi: 10.1073/pnas.81.14.4586

Cudeiro J, Sillito AM (2006) Looking back: corticothalamic feedback and early visual processing. Trends Neurosci. 29:298–306.

Culling JF, Darwin CJ (1994) Perceptual and computational separation of simultaneous vowels: Cues arising from low-frequency beating. J Acoust Soc Am 95:1559–1569. doi: 10.1121/1.408543

Culling JF, Hawley ML, Litovsky RY (2004) The role of head-induced interaural time and level differences in the speech reception threshold for multiple interfering sound sources. J Acoust Soc Am 116:1057. doi: 10.1121/1.1772396

Dannenbring GL, Bregman AS (1978) Streaming vs. fusion of sinusoidal components of complex tones. Percept Psychophys 24:369–376. doi: 10.3758/BF03204255

Darwin CJ (1984) Perceiving vowels in the presence of another sound: constraints on formant perception. J Acoust Soc Am 76:1636–1647. doi: 10.1121/1.391610

Darwin CJ, Hukin RW (1999) Auditory objects of attention: the role of interaural time differences. J Exp Psychol Hum Percept Perform 25:617–629. doi: 10.1037/0096-1523.25.3.617

Darwin CJ, Sutherland NS (1984) Grouping frequency components of vowels: When is a harmonic not a harmonic? Q J Exp Psychol Sect A 36:193–208. doi: 10.1080/14640748408402155

De Cheveigné A (1997) Concurrent vowel identification. III. A neural model of harmonic interference cancellation. J Acoust Soc Am 101:2857. doi: 10.1121/1.419480

De Cheveigné A (1995) Identification of concurrent harmonic and inharmonic vowels: A test of the theory of harmonic cancellation and enhancement. J Acoust Soc Am 97:3736. doi: 10.1121/1.412389

De Cheveigné A, Kawahara H, Tsuzaki M, Aikawa K (1997a) Concurrent vowel identification. I. Effects of relative amplitude and F[sub 0] difference. J Acoust Soc Am 101:2839. doi: 10.1121/1.418517

De Cheveigné A, McAdams S, Marin CMH (1997b) Concurrent vowel identification. II. Effects of phase, harmonicity, and task. J Acoust Soc Am 101:2848. doi: 10.1121/1.419476

De La Mothe LA, Blumell S, Kajikawa Y, Hackett TA (2006) Thalamic connections of the auditory cortex in marmoset monkeys: Core and medial belt regions. J Comp Neurol 496:72–96. doi: 10.1002/cne.20924

Dooling RJ, Leek MR, Gleich O, Dent ML (2002) Auditory temporal resolution in birds: discrimination of harmonic complexes. J Acoust Soc Am 112:748–759. doi: 10.1121/1.1494447

Dorfman DD, Biderman M (1971) A learning model for a continuum of sensory states. J Math Psychol 8:264–284. doi: 10.1016/0022-2496(71)90017-4

Edeline JM, Manunta Y, Nodal FR, Bajo VM (1999) Do auditory responses recorded from awake animals reflect the anatomical parcellation of the auditory thalamus? Hear Res 131:135–52.

Eramudugolla R, McAnally KI, Martin RL, et al (2008) The role of spatial location in auditory search. Hear Res 238:139–146. doi: 10.1016/j.heares.2007.10.004

Eyding D, Macklis JD, Neubacher U, et al (2003) Selective elimination of corticogeniculate feedback abolishes the electroencephalogram dependence of primary visual cortical receptive fields and reduces their spatial specificity. J Neurosci 23:7021–33.

Farley SD, Lehner PN, Clark T, Trost C (1987) Vocalizations of the Siberian Ferret (Mustela eversmanni) and Comparisons with Other Mustelids. J Mammal 68:413–416. doi: 10.2307/1381487

Fay RR (1988) Hearing in Vertebrates: A Psychophysics Databook. Hill-Fay Associates, Winnetka, IL, pp 451–458

Fay RR (1992) Structure and Function in Sound Discrimination Among Vertebrates. In: The Evolutionary Biology of Hearing. pp 229–263

Fenno L, Yizhar O, Deisseroth K (2011) The development and application of optogenetics. Annu Rev Neurosci 34:389–412. doi: 10.1146/annurev-neuro-061010-113817

Fishman YI, Micheyl C, Steinschneider M (2013) Neural representation of harmonic complex tones in primary auditory cortex of the awake monkey. J Neurosci 33:10312–10323. doi: 10.1523/JNEUROSCI.0020-13.2013

Fishman YI, Steinschneider M (2010) Neural correlates of auditory scene analysis based on inharmonicity in monkey primary auditory cortex. J Neurosci 30:12480–12494. doi: 10.1523/JNEUROSCI.1780-10.2010

Fishman YI, Steinschneider M, Micheyl C (2014) Neural Representation of Concurrent Harmonic Sounds in Monkey Primary Auditory Cortex: Implications for Models of Auditory Scene Analysis. J Neurosci 34:12425–12443. doi: 10.1523/JNEUROSCI.0025-14.2014

Fritz JB, Elhilali M, Shamma SA (2005) Differential dynamic plasticity of A1 receptive fields during multiple spectral tasks. J Neurosci 25:7623–7635. doi: 10.1523/JNEUROSCI.1318-05.2005

Games K, Winer J a (1988) Layer V in rat auditory cortex: Projections to the inferior colliculus and contralateral cortex. Hear Res 34:1–25. doi: 10.1016/0378-5955(88)90047-0

Gao E, Suga N (1998) Experience-dependent corticofugal adjustment of midbrain frequency map in bat auditory system. Proc Natl Acad Sci U S A 95:12663–12670. doi: 10.1073/pnas.95.21.12663

Godwin DW, Van Horn SC, Erişir A, et al (1996) Ultrastructural localization suggests that retinal and cortical inputs access different metabotropic glutamate receptors in the lateral geniculate nucleus. J Neurosci 16:8181–92.

Gold JR, Nodal FR, Peters F, et al (2015) Auditory gap-in-noise detection behavior in ferrets and humans. Behav Neurosci 129:473–490. doi: 10.1037/bne0000065

Goldberg JM, Brown PB (1969) Response of binaural neurons of dog superior olivary complex to dichotic tonal stimuli: some physiological mechanisms of sound localization. J Neurophysiol 32:613–636. doi: 10.1007/978-1-4612-2700-7_3

Goldstein JL (1973) An optimum processor theory for the central formation of the pitch of complex tones. J Acoust Soc Am 54:1496–1516. doi: 10.1121/1.1978261

González-Hernández TH, Galindo-Mireles D, Castañeyra-Perdomo A, Ferres-Torres R (1991) Divergent projections of projecting neurons of the inferior colliculus to the medial geniculate body and the contralateral inferior colliculus in the rat. Hear Res 52:17–21. doi: 10.1016/0378-5955(91)90184-B

Granseth B (2004) Dynamic properties of corticogeniculate excitatory transmission in the rat dorsal lateral geniculate nucleus in vitro. J Physiol 556:135–146. doi: 10.1113/jphysiol.2003.052720

Guinan JJ, Norris BE, Guinan SS (1972) Single Auditory Units in the Superior Olivary Complex: II: Locations of Unit Categories and Tonotopic Organization. Int J Neurosci 4:147–166. doi: 10.3109/00207457209164756

Hackett T a, Barkat TR, O'Brien BMJ, et al (2011) Linking topography to tonotopy in the mouse auditory thalamocortical circuit. J Neurosci 31:2983–95. doi: 10.1523/JNEUROSCI.5333-10.2011

Hackett T a., Preuss TM, Kaas JH (2001) Architectonic identification of the core region in auditory cortex of macaques, chimpanzees, and humans. J Comp Neurol 441:197–222. doi: 10.1002/cne.1407

Hall JW, Haggard MP, Fernandes MA (1984) Detection in noise by spectro-temporal pattern analysis. J Acoust Soc Am 76:50–56. doi: 10.1121/1.391005

Hartmann WM, McAdams S, Smith BK (1990) Hearing a mistuned harmonic in an otherwise periodic complex tone. J Acoust Soc Am 88:1712–1724. doi: 10.1121/1.400246

He J (2003) Corticofugal modulation of the auditory thalamus. Exp Brain Res 153:579–590. doi: 10.1007/s00221-003-1680-5

He J (1997) Modulatory effects of regional cortical activation on the onset responses of the cat medial geniculate neurons. J Neurophysiol 77:896–908.

He J, Yu Y-Q, Xiong Y, et al (2002) Modulatory effect of cortical activation on the lemniscal auditory thalamus of the Guinea pig. J Neurophysiol 88:1040–50.

Heathcote A, Popiel SJ, Mewhort DJ (1991) Analysis of response time distributions: An example using the Stroop task. Psychol. Bull. 109:340–347.

Heffner HE, Heffner RS (1986) Hearing loss in Japanese macaques following bilateral auditory cortex lesions. J Neurophysiol 55:256–271.

Heil P, Peterson AJ (2015) Basic response properties of auditory nerve fibers: a review. Cell Tissue Res. 129–158.

Hill NI, Darwin CJ (1996) Lateralization of a perturbed harmonic : Effects of onset asynchrony and mistuning a). 100:2352–2364.

Hohle RH (1965) Inferred components of reaction times as functions of foreperiod duration. J Exp Psychol 69:382–386. doi: 10.1037/h0021740

Horst JW, Javel E, Farley GR (1986) Coding of spectral fine structure in the auditory nerve. I. Fourier analysis of period and interspike interval histograms. J Acoust Soc Am 79:398–416. doi: 10.1121/1.393528

Houtsma AJM, Smurzynski J (1990) Pitch identification and discrimination for complex tones with many harmonics. J Acoust Soc Am 87:304–310. doi: 10.1121/1.399297

Huang CL, Larue DT, Winer J a. (1999) GABAergic organization of the cat medial geniculate body. J Comp Neurol 415:368–392. doi: 10.1002/(SICI)1096-9861(19991220)415:3<368::AID-CNE4>3.0.CO;2-I

Huang CL, Winer J a. (2000) Auditory thalamocortical projections in the cat: Laminar and areal patterns of input. J Comp Neurol 427:302–331. doi: 10.1002/1096-9861(20001113)427:2<302::AID-CNE10>3.0.CO;2-J

Huetz C, Philibert B, Edeline J-M (2009) A spike-timing code for discriminating conspecific vocalizations in the thalamocortical system of anesthetized and awake guinea pigs. J Neurosci 29:334–350. doi: 10.1523/JNEUROSCI.3269-08.2009

Jaramillo S, Zador AM (2011) The auditory cortex mediates the perceptual effects of acoustic temporal expectation. Nat Neurosci 14:246–251. doi: 10.1038/nn.2688

Jeffress L a (1948) A place theory of sound localization. J Comp Physiol Psychol 41:35–39. doi: 10.1037/h0061495

Jones EG (1975) Some aspects of the organization of the thalamic reticular complex. J Comp Neurol 162:285–308. doi: 10.1002/cne.901620302

Jones EG (2001) The thalamic matrix and thalamocortical synchrony. Trends Neurosci 24:595–601. doi: 10.1016/S0166-2236(00)01922-6

Jones EG (ed) (1985) The Thalamus. Springer US, Boston, MA

Jones HE, Andolina IM, Ahmed B, et al (2012) Differential feedback modulation of center and surround mechanisms in parvocellular cells in the visual thalamus. J Neurosci 32:15946–51. doi: 10.1523/JNEUROSCI.0831-12.2012

Kadia SC, Wang X (2003) Spectral integration in A1 of awake primates: neurons with single- and multipeaked tuning characteristics. J Neurophysiol 89:1603–22. doi: 10.1152/jn.00271.2001

Kalappa BI, Brozoski TJ, Turner JG, Caspary DM (2014) Single unit hyperactivity and bursting in the auditory thalamus of awake rats directly correlates with behavioural evidence of tinnitus. J Physiol 592:5065–5078. doi: 10.1113/jphysiol.2014.278572

Kalluri S, Depireux DA, Shamma SA (2008) Perception and cortical neural coding of harmonic fusion in ferrets. J Acoust Soc Am 123:2701–2716. doi: 10.1121/1.2902178

Kavanagh GL, Kelly JB (1988) Hearing in the ferret (Mustela putorius): effects of primary auditory cortical lesions on thresholds for pure tone detection. J Neurophysiol 60:879–88. doi: 10.1016/0378-5955(86)90025-0

Kavanagh GL, Kelly JB (1987) Contribution of auditory cortex to sound localization by the ferret (Mustela putorius). J Neurophysiol 57:1746–1766.

Keating P, Dahmen JC, King AJ (2013) Context-specific reweighting of auditory spatial cues following altered experience during development. Curr Biol 23:1291–1299. doi: 10.1016/j.cub.2013.05.045

Keating P, Nodal FR, King AJ (2014) Behavioural sensitivity to binaural spatial cues in ferrets: Evidence for plasticity in the duplex theory of sound localization. Eur J Neurosci 39:197–206. doi: 10.1111/ejn.12402

Keilson SE, Richards VM, Wyman BT, Young ED (1997) The representation of concurrent vowels in the cat anesthetized ventral cochlear nucleus: evidence for a periodicity-tagged spectral representation. J Acoust Soc Am 102:1056–1071. doi: 10.1121/1.419859

Kelly JB, Kavanagh GL, Dalton JC (1986) Hearing in the ferret (Mustela putorius): thresholds for pure tone detection. Hear Res 24:269–275. doi: 10.1016/0378-5955(86)90025-0

Kilgard MP, Merzenich MM (1998) Plasticity of temporal information processing in the primary auditory cortex. Nautre Neoscience 1:727–731. doi: 10.1038/3729

Kilgard MP, Pandya PK, Vazquez J, et al (2001) Sensory input directs spatial and temporal plasticity in primary auditory cortex. J Neurophysiol 86:326–338.

Kimura A, Imbe H, Donishi T (2009) Axonal projections of auditory cells with short and long response latencies in the medial geniculate nucleus: Distinct topographies in the connection with the thalamic reticular nucleus. Eur J Neurosci 30:783–799. doi: 10.1111/j.1460-9568.2009.06880.x

Klinge A, Itatani N, Klump GM (2010) A Comparative View on the Perception of Mistuning: Constraints of the Auditory Periphery. In: Lopez-Poveda EA, Palmer AR, Meddis R (eds) Neurophysiological Bases of Auditory Perception. Springer New York, New York, NY, pp 465–475

Klinge A, Klump GM (2010) Mistuning detection and onset asynchrony in harmonic complexes in Mongolian gerbils. J Acoust Soc Am 128:280–290. doi: 10.1121/1.3436552

Klinge A, Klump GM (2009) Frequency difference limens of pure tones and harmonics within complex stimuli in Mongolian gerbils and humans. J Acoust Soc Am 125:304–314. doi: 10.1121/1.3021315

Knight PL (1977) Representation of the cochlea within the anterior auditory field (AAF) of the cat. Brain Res 130:447–467. doi: 10.1016/0006-8993(77)90108-1

Kowalski N, Versnel H, Shamma S a (1995) Comparison of responses in the anterior and primary auditory fields of the ferret cortex. J Neurophysiol 73:1513–1523.

Kuwada S, Yin TC, Syka J, et al (1984) Binaural interaction in low-frequency neurons in inferior colliculus of the cat. IV. Comparison of monaural and binaural response properties. J Neurophysiol 51:1306–1325.

Lacouture Y, Cousineau D (2008) How to use MATLAB to fit the ex - Gaussian and other probability functions to a distribution of response times. Tutor Quant Methods Psychol 4:35–45.

Lam Y-W, Sherman SM (2010) Functional organization of the somatosensory cortical layer 6 feedback to the thalamus. Cereb Cortex 20:13–24. doi: 10.1093/cercor/bhp077

Langner G (1992) Periodicity coding in the auditory system. Hear Res 60:115–142. doi: 10.1016/0378-5955(92)90015-F

Langner G, Dinse HR, Godde B (2009) A map of periodicity orthogonal to frequency representation in the cat auditory cortex. Front Integr Neurosci 3:3662–9. doi: 10.3389/neuro.07.027.2009

Langner G, Schreiner CE (1988) Periodicity coding in the inferior colliculus of the cat. I. neuronal mechanisms. J Neurophysiol 60:1799–1822.

Las L, Stern E a, Nelken I (2005) Representation of tone in fluctuating maskers in the ascending auditory system. J Neurosci 25:1503–13. doi: 10.1523/JNEUROSCI.4007-04.2005

Leach ND, Nodal FR, Cordery PM, et al (2013) Cortical cholinergic input is required for normal auditory perception and experience-dependent plasticity in adult ferrets. J Neurosci 33:6659–6671. doi: 10.1523/JNEUROSCI.5039-12.2013

LeDoux JE, Farb CR, Romanski LM (1991) Overlapping projections to the amygdala and striatum from auditory processing areas of the thalamus and cortex. Neurosci Lett 134:139–144. doi: 10.1016/0304-3940(91)90526-Y

LeDoux JE, Ruggiero DA, Reis DJ (1985) Projections to the subcortical forebrain from anatomically defined regions of the medial geniculate body in the rat. J Comp Neurol 242:182–213. doi: 10.1002/cne.902420204

Lee CC (2013) Thalamic and cortical pathways supporting auditory processing. Brain Lang 126:22–28. doi: 10.1016/j.bandl.2012.05.004

Lee CC, Sherman SM (2009) Modulator property of the intrinsic cortical projection from layer 6 to layer 4. Front Syst Neurosci 3:3. doi: 10.3389/neuro.06.003.2009

Lee CC, Sherman SM (2008) Synaptic Properties of Thalamic and Intracortical Inputs to Layer 4 of the First- and Higher-Order Cortical Areas in the Auditory and Somatosensory Systems. J Neurophysiol 100:317–326. doi: 10.1152/jn.90391.2008

Lee CC, Winer J a (2008a) Connections of cat auditory cortex: III. Corticocortical system. J Comp Neurol 507:1920–43. doi: 10.1002/cne.21613

Lee CC, Winer J a (2008b) Connections of cat auditory cortex: II. Commissural system. J Comp Neurol 507:1901–19. doi: 10.1002/cne.21613

Lee CC, Winer JA (2008c) Connections of cat auditory cortex: I. Thalamocortical system. J Comp Neurol 507:1879–1900. doi: 10.1002/cne.21611

Liberman MC, Simmons DD (1985) Applications of neuronal labeling techniques to the study of the peripheral auditory system. J Acoust Soc Am 78:312–319. doi: 10.1121/1.392492

Licklider JCR (1951) A duplex theory of pitch perception. Experientia 7:128–134. doi: 10.1007/BF02156143

Lin JY, Hartmann WM (1998) The pitch of a mistuned harmonic: evidence for a template model. J Acoust Soc Am 103:2608–2617. doi: 10.1121/1.422781

Linden JF, Schreiner CE (2003) Columnar transformations in auditory cortex? A comparison to visual and somatosensory cortices. Cereb cortex 13:83–89. doi: 10.1093/cercor/13.1.83

Liu L-F, Palmer AR, Wallace MN (2006) Phase-locked responses to pure tones in the inferior colliculus. J Neurophysiol 95:1926–1935. doi: 10.1152/jn.00497.2005

Liu X, Basavaraj S, Krishnan R, Yan J (2011) Contributions of the thalamocortical system towards sound-specific auditory plasticity. Neurosci Biobehav Rev 35:2155–2161. doi: 10.1016/j.neubiorev.2011.02.010

Llano D a, Sherman SM (2008) Evidence for nonreciprocal organization of the mouse auditory thalamocortical-corticothalamic projection systems. J Comp Neurol 507:1209–1227. doi: 10.1002/cne.21602

Loftus WC, Bishop DC, Saint Marie RL, Oliver DL (2004) Organization of binaural excitatory and inhibitory inputs to the inferior colliculus from the superior olive. J Comp Neurol 472:330–44. doi: 10.1002/cne.20070

Lohr B, Dooling RJ (1998) Detection of changes in timbre and harmonicity in complex sounds by zebra finches (Taeniopygia guttata) and budgerigars (Melopsittacus undulatus). J Comp Psychol 112:36–47. doi: 10.1037/0735-7036.112.1.36

Lu T, Liang L, Wang X (2001) Temporal and rate representations of time-varying signals in the auditory cortex of awake primates. Nat Neurosci 4:1131–1138. doi: 10.1038/nn737

Lu T, Wang X (2000) Temporal discharge patterns evoked by rapid sequences of wide- and narrowband clicks in the primary auditory cortex of cat. J Neurophysiol 84:236–246.

Luce RD (1986) Response times: Their role in inferring elementary mental organization. Oxford University Press, New York, NY, pp 99–105

Luo F, Liu X, Wang C, Yan J (2011) The pedunculopontine tegmental nucleus: a second cholinergic source for frequency-specific auditory plasticity. J Neurophysiol 105:107–16. doi: 10.1152/jn.00546.2010

Luo F, Wang Q, Kashani A, Yan J (2008) Corticofugal modulation of initial sound processing in the brain. J Neurosci 28:11615–21. doi: 10.1523/JNEUROSCI.3972-08.2008

Ma X, Suga N (2001) Plasticity of bat's central auditory system evoked by focal electric stimulation of auditory and/or somatosensory cortices. J Neurophysiol 85:1078–1087.

Ma X, Suga N (2004) Lateral inhibition for center-surround reorganization of the frequency map of bat auditory cortex. J Neurophysiol 92:3192–3199. doi: 10.1152/jn.00301.2004

Ma X, Suga N (2005) Long-term cortical plasticity evoked by electric stimulation and acetylcholine applied to the auditory cortex. Proc Natl Acad Sci U S A 102:9335–9340. doi: 10.1073/pnas.0503851102

Ma X, Suga N (2007) Multiparametric corticofugal modulation of collicular duration-tuned neurons: modulation in the amplitude domain. J Neurophysiol 97:3722–30. doi: 10.1152/jn.01268.2006

Macklis JD (1993) Transplanted neocortical neurons migrate selectively into regions of neuronal degeneration produced by chromophore-targeted laser photolysis. J Neurosci 13:3848–63.

Madison R, Macklis JD, Thies C (1990) Latex nanosphere delivery system (LNDS): novel nanometer-sized carriers of fluorescent dyes and active agents selectively target neuronal subpopulations via uptake and retrograde transport. Brain Res 522:90–8.

Magavi SS, Leavitt BR, Macklis JD (2000) Induction of neurogenesis in the neocortex of adult mice. Nature 405:951–5. doi: 10.1038/35016083

Mardia K, Jupp P (2000) Directional Statistics. Wiley, New York, NY

Matzke D, Wagenmakers EJ (2009) Psychological interpretation of the ex-Gaussian and shifted Wald parameters: a diffusion model analysis. Psychon Bull Rev 16:798–817. doi: 10.3758/PBR.16.5.798

McAlonan K, Cavanaugh J, Wurtz RH (2008) Guarding the gateway to cortex with attention in visual thalamus. Nature 456:391–4. doi: 10.1038/nature07382

McAlpine D, Jiang D, Palmer AR (2001) A neural code for low-frequency sound localization in mammals. Nat Neurosci 4:396–401. doi: 10.1038/86049

McCourt ME, Boyapati J, Henry GH (1986) Layering in lamina 6 of cat striate cortex. Brain Res 364:181–5.

McGill W (1963) Stochastic latency mechanisms. In: Luce D, Bush R, Galanter E (eds) Handbook of mathematical psychology. Wiley, New York, NY, pp vol.1, 309–360

McGurk H, MacDonald J (1976) Hearing lips and seeing voices. Nature 264:746–8.

Meddis R, Hewitt MJ (1991a) Virtual pitch and phase sensitivity of a computer model of the auditory periphery. I: Pitch identification. J Acoust Soc Am 89:2866. doi: 10.1121/1.400725

Meddis R, Hewitt MJ (1991b) Virtual pitch and phase sensitivity of a computer model of the auditory periphery. II: Phase sensitivity. J Acoust Soc Am 89:2883. doi: 10.1121/1.400726

Middlebrooks JC, Green DM (1991) Sound localization by human listeners. Annu Rev Psychol 42:135–159. doi: 10.1146/annurev.ps.42.020191.001031

Middlebrooks JC, Onsan Z a (2012) Stream segregation with high spatial acuity. J Acoust Soc Am 132:3896–3911. doi: 10.1121/1.4764879

Mill RW, Alves-Pinto A, Sumner CJ (2014) Decision criterion dynamics in animals performing an auditory detection task. PLoS One 9:e114076. doi: 10.1371/journal.pone.0114076

Miller GA, Heise GA (1950) The Trill Threshold. J Acoust Soc Am 22:637. doi: 10.1121/1.1906663

Miller LM, Escabí M a, Read HL, Schreiner CE (2002) Spectrotemporal receptive fields in the lemniscal auditory thalamus and cortex. J Neurophysiol 87:516–27.

Moore BC, Glasberg BR, Peters RW (1986) Thresholds for hearing mistuned partials as separate tones in harmonic complexes. J Acoust Soc Am 80:479–83.

Moore BCJ (1973) Frequency difference limens for short-duration tones. J Acoust Soc Am 54:610–619. doi: 10.1121/1.1913640

Moore BCJ (2008) The role of temporal fine structure processing in pitch perception, masking, and speech perception for normal-hearing and hearing-impaired people. J Assoc Res Otolaryngol 9:399–406. doi: 10.1007/s10162-008-0143-x

Moore BCJ, Gockel HE (2011) Resolvability of components in complex tones and implications for theories of pitch perception. Hear Res 276:88–97. doi: 10.1016/j.heares.2011.01.003

Moore BCJ, Peters RW, Glasberg BR (1985) Thresholds for the detection of inharmonicity in complex tones. J Acoust Soc Am 77:1861–7. doi: 10.1121/1.391937

Moore DR, Semple MN, Addison PD (1983) Some acoustic properties of neurones in the ferret inferior colliculus. Brain Res 269:69–82. doi: 10.1016/0006-8993(83)90963-0

Morel A, Imig TJ (1987) Thalamic projections to fields A, AI, P, and VP in the cat auditory cortex. J Comp Neurol 265:119–144. doi: 10.1002/cne.902650109

Morel A, Rouiller E, de Ribaupierre Y, de Ribaupierre F (1987) Tonotopic organization in the medial geniculate body (MGB) of lightly anesthetized cats. Exp Brain Res 69:24–42. doi: 10.1007/BF00247026

Nakamoto KT, Shackleton TM, Magezi D a., Palmer AR (2015) A function for binaural integration in auditory grouping and segregation in the inferior colliculus. J Neurophysiol 113:1819–1830. doi: 10.1152/jn.00472.2014

Nelken I, Bizley JK, Nodal FR, et al (2004) Large-scale organization of ferret auditory cortex revealed using continuous acquisition of intrinsic optical signals. J Neurophysiol 92:2574–88. doi: 10.1152/jn.00276.2004

Nelken I, Bizley JK, Nodal FR, et al (2008) Responses of auditory cortex to complex stimuli: functional organization revealed using intrinsic optical signals. J Neurophysiol 99:1928–1941. doi: 10.1152/jn.00469.2007

Nelken I, Rotman Y, Yosef OB (1999) Responses of auditory-cortex neurons to structural features of natural sounds. 397:0–3.

Neuert V (2004) Responses of Dorsal Cochlear Nucleus Neurons to Signals in the Presence of Modulated Maskers. J Neurosci 24:5789–5797. doi: 10.1523/JNEUROSCI.0450-04.2004

Nodal FR, Bajo VM, Bizley JK, King AJ (2006) Cortico-Thalamic Connectivity of Ferret Auditory Cortex. In: ARO Midwinter Meeting. p 238

Nodal FR, Bajo VM, King AJ (2012) Plasticity of spatial hearing: behavioural effects of cortical inactivation. J Physiol 590:3965–3986. doi: 10.1113/jphysiol.2011.222828

Nodal FR, Bajo VM, Parsons CH, et al (2008) Sound localization behavior in ferrets: Comparison of acoustic orientation and approach-to-target responses. Neuroscience 154:397–408. doi: 10.1016/j.neuroscience.2007.12.022

Nodal FR, Kacelnik O, Bajo VM, et al (2010) Lesions of the auditory cortex impair azimuthal sound localization and its recalibration in ferrets. J Neurophysiol 103:1209–1225. doi: 10.1152/jn.00991.2009

O'Connor DH, Fukui MM, Pinsk M a, Kastner S (2002) Attention modulates responses in the human lateral geniculate nucleus. Nat Neurosci 5:1203–9. doi: 10.1038/nn957

O'Connor KN, Sutter ML (2000) Global spectral and location effects in auditory perceptual grouping. J Cogn Neurosci 12:342–354. doi: 10.1162/089892900562020

Ohl FW, Wetzel W, Wagner T, et al (1999) Bilateral ablation of auditory cortex in Mongolian gerbil affects discrimination of frequency modulated tones but not of pure tones. Learn Mem 6:347–62. doi: 10.1101/lm.6.4.347

Ojima H (1994) Terminal morphology and distribution of corticothalamic fibers originating from layers 5 and 6 of cat primary auditory cortex. Cereb Cortex 4:646–63.

Oliver D, Beckius G, Bishop DC, Kuwada S (1997) Simultaneous anterograde labeling of axonal layers from lateral superior olive and dorsal cochlear nucleus in the inferior colliculus of cat. J Comp Neurol 382:215–229.

Oliver DL, Winer J a, Beckius GE, Saint Marie RL (1994) Morphology of GABAergic neurons in the inferior colliculus of the cat. J Comp Neurol 340:27–42. doi: 10.1002/cne.903400104

Olsen SR, Bortone DS, Adesnik H, Scanziani M (2012) Gain control by layer six in cortical circuits of vision. Nature 483:47–52. doi: 10.1038/nature10835

Ono K, Kudoh M, Shibuki K (2006) Roles of the auditory cortex in discrimination learning by rats. Eur J Neurosci 23:1623–1632. doi: 10.1111/j.1460-9568.2006.04695.x

Orman SS, Humphrey GL (1981) Effects of changes in cortical arousal and of auditory cortex cooling on neuronal activity in the medial geniculate body. Exp brain Res 42:475–82.

Palmer a R, Russell IJ (1986) Phase-locking in the cochlear nerve of the guinea pig and its relation to the receptor potential of inner hair cells.

Peruzzi D, Bartlett E, Smith PH, Oliver DL (1997) A monosynaptic GABAergic input from the inferior colliculus to the medial geniculate body in rat. J Neurosci 17:3766–3777.

Pfeiffer RR (1966) Classification of response patterns of spike discharges for units in the cochlear nucleus: Tone-burst stimulation. Exp Brain Res 1:220–235. doi: 10.1007/BF00234343

Phillips DP, Judge PW, Kelly JB (1988) Primary auditory cortex in the ferret (Mustela putorius): neural response properties and topographic organization. Brain Res 443:281–294.

Polley DB, Steinberg EE, Merzenich MM (2006) Perceptual learning directs auditory cortical map reorganization through top-down influences. J Neurosci 26:4970–4982. doi: 10.1523/JNEUROSCI.3771-05.2006

Pressnitzer D, Meddis R, Delahaye R, Winter IM (2001) Physiological correlates of comodulation masking release in the mammalian ventral cochlear nucleus. J Neurosci 21:6377–6386. doi: 21/16/6377 [pii]

Prieto J, Winer J (1999) Layer VI in cat primary auditory cortex: Golgi study and sublaminar origins of projection neurons. J Comp Neurol 404:332–58. doi: 10.1002/(SICI)1096-9861(19990215)404:3<332::AID-CNE5>3.0.CO;2-R

Read HL, Nauen DW, Escabi M a, et al (2011) Distinct core thalamocortical pathways to central and dorsal primary auditory cortex. Hear Res 274:95–104. doi: 10.1016/j.heares.2010.11.010

Reale R a, Imig TJ (1980) Tonotopic organization in auditory cortex of the cat. J Comp Neurol 192:265–91. doi: 10.1002/cne.901920207

Redies H, Brandner S (1991) Functional organization of the auditory thalamus in the guinea pig. Exp Brain Res 86:384–392. doi: 10.1007/BF00228962

Roberts B, Bailey PJ (1993) Spectral Pattern and the Perceptual Fusion of Harmonics .2. A Special Status for Added Components? J Acoust Soc Am 94:3165–3177.

Roberts B, Bailey PJ (1996a) Spectral regularity as a factor distinct from harmonic relations in auditory grouping. J Exp Psychol Hum Percept Perform 22:604–14.

Roberts B, Bailey PJ (1996b) Regularity of spectral pattern and its effects on the perceptual fusion of harmonics. Percept Psychophys 58:289–299. doi: 10.3758/BF03211882

Roberts B, Bregman AS (1991) Effects of the pattern of spectral spacing on the perceptual fusion of harmonics. J Acoust Soc Am 90:3050. doi: 10.1121/1.401779

Roberts B, Holmes SD (2007) Contralateral influences of wideband inhibition on the effect of onset asynchrony as a cue for auditory grouping. J Acoust Soc Am 121:3655–65. doi: 10.1121/1.2721874

Roberts B, Holmes SD (2006) Asynchrony and the grouping of vowel components: Captor tones revisited. J Acoust Soc Am 119:2905. doi: 10.1121/1.2190164

Rodrigues-Dagaeff C, Simm G, De Ribaupierre Y, et al (1989) Functional organization of the ventral division of the medial geniculate body of the cat: evidence for a rostro-caudal gradient of response properties and cortical projections. Hear Res 39:103–125. doi: 10.1016/0378-5955(89)90085-3

Rose JE, Brugge JF, Anderson DJ, Hind JE (1967) Phase-locked response to low-frequency tones in single auditory nerve fibers of the squirrel monkey. J Neurophysiol 30:769–793.

Rouiller E, de Ribaupierre Y, de Ribaupierre F (1979) Phase-locked responses to low frequency tones in the medial geniculate body. Hear. Res. 1:213–226.

Rouiller E, de Ribaupierre Y, Toros-Morel A, de Ribaupierre F (1981) Neural coding of repetitive clicks in the medial geniculate body of cat. Hear Res 5:81–100. doi: 10.1016/0378-5955(81)90028-9

Rouiller EM, de Ribaupierre F (1985) Origin of afferents to physiologically defined regions of the medial geniculate body of the cat: ventral and dorsal divisions. Hear Res 19:97–114. doi: 10.1016/0378-5955(85)90114-5

Rouiller EM, de Ribaupierre F (1989) Note on the tonotopic organization in the cat medial geniculate body: influence of sampling of units. Exp Brain Res 74:220–6.

Rouiller EM, Rodrigues-Dagaeff C, Simm G, et al (1989) Functional organization of the medial division of the medial geniculate body of the cat: tonotopic organization, spatial distribution of response properties and cortical connections. Hear Res 39:127–42.

Rouiller EM, Welker E (1991) Morphology of corticothalamic terminals arising from the auditory cortex of the rat: a Phaseolus vulgaris-leucoagglutinin (PHA-L) tracing study. Hear Res 56:179–90. doi: 10.1016/0378-5955(91)90168-9

Ryan A (1976) Hearing sensitivity of the mongolian gerbil, Meriones unguiculatis. J Acoust Soc Am 59:1222–1226. doi: 10.1121/1.380961

Ryugo DK, Weinberger NM (1976) Corticofugal Modulation of the Medial Geniculate Body. Exp Neurol 391:377–391. doi: 0014-4886(76)90262-4 [pii]

Saberi K, Perrott DR (1999) Cognitive restoration of reversed speech. Nature 398:760–760. doi: 10.1038/19652

Sakai M, Suga N (2002) Centripetal and centrifugal reorganizations of frequency map of auditory cortex in gerbils. Proc Natl Acad Sci U S A 99:7108–7112. doi: 10.1073/pnas.102165399

Sanes DH (1990) An in vitro analysis of sound localization mechanisms in the gerbil lateral superior olive. J Neurosci 10:3494–3506.

Scheffers MTM (1983) Sifting vowels. Auditory pitch analysis and sound segregation.

Schnupp JWH, Hall TM, Kokelaar RF, Ahmed B (2006) Plasticity of temporal pattern codes for vocalization stimuli in primary auditory cortex. J Neurosci 26:4785–95. doi: 10.1523/JNEUROSCI.4330-05.2006

Schnupp JWH, Nelken I, King AJ (2011) Auditory neuroscience: making sense of sound. The MIT Press, Cambridge, MA

Schreiner CE, Polley DB (2014) Auditory map plasticity: Diversity in causes and consequences. Curr Opin Neurobiol 24:143–156. doi: 10.1016/j.conb.2013.11.009

Schulze H, Hess A, Ohl FW, Scheich H (2002) Superposition of horseshoe-like periodicity and linear tonotopic maps in auditory cortex of the Mongolian gerbil. Eur J Neurosci 15:1077–1084. doi: 10.1046/j.1460-9568.2002.01935.x

Shamma S a., Elhilali M, Micheyl C (2011) Temporal coherence and attention in auditory scene analysis. Trends Neurosci 34:114–123. doi: 10.1016/j.tins.2010.11.002

Sheen VL, Macklis JD (1994) Apoptotic mechanisms in targeted neuronal cell death by chromophore-activated photolysis. Exp Neurol 130:67–81. doi: 10.1006/exnr.1994.1186

Sherman SM (2001) Tonic and burst firing: Dual modes of thalamocortical relay. Trends Neurosci 24:122–126. doi: 10.1016/S0166-2236(00)01714-8

Sherman SM, Guillery RW (1998) On the actions that one nerve cell can have on another: distinguishing "drivers" from "modulators". Proc Natl Acad Sci U S A 95:7121–7126. doi: 10.1073/pnas.95.12.7121

Sherman SM, Guillery RW (2011) Distinct functions for direct and transthalamic corticocortical connections. J Neurophysiol 106:1068–77. doi: 10.1152/jn.00429.2011

Sherman SM, Guillery RW (2013) Functional Connections of Cortical Areas: A New View from the Thalamus, 1st edn. Cambridge, MA

Sinex DG (2008) Responses of cochlear nucleus neurons to harmonic and mistuned complex tones. Hear Res 238:39–48. doi: 10.1016/j.heares.2007.11.001

Sinex DG, Guzik H, Li H, et al (2003) Responses of auditory nerve fibers to harmonic and mistuned complex tones. Hear Res 182:130–139. doi: 10.1016/S0378-5955(03)00189-8

Sinex DG, Henderson Sabes J, Li H (2002) Responses of inferior colliculus neurons to harmonic and mistuned complex tones. Hear Res 168:150–162. doi: 10.1016/S0378-5955(02)00366-0

Sinex DG, Li H (2007) Responses of inferior colliculus neurons to double harmonic tones. J Neurophysiol 98:3171–84. doi: 10.1152/jn.00516.2007

Sinex DG, Li H, Velenovsky DS (2005) Prevalence of stereotypical responses to mistuned complex tones in the inferior colliculus. J Neurophysiol 94:3523–3537. doi: 10.1152/jn.01194.2004

Steinschneider M, Reser DH, Fishman YI, et al (1998) Click train encoding in primary auditory cortex of the awake monkey: evidence for two mechanisms subserving pitch perception. J Acoust Soc Am 104:2935–2955. doi: 10.1121/1.423877

Sternson SM, Roth BL (2014) Chemogenetic Tools to Interrogate Brain Functions. Annu Rev Neurosci. doi: 10.1146/annurev-neuro-071013-014048

Storace D a., Higgins NC, Read HL (2010) Thalamic label patterns suggest primary and ventral auditory fields are distinct core regions. J Comp Neurol 518:1630–1646. doi: 10.1002/cne.22345

Stratford KJ, Tarczy-Hornoch K, Martin KAC, et al (1996) Excitatory synaptic inputs to spiny stellate cells in cat visual cortex. Nature 382:258–261. doi: 10.1038/382258a0

Suga N (2012) Tuning shifts of the auditory system by corticocortical and corticofugal projections and conditioning. Neurosci Biobehav Rev 36:969–88. doi: 10.1016/j.neubiorev.2011.11.006

Suga N, Ma X (2003) Multiparametric corticofugal modulation and plasticity in the auditory system. Nat Rev Neurosci 4:783–94. doi: 10.1038/nrn1222

Sumner CJ, Palmer AR (2012) Auditory nerve fibre responses in the ferret. Eur J Neurosci 36:2428–2439. doi: 10.1111/j.1460-9568.2012.08151.x

Sutter ML, Schreiner CE (1991) Physiology and topography of neurons with multipeaked tuning curves in cat primary auditory cortex. J Neurophysiol 65:1207–1226.

Talwar SK, Gerstein GL (2001) Reorganization in awake rat auditory cortex by local microstimulation and its effect on frequency-discrimination behavior. J Neurophysiol 86:1555–1572.

Talwar SK, Musial PG, Gerstein GL (2001) Role of mammalian auditory cortex in the perception of elementary sound properties. J Neurophysiol 85:2350–8.

Temereanca S, Simons DJ (2004) Functional Topography of Corticothalamic Feedback Enhances Thalamic Spatial Response Tuning in the Somatosensory Whisker/Barrel System. Neuron 41:639–651. doi: 10.1016/S0896-6273(04)00046-7

Terhardt E (1974) Pitch, consonance, and harmony. J Acoust Soc Am 55:1061–1069. doi: 10.1121/1.1914648

Thomas EAC (1975) Criterion adjustment and probability matching. Percept Psychophys 18:158–162.

Tollin DJ, Yin TCT (2002a) The coding of spatial location by single units in the lateral superior olive of the cat. II. The determinants of spatial receptive fields in azimuth. J Neurosci 22:1468–79. doi: 22/4/1454 [pii]

Tollin DJ, Yin TCT (2002b) The coding of spatial location by single units in the lateral superior olive of the cat. I. spatial receptive fields in azimuth. J Neurosci 22:1454–67. doi: 22/4/1454 [pii]

Tolnai S, Dolležal L-V, Klump GM (2015) Binaural cues provide for a release from informational masking. Behav Neurosci 129:589–98. doi: 10.1037/bne0000091

Tolnai S, Litovsky RY, King AJ (2014) The precedence effect and its buildup and breakdown in ferrets and humans. J Acoust Soc Am 135:1406–1418. doi: 10.1121/1.4864486

Town SM, Atilgan H, Wood KC, Bizley JK (2015) The role of spectral cues in timbre discrimination by ferrets and humans. J Acoust Soc Am 137:2870–2883. doi: 10.1121/1.4916690

Tsuchitani C, Boudreau JC (1966) Single unit analysis of cat superior olive S segment with tonal stimuli. J Neurophysiol 29:684–97.

Van Horn SC, Erisir A, Sherman SM (2000) Relative distribution of synapses in the A-laminae of the lateral geniculate nucleus of the cat. J Comp Neurol 416:509–520. doi: 10.1002/(SICI)1096-9861(20000124)416:4<509::AID-CNE7>3.0.CO;2-H

Van Noorden LPAS (1975) Temporal coherence in the perception of tone sequences. The Netherlands Technical University

Versnel H, Mossop JE, Mrsic-Flogel TD, et al (2002) Optical imaging of intrinsic signals in ferret auditory cortex: responses to narrowband sound stimuli. J Neurophysiol 88:1545–1558.

Vidnyanszky Z, Gorcs TJ, Negyessy L, et al (1996) Immunocytochemical visualization of the mGluR1a metabotropic glutamate receptor at synapses of corticothalamic terminals originating from area 17 of the rat. Eur J Neurosci 8:1061–71.

Villa a. EP, Rouiller EM, Simm GM, et al (1991) Corticofugal modulation of the information processing in the auditory thalamus of the cat. Exp Brain Res 86:506–517. doi: 10.1007/BF00230524

Walker KMM (2008) The Perception and Cortical Processing of Communication Sounds. University of Oxford

Walker KMM, Bizley JK, King AJ, Schnupp JWH (2011) Multiplexed and robust representations of sound features in auditory cortex. J Neurosci 31:14565–76. doi: 10.1523/JNEUROSCI.2074-11.2011

Walker KMM, McDermott JH, Kang J, King AJ (2014) Ferret pitch perception is dominated by temporal cues, unlike that of humans. In: ARO Midwinter Meeting. p 509

Walker KMM, Schnupp JWH, Hart-Schnupp SMB, et al (2009) Pitch discrimination by ferrets for simple and complex sounds. J Acoust Soc Am 126:1321–1335. doi: 10.1121/1.3179676

Wallace MN, Anderson L a, Palmer AR (2007) Phase-locked responses to pure tones in the auditory thalamus. J Neurophysiol 98:1941–1952. doi: 10.1152/jn.00697.2007

Wallace MN, He J (2011) Intrinsic Connections of the Auditory Cortex. In: Winer JA, Schreiner CE (eds) The Auditory Cortex. Springer US, Boston, MA, pp 133–145

Wallace MN, Shackleton TM, Palmer AR (2002) Phase-locked responses to pure tones in the primary auditory cortex. Hear Res 172:160–171. doi: 10.1016/S0378-5955(02)00580-4

Wang X, Kadia SC (2001) Differential representation of species-specific primate vocalizations in the auditory cortices of marmoset and cat. J Neurophysiol 86:2616–2620.

Wang X, Lu T, Bendor D, Bartlett E (2008) Neural coding of temporal information in auditory thalamus and cortex. Neuroscience 157:484–493. doi: 10.1016/j.neuroscience.2008.07.050

Wang X, Merzenich MM, Beitel R, et al (1995) Representation of a species-specific vocalization in the primary auditory cortex of the common marmoset: temporal and spectral characteristics. J Neurophysiol 74:2685–706.

Wickens T (2002) Elementary Signal Detection Theory. Oxford University Press, New York, NY

Winer J a, Diehl JJ, Larue DT (2001) Projections of auditory cortex to the medial geniculate body of the cat. J Comp Neurol 430:27–55.

Winer J a, Larue DT (1996) Evolution of GABAergic circuitry in the mammalian medial geniculate body. Proc Natl Acad Sci U S A 93:3083–3087. doi: 10.1073/pnas.93.7.3083

Winer J a, Morest DK (1983a) The medial division of the medial geniculate body of the cat: implications for thalamic organization. J Neurosci 3:2629–51.

Winer J a, Morest DK (1983b) The neuronal architecture of the dorsal division of the medial geniculate body of the cat. A study with the rapid Golgi method. J Comp Neurol 221:1–30. doi: 10.1002/cne.902210102

Winer J a, Morest DK, Diamond IT (1988) A cytoarchitectonic atlas of the medial geniculate body of the opossum, Didelphys virginiana, with a comment on the posterior intralaminar nuclei of the thalamus. J Comp Neurol 274:422–448. doi: 10.1002/cne.902740310

Winer J a, Prieto JJ (2001) Layer V in cat primary auditory cortex (AI): cellular architecture and identification of projection neurons. J Comp Neurol 434:379–412. doi: 10.1002/cne.1183

Winer J a, Saint Marie RL, Larue DT, Oliver DL (1996) GABAergic feedforward projections from the inferior colliculus to the medial geniculate body. Proc Natl Acad Sci U S A 93:8005–8010. doi: 10.1073/pnas.93.15.8005

Winer J a. (2006) Decoding the auditory corticofugal systems. Hear Res 212:1–8. doi: 10.1016/j.heares.2005.06.014

Winer J a., Larue DT, Huang CL (1999) Two systems of giant axon terminals in the cat medial geniculate body: Convergence of cortical and GABAergic inputs. J Comp Neurol 413:181–197. doi: 10.1002/(SICI)1096-9861(19991018)413:2<181::AID-CNE1>3.0.CO;2-7

Winer J a., Lee CC (2007) The distributed auditory cortex. Hear Res 229:3–13. doi: 10.1016/j.heares.2007.01.017

Wu Y, Yan J (2007) Modulation of the receptive fields of midbrain neurons elicited by thalamic electrical stimulation through corticofugal feedback. J Neurosci 27:10651–10658. doi: 10.1523/JNEUROSCI.1320-07.2007

Xiong Q, Znamenskiy P, Zador AM (2015) Selective corticostriatal plasticity during acquisition of an auditory discrimination task. Nature 1–16. doi: 10.1038/nature14225

Yan J, Ehret G (2002) Corticofugal modulation of midbrain sound processing in the house mouse. Eur J Neurosci 16:119–128. doi: 10.1046/j.1460-9568.2002.02046.x

Yan J, Suga N (1996) Corticofugal modulation of time-domain processing of biosonar information in bats. Science 273:1100–3. doi: 10.1126/science.273.5278.1100

Yap MJ, Balota DA, Cortese MJ, Watson JM (2006) Single- versus dual-process models of lexical decision performance: insights from response time distributional analysis. J Exp Psychol Hum Percept Perform 32:1324–1344. doi: 10.1037/0096-1523.32.6.1324

Yin P, Fritz JB, Shamma SA (2010) Do ferrets perceive relative pitch? J Acoust Soc Am 127:1673–1680. doi: 10.1121/1.3290988

Yin TC, Chan JC (1990) Interaural time sensitivity in medial superior olive of cat. J Neurophysiol 64:465–488.

Young ED, Brownell WE (1976) Responses to tones and noise of single cells in dorsal cochlear nucleus of unanesthetized cats. J Neurophysiol 39:282–300.

Yu Y-Q, Xiong Y, Chan Y-S, He J (2004) Corticofugal gating of auditory information in the thalamus: an in vivo intracellular recording study. J Neurosci 24:3060–9. doi: 10.1523/JNEUROSCI.4897-03.2004

Zhang Y, Suga N (2005) Corticofugal feedback for collicular plasticity evoked by electric stimulation of the inferior colliculus. J Neurophysiol 94:2676–82. doi: 10.1152/jn.00549.2005

Zhang Y, Suga N (1997) Corticofugal amplification of subcortical responses to single tone stimuli in the mustached bat. J Neurophysiol 78:3489–3492.

Zhang Y, Suga N (2000) Modulation of responses and frequency tuning of thalamic and collicular neurons by cortical activation in mustached bats. J Neurophysiol 84:325–333.

Zhang Y, Suga N, Yan J (1997) Corticofugal modulation of frequency processing in bat auditory system. Nature 387:900–3. doi: 10.1038/43180

Zhang Y, Yan J (2008) Corticothalamic Feedback for Sound- Specific Plasticity of Auditory Thalamic Neurons Elicited by Tones Paired with Basal Forebrain Stimulation. Cereb Cortex 18:1521–1528. doi: 10.1093/cercor/bhm188

Zhang Z, Liu C-H, Yu Y-Q, et al (2008) Corticofugal projection inhibits the auditory thalamus through the thalamic reticular nucleus. J Neurophysiol 99:2938–45. doi: 10.1152/jn.00002.2008

Znamenskiy P, Zador AM (2013) Corticostriatal neurons in auditory cortex drive decisions during auditory discrimination. Nature 497:482–5. doi: 10.1038/nature12077

Zwicker UT (1984) Auditory recognition of diotic and dichotic vowel pairs. Speech Commun 3:265–277. doi: 10.1016/0167-6393(84)90023-2

Zychaluk K, Foster DH (2009) Model-free estimation of the psychometric function. Atten Percept Psychophys 71:1414–25. doi: 10.3758/APP.71.6.1414